BODIPY-linked *cis*-dichlorido zinc(II) conjugates: strategic design of organelle-specific next generation theranostic photosensitizers

Arnab Bhattacharyya,[a] Aida Jameei,[b] Rupak Saha,[a] Aditya Garai,[a] Anjali A. Karande,*[b] and Akhil R. Chakravarty*[a]

[a] Department of Inorganic and Physical Chemistry and [b] Department of Biochemistry, Indian Institute of Science, Bangalore 560 012, India. Email: arc@iisc.ac.in, anjali@alum.iisc.ac.in.

Electronic Supplementary Information (ESI)

Table of contents

Scheme S2 – General synthetic scheme for the preparation of complexes **1-3**

Figures –

Figure S1 – UV-vis absorption spectra of ligands L^2 and L^3

Figure S2 – Emission spectra of ligands L^2 and L^3

Figures S3-S10 – NMR (^1H, ^{13}C, ^{11}B) spectra of ligands L^1-L^3

Figures S11-S13 – ESI-MS spectra of complexes **1-3**

Figure S14 – UV-vis absorption spectra of complexes **1-3**

Figure S15 – Emission spectra of complexes **2**,**3**

Figures S16, S17 – FTIR spectra of complexes **2,3**

Figures S18-S25 – NMR (^1H, ^{13}C, ^{11}B) spectra of complexes **1**-**3**

Figures S26, S27 – Cyclic voltammogram of complexes **2**,**3**

Figures S28, S29 – Unit cell packing diagram of complexes **2,3**

Figure S30 – Energy optimized structure of complex **1** showing frontier orbitals

Figure S31 – HOMO–1 and LUMO+1 energy level diagrams of complexes **1-3**

Figures S32-S34 – Time dependent stability studies of complexes **1**-**3** under dark conditions in biological media

Figures S35, S36 – Time dependent photo-stability studies of complexes **2**,**3** in biological media

Figures S37-S42 – Cell viability plots of complexes **1-3** in HeLa and MCF-7 cells

Figure S43 – Cellular uptake plot of complex **2** in HeLa cells

Figures S44, S45 – Confocal microscopy images of complex **2** in HeLa and MCF-7 cells showing back ground colours and controls

Experimental section

Materials and measurements:

The chemicals and solvents were bought from SD Fine chemicals, India. 2,4-Dimethylpyrrole, 2-pyridylmethyl amine and 4-chloromethyl benzoyl chloride, pyridine-2-carboxaldehyde were obtained from Sigma-Adrich (Merck), India and TCI Chemicals, India. DPBF (1,3-diphenylisobenzofuran) and Rose Bengal (RB) were purchased from TCI Chemicals, India. Solvents were distilled and purified before use following literature methods.[S1] HeLa and MCF-7 cells were procured from NCCS (National Centre for Cell Science), India. Dulbecco's modified eagle medium (DMEM) for cell culture, Dulbecco's phosphate buffered saline (DPBS), Hoechst dye (33258), propidium iodide (PI), MTT (4,5-dimethylthiazol-2-yl)-2,5-diphenyltetrazolium bromide, DCFDA (dichlorofluorescein diacetate) were purchased from Sigma-Aldrich (Merck). FBS (fetal bovine serum) and red emissive mitochondrial tracker dye (MTR, product specification no. M 22426) were obtained from Invitrogen, India. ct-DNA (ct, calf thymus) and supercoiled CsCl purified pUC19 DNA were bought from Sigma-Aldrich (Merck) and Bangalore Genie (India) respectively. TEMP (2,2,6,6-tetramethyl-4-piperidone), NaN_3, KI, DMSO and EB (ethidium bromide) etc. were procured from Sigma-Aldrich (Merck).

Thermo Finnigan CHNS analyzer (Model FLASH EA 1112) with Eager 300 software was used for elemental analysis. The absorption and IR spectra were recorded using Perkin Elmer Shimadzu UV-2600 UV-vis spectrophotometer and Bruker Alpha-P spectrometer respectively. Emission spectral measurements were done using Horiba Model Jobin–Yvon Fluoromax-4 spectrophotometer. Fluorescence quantum yield measurements were carried out following standard protocols using fluorescein as a standard in NaOH. ESI-MS measurements were made using Agilent Model 6538 Ultra high definition (UHD) accurate Mass Q-TOF (LC-HRMS) and Micromass Q-TOF (ESI-HRMS) spectrometers. The NMR spectra were recorded using Bruker Avance NMR spectrometer (400 MHz). Cyclic voltammetric measurements were performed by CHI 645D electrochemical workstation, CH instruments, USA. The setup comprises three electrodes where glassy carbon acts as a working electrode, platinum as auxiliary and saturated calomel as reference electrodes. Ferrocene and TBAP (tetrabutylammonium perchlorate, 0.1 M) were used as standard and supporting electrolyte, respectively [***Caution!*** *TBAP was used in small quantities and with care*]. Photo-irradiation of the samples for different chemical and

biological experiments was done using Luzchem photoreactor made of Ontario, Canada (Model LZC-1) fitted with eight Sylvania white fluorescent tubes (400-700 nm) producing a broad band white light. To record the data for MTT assay, TECAN micro plate reader was used. Fluorescence activated cell sorting experiments were carried out by FACS Calibur BD (Becton Dickinson) cell analyzer while confocal microscopy images were captured using Leica TCS (Model SP8 DM 6000) containing laser scanning facility and 63× magnification ability.

Synthesis and characterization of ligands L^1-L^3 and complex 1:

Synthesis of ligand L^1: The synthesis of di-(2-picolyl)amine [bis-(2-pyridylmethyl)amine] ligand (L^1) was done following a standard literature procedure.[S2]

L^1: ^{1}H NMR (400 MHz, $CDCl_3$); δ (ppm): 8.43 (dd, 2 H, *J* = 4.8 Hz), 7.51 (dt, 2 H, *J* = 7.6 Hz), 7.24 (d, 2 H, *J* = 7.8 Hz), 7.03 (dt, 2 H, *J* = 6.1 Hz); (d, doublet; dd, doublet of doublet, dt, doublet of triplet); ^{13}C NMR (100 MHz, $CDCl_3$); δ (ppm): 159.8, 149.6, 136.8, 122.7, 122.3, 54.9.

Synthesis of ligands L^2 and L^3 (Scheme S1):

Synthesis of precursor A: The precursor species **A** was synthesized following the synthetic procedure reported by C. J. Chang *et al.*[S3]

Synthesis of ligand L^2: In a dry round bottomed flask, the precursor **A** (0.37 g, 1 mmol, 1.0 eq.) was taken in 25 mL acetonitrile. K_2CO_3 (0.28 g, 2 mmol, 2.0 eq.) and KI (0.33 g, 2 mmol, 2.0 eq.) dissolved in 10 mL of distilled water were subsequently added to the flask. Bis-(2-pyridylmethyl)amine (1 g, 5 mmol, 5.0 eq.) taken in 10 mL CH_3CN was finally added to this mixture and the resulting solution was heated at 80° C for 6 h. The solvents were then evaporated under reduced pressure and resulting residue thus obtained was dissolved in dichloromethane. The organic layer was then washed with water and brine solution, dried over anhydrous Na_2SO_4, filtered and concentrated under reduced pressure to procure the crude BODIPY ligand. Purification of the crude was finally done by silica gel column chromatography using EtOAc/Hexane as eluent (9:1) to afford the emissive BODIPY ligand L^2 as a dark orange solid (0.38 g, 0.71 mmol, ~71% yield).

L^2: ^{1}H NMR (400 MHz, $CDCl_3$); δ (ppm): 8.56 (d, 2 H, *J* = 4.7 Hz), 7.70 (dt, 2 H, *J* = 7.6 Hz), 7.55 (q, 4 H), 7.26 (t, 2 H, *J* = 7.0 Hz), 7.18 (t, 2 H, *J* = 5.5 Hz), 5.96 (s, 2 H), 3.84 (s, 4 H), 3.79 (s, 2 H), 2.56 (s, 6 H), 1.34 (s, 6 H) (s, singlet; d, doublet; t; triplet, q, quartet; dt, doublet of triplet); ^{13}C NMR (100 MHz, $CDCl_3$); δ (ppm): 159.9, 155.8, 149.5, 143.5, 142.1, 140.3, 136.9, 134.3, 131.9, 130.3, 128.4, 123.3, 122.5, 121.6, 60.2, 58.5, 15.0, 14.7; ^{11}B NMR (100 MHz, $CDCl_3$), δ (ppm): 0.77 (t, 1 B, *J* = 25.8 Hz). UV-visible in 10% DMSO-DPBS buffer (pH = 7.4) [λ_{max}/ nm (ε/ dm^3 mol^{-1} cm^{-1})]: 249 (10,240), 334 (2,940), 500 (46,600). Emission in 10% DMSO-DPBS buffer (pH = 7.4) [λ_{em}/ nm (λ_{ex}/ nm)]: 506 (450).

Synthesis of ligand L^3: Non-iodinated BODIPY ligand L^2 (0.53 g, 1.0 mmol, 1.0 eq.) was taken in an oven dried round bottomed flask and dissolved in 30 ml of dry dicholoromethane. Under flow of nitrogen, N-iodo succinimide (NIS) (1.35 g, 6.0 mmol, 6.0 eq.) was then added to the flask. The reaction mixture was stirred under inert atmosphere at room temperature until full consumption of L^2 was noticed by thin layer chromatography (TLC). The organic layer was then washed with water and brine, dried over anhydrous Na_2SO_4, filtered and the solvent was removed using a rotary evaporator. The crude product was finally purified by silica gel column chromatography using EtOAc/hexane as eluent (9:1 v/v) to obtain di-iodinated BODIPY ligand L^3 as a dark red solid (0.59 g, 0.75 mmol, ~75% yield).

L^3: ^{1}H NMR (400 MHz, $CDCl_3$); δ (ppm): 8.60 (d, 2 H, *J* = 4.4 Hz), 7.75 (dt, 2 H, *J* = 7.6 Hz), 7.62 (q, 4 H), 7.24 (t, 4 H), 3.96 (s, 4 H), 3.93 (s, 2 H), 2.65 (s, 6 H), 1.35 (s, 6 H); ^{13}C NMR (100 MHz, $CDCl_3$); δ (ppm): 158.6, 157.2, 149.3, 145.6, 141.6, 137.5, 134.3, 131.7, 130.8, 128.4, 123.8, 123.8, 123.0, 86.1, 59.6, 58.3, 30.8, 30.1, 17.4, 16.5; ^{11}B NMR (100 MHz, $CDCl_3$); δ (ppm): 0.54 (t, 1 B, *J* = 25.1 Hz). UV-vis in 10% DMSO-DPBS buffer (pH = 7.4) [λ_{max}/ nm (ε/ dm^3 mol^{-1} cm^{-1})]: 249 (19,100), 383 (8,200), 535 (37,900). Emission in 10% DMSO-DPBS buffer (pH = 7.4) [λ_{em}/ nm (λ_{ex}/ nm)]: 554 (500).

Synthesis of complex 1 (Scheme S2):

Complex **1** was prepared using a modified procedure previously reported by Fernandes *et al.*[S4] $ZnCl_2.2H_2O$ (16 mg, 1.2 mmol, 1.2 eq.) was initially dissolved in minimum volume of methanol. A methanolic solution of dipicolylamine ligand (dpa, L^1, 20 mg, 1.0 mmol, 1.0 eq.) was added to it in drop-wise manner. A white coloured solid was obtained which was collected by filtration

after 30 min of stirring, washed multiple times with cold water, diethyl ether and dried in vacuum over P_4O_{10} to obtain complex **1**.

[ZnL^{1}Cl$_2$] (**1**): yield: 29 mg, ~87%. Anal Calcd. for $C_{12}H_{13}Cl_2N_3Zn$ (Fw / g M^{-1}: 335.5370): C, 42.96; H, 3.91; N, 12.52. Found: C, 43.08; H, 3.97; N, 12.44. ESI-MS in acetonitrile (m/z): calculated for $[M–Cl]^+$: 298.0089; Found: 298.0125. UV-vis in 1.0% DMSO-DPBS buffer (pH = 7.4) [λ_{max}/ nm (ε/ dm^3 mol^{-1} cm^{-1})]: 261 (18,000). ^{1}H NMR (400 MHz, DMSO-D_6); δ (ppm): 8.78 (d, 2 H, *J* = 4.8 Hz), 8.01 (dt, 2 H, *J* = 7.7 Hz), 7.56 (q, 4 H), 4.86 (s, 1 H), 4.13 (s, 4 H); ^{13}C NMR (100 MHz, DMSO-D_6); δ (ppm): 156.4, 148.3, 140.4, 124.8, 123.9, 51.1. Molar conductivity (Λ_M) in acetonitrile (in aqueous DMSO 9:1 v/v): 17 (217) S m^2 mol^{-1}.

X-ray crystallographic discussion:

The chelate acute bite angles for the crystal structure of complex **2** corresponding to N(1)-Zn(1)-N(3) and N(2)-Zn(1)-N(3) are 74.29(8)° and 74.32(9)°, while for complex **3** the values are 74.98(18)° and 75.28(19)°. The shorter and stronger equatorial Zn-N bonds [Zn(1)-N(1) = 2.098(2) Å, Zn(1)-N(2) = 2.124(2) Å for complex **2** and Zn(1)-N(1) = 2.115(5) Å, Zn(1)-N(2) = 2.115(6) Å for complex **3**] are formed by the overlap of the metal ion orbitals with the pyridine (sp^2) nitrogen atoms which are electron rich while the elongated Zn-N axial bonds [Zn(1)-N(3) = 2.404(2) Å for complex **2** and Zn(1)-N(3) = 2.376(4) Å for complex **3**] have overlap of amine (sp^3) nitrogen atoms with the respective zinc(II) centres. Similarly, basal Zn-Cl bonds [Zn(1)-Cl(1) = 2.2554(8) Å for complex **2** and Zn(1)-Cl(1) = 2.2861(19) Å for complex **3**], where the sp^2 hybrid orbitals of metal are involved, are reported to be stronger than the axial Zn-Cl bonds [Zn(1)-Cl(2) = 2.2940(9) Å for complex **2** and Zn(1)-Cl(2) = 2.375(2) Å for complex **3**]. Boron atom from BODIPY unit lies in the dipyrrin plane and coordinates to the adjacent fluorine atoms (B-N bond distance ~1.55 Å and B-F distance ~1.39 Å) in a typical tetrahedral fashion. The iodine atoms I(1) and I(2) from L^3 in complex **3** gave a distance of ~2.1 Å with the adjacent carbon atoms. Important intermolecular short contacts were also found to exist between Cl(2)…H(12) and F(1)…H(18) pair in complex **2** and Cl(2)…H(25) and I(1)…C(3) pair in complex **3**. The solid state structures showed the presence of a *cis*-dichlorido zinc(II) motif, while the solution conductivity measurements displayed dissociation of two chlorido ligands in aqueous DMSO.[S5]

Theoretical procedures:

Gaussian 09 software program package was utilized to find out the geometrical and electronic parameters of the ground and excited states of **1-3**. Density functional theory (DFT) was used to obtain the energy minimized structures of the complexes and B3LYP level of theory was applied for the studies.[S6] LANL2DZ basis set was chosen for iodine atoms only while 6-31G (d, p) basis set for all non-iodine atoms was selected. IEF-PCM model was also included in the study to account for the bulk solvent effect (water) on the ground state geometry and frontier molecular orbitals of the complexes **1-3**. The initial coordinates required for theoretical calculations were taken from the crystallographic parameters reported by Fernandes *et al.* for complex **1** while the initial coordinates for BODIPY containing complexes **2** and **3** were taken from the present crystallographic parameters.[S4] The calculated/optimized coordinates are provided in Tables S2-S4.

In vitro cellular experiments:

Cell culture:

HeLa (human cervical carcinoma) and MCF-7 (human breast adenocarcinoma) cells were cultured in Dulbecco's modified eagle medium (DMEM, pH = 7.4) containing 10% fetal bovine serum (FBS), 100 IU mL^{-1} of penicillin, 100 μg mL^{-1} of streptomycin and 2.0 mM of Glutamax at 37 °C in a CO_2 (5%) incubator. The adherent cultures were grown as monolayer. They were passaged once in 4–5 days by trypsinizing with 0.25% trypsin–EDTA.

Cell viability (MTT) assay:

Approximately 1×10^4 HeLa and MCF-7 cells were plated in each well of a 96-well culture plate in DMEM supplemented with 10% fetal bovine serum (10% FBS-DMEM) and cultured overnight. The MTT assay was performed using standard protocols reported earlier.[S7] Complexes **1-3** were first dissolved in 1% DMSO and then diluted in 10% FBS-DMEM medium using successive dilution technique and finally added to the cells at varying concentrations in two separate batches. Incubation was then continued for 4 h in the dark with subsequent photo-irradiation for 1 h in visible light (400-700 nm) for the light exposed batch of cells using Luzchem Photoreactor (Model LZC-1, Ontario, Canada) equipped with Sylvania make 8 white

fluorescent tubes giving an overall fluence rate of 2.4 mW cm^{-2} to provide a total dose of 10 *J* cm^{-2}. Prior to photo irradiation, the culture medium was changed to Dulbecco's phosphate buffered saline (DPBS, pH = 7.4) for this batch of cells. The light unexposed batch of cells, on the other hand, was kept in dark simultaneously for 1 h after changing the culture medium with fresh 10% FBS-DMEM. Both batches of cells were then further incubated for 19 h in culture medium. A 25 μL of MTT (4.0 mg ml^{-1} in DPBS) was then added to each well and kept for 4 h in dark. The culture medium was removed and 100 μL of HPLC grade DMSO was then added to dissolve the formazan thus formed inside viable cells. The intensity of formazan was then estimated by measuring its absorbance in DMSO at 540 nm using an ELISA microplate reader (BioRad, Hercules, CA, USA). Cytotoxicity of each sample was calculated as the percentage ratio of the absorbance of the treated cells over the untreated controls. The IC_{50} values in the dark and in light were determined using nonlinear regression analysis method by plotting "log(inhibitor) vs. normalised response (variable slope)" using GraphPad Prism version 6.[S8] The errors were calculated by taking the average of the deviation obtained by repeating the experiment three times.

Confocal microscopy experiments:

HeLa and MCF-7 cells (~4×10^4 cells per mm^2) cultured overnight on cover slips, were incubated with emissive complex **2** (concentration = 1.0 μM) for 4 h in the dark in 10% FBS-DMEM. The culture medium was then changed. Cells were then fixed with 4% paraformaldehyde for 10 min at room temperature and washed with DPBS. Cell nuclei were stained with blue emissive Hoechst 33258 dye (5 μg ml^{-1}) for 10 min at 37 °C. After washing, cells were mounted in 90% glycerol solution and sealed. Mowiol was used as an anti fade agent. Confocal microscopy images were then acquired using confocal scanning electron microscope (Leica, TCS SP5 DM6000) at 63× magnification. To detect intra-cellular localization of the complexes, HeLa and MCF-7 cells (~4×10^4 cells per square mm) were incubated similarly with 1.0 μM of complex **2** for 4 h in the dark. The cells were then stained with 0.1 μM of mitotracker red (MTR) for 30 min at 37 °C. After washing with DPBS, the cover slips with cells were mounted on slides, treated with Mowiol and sealed. The images were then captured using Leica TCS (SP5 DM6000) laser scanning confocal microscope at 63× magnification. To monitor the excitation of nuclear localizing Hoechst 33258 dye, a blue diode laser of 405 nm wavelength was

used and the resulting emission was measured at 460 nm. A 488 nm argon laser source was utilized to excite the fluorophoric BODIPY containing complex **2** (λ_{max} = 500 nm) and subsequent emission was monitored at 520 nm. Mitotracker red has absorption maxima at ~579 nm and a red Helium–Neon (He-Ne) mixed gas laser was used for the excitation followed by detection of its emission at ~599 nm. The experimental data was processed with LAS AF Lite software.

Annexin V-FITC/PI assay for apoptosis:

HeLa (~4×10^5 cells per ml) cells were incubated with photosensitizing complex **3** (0.03 μM) in 10% FBS-DMEM and kept in the dark for 4 h in two separate batches. The light exposed batch of cells was then irradiated with visible light (400-700 nm, dose 10 *J* cm^{-2}) in DPBS for 1 h and light unexposed batch of cells was kept in dark simultaneously for 1 h after changing the culture medium. The cells were then cultured for another 19 h in complete medium, harvested and washed twice with chilled DPBS at 4 °C. The cells were re-suspended in 100 μL Annexin V binding buffer (100 mM HEPES/NaOH, pH = 7.4 containing 140 mM NaCl and 2.5 mM $CaCl_2$), stained with Annexin V-FITC and propidium iodide (PI) respectively and incubated for 15 min at 37 °C in the dark. Finally, 400 μL of binding buffer was added to the HeLa cells and flow cytometric analysis was performed immediately.[S9] FACS Suite software was used to process the raw data of Annexin V-FITC/PI assay.

DCFDA assay for the detection of ROS:

HeLa cells (~1×10^6 cells per ml) were treated with the most active complex **3** (0.03 μM) in 10% FBS-DMEM for 4 h in the dark in two separate batches. Cells were then harvested by trypsinization and single cell suspensions were prepared in DPBS. The suspensions were then treated with 10 μM DCFDA solution prepared in DMSO and kept in the dark for 30 min at 37 °C. The medium was discarded and one batch of suspended cells was further incubated under dark conditions for 1 h while the other batch of cell suspension was irradiated with visible light (400-700 nm, 10 *J* cm^{-2}) source for 1 h in DPBS. Flow cytometric analysis was finally performed for the quantification of the intracellular ROS produced under different conditions.[S10] The raw data was then processed with the help of Flowing software version 2.5.1.

JC-1 assay for the detection in alteration of mitochondrial membrane potential:

HeLa cells (~2 × 10^6 cells/ml) were treated in two different batches with complex **3** (0.03 μM) for 4 h in dark in 10% FBS-DMEM medium followed by photo irradiation of the light exposed batch of cells to visible light source (400-700 nm) for 1 h in Dulbecco's phosphate buffered saline (DPBS) medium. Light unexposed cells were kept under dark conditions for 1 h also in fresh culture medium. Cells were then harvested by trypsinization and single cell suspensions (~1 × 10^6 cells/ml) were made. JC-1 dye (10 μL, 200 μM) was added to the cell suspensions to make a 2 μM final dye concentration and the incubation was continued for 15 minutes at 25° C. Cells were then washed with DPBS, re-suspended and FACS analysis was performed immediately.[S11] The raw data was processed using Cyflogic software version 1.2.1.

DNA binding, docking and cleavage experiments:

DNA binding studies by UV-vis absorption titration method:

DNA binding experiments were done for complexes **1-3** in Tris-HCl/NaCl buffer (pH = 7.2) medium and calf thymus (ct) DNA was used as the DNA source for all the studies. For the determination of intrinsic equilibrium DNA binding constant (K_b) of the complexes, UV−visible absorption titration experiments were performed where each of the complexes **1-3** (50 μM) taken in 5 mM Tris-HCl/NaCl buffer (pH = 7.2) containing 5% DMF was gradually titrated against 200 μM of ct-DNA (10 μL addition each time) and the change in absorbance was monitored at the respective absorption maxima until saturation point appeared. Binding constant values were then calculated by McGhee−von Hippel (MvH) method using the expression of Bard and co-workers.[S12] The non-linear regression analysis equation is as follows: $(\varepsilon_a - \varepsilon_f)/(\varepsilon_b - \varepsilon_f) = (b - (b^2 - 2K_b{}^2C_t[DNA]_t/s)^{1/2})/2K_bC_t$, where $b = 1 + K_bC_t + K_b[DNA]_t/2s$, ε_a is the molar extinction coefficient at a given DNA concentration, ε_f is the molar extinction coefficient of DNA unbound complex, ε_b is molar extinction coefficient of complex in fully bound form, C_t is total complex concentration, $[DNA]_t$ is the DNA concentration and s is the MvH fitting parameter. Relative fitting parameter (s) values for complexes **1-3** were also calculated using MvH method.

DNA binding studies by ethidium bromide (EB) displacement assay:

For a better understanding of the nature and mode of interaction of complexes **1-3** with ct-DNA, competitive DNA binding studies have been performed in presence of ethidium bromide (3,8-diamino-5-ethyl-6-phenylphenanthridine bromide) and complexes. Fluorescence spectral

measurements for ethidium bromide (2 µM) bound ct-DNA (100 µM) solutions were done in Tris-HCl/NaCl buffer medium (pH = 7.2). The quenching in the fluorescence intensity of DNA bound ethidium bromide was monitored at 600 nm (λ_{ex} = 546 nm) with an increasing concentration of the complexes **1**-**3** (0-60 µM). Free ethidium bromide, however, did not show any detectable emission in the Tris-HCl/NaCl buffer medium as a result of fluorescence quenching of EB by the solvent molecules. The quenching parameters were calculated using the following Stern−Volmer equation: $I_0/I = K_q[Q] + 1$; where I_0 is the emission intensity of EB-ct DNA in the absence of the quencher (complexes **1**-**3**), I is the emission intensity of EB-ct DNA in the presence of the quencher (complexes **1**-**3**), K_q is the quenching constant and [Q] represents the concentration of the quencher (complexes **1**-**3**). The apparent DNA binding constant (K_{app}) of the complexes **1**-**3** were also calculated from the equation: $K_{app} \times [complex]_{50} = K_{EB} \times [EB]$; where K_{app} is the apparent DNA binding constant of the complexes studied, $[complex]_{50}$ is the concentration of the complexes **1**-**3** when 50% quenching of ct-DNA bound ethidium bromide is observed, K_{EB} is the DNA binding constant of ethidium bromide (1.0×10^7 M^{-1}) and [EB] is the concentration of ethidium bromide (2 µM) used for the studies.

Molecular docking studies:

Molecular docking studies between complexes **1**-**3** with DNA were performed using HEX 8.0.0 software for a better understanding of the possible mode and mechanism of interactions between the complexes and DNA. This software is an interactive molecular graphics program specifically designed for interaction and docking calcultaions in order to find out the required knowledge of feasible DNA binding sites and respective binding affinities of biomolecules. B-DNA was used as the reference DNA source for docking studies and the crystal structure of B-DNA (PDB ID: 1BNA) was downloaded from the protein data bank (http://www.rcsb.org./pdb) in .pdb format. Initial coordinates of the complexes **1**-**3** for docking studies were taken from their solution phase DFT optimized structures as .mol file and converted to required .pdb format using CHIMERA 1.13.1 software. For docking calculations, default software parameters were used which are as following; correlation type-shape only, FFT mode-3D level, grid dimesion-6, receptor range-180, ligand range-180, twist range-360 and distance range-40. Finally, the results of docking studies were visualized and interpreted with the help of Discovery Studio 3.5 software.[S13]

DNA cleavage experiments:

DNA cleavage activities of the zinc(II) complexes **1**-**3** were performed with supercoiled (SC) pUC19 DNA (Plasmid, University of California, 30 μM, 0.2 μg, 2686 base-pairs) using agarose gel electrophoresis method in 50 mM Tris-HCl [tris-(hydroxymethyl)methane-HCl] buffer of pH = 7.2 containing 50 mM NaCl.[S14] To monitor relative DNA cleavage activities both in dark and under light irradiated conditions, complexes **1**-**3** in varying concentrations were incubated with DNA (1 μL) in Tris-HCl/NaCl buffer (total sample volume = 20 μL) and kept in the dark for 1 h at 37° C followed by exposure to laser light source for another 1 h or continued to be kept under dark conditions as per requirement. After the incubation period, all the samples were added to the loading buffer (0.25% bromophenol blue, 0.25% xylene cyanol, 30% glycerol, 3 μL) and then loaded on 1% agarose gel containing 1.0 μg/ml ethidium bromide. Gel electrophoresis was then carried out in a dark chamber for 2 h at 65 V in TAE (Tris-acetate EDTA) buffer (pH ~ 8.5). For DNA photo cleavage studies, the light irradiation of each sample was performed with a CW (continuous wave) diode laser (532 nm, power 100 mW, beam diameter 0.32 ± 0.02 mm, single mode, model no. EXLSR-532-100-CDRH) made of Newport Corporation, Spectra Physics Laser Division, Santa Clara, C.A, U.S.A. following standard protocols.[S14] For mechanistic studies, different additives as quenchers of singlet oxygen (NaN_3, 5 mM; TEMP, 5 mM) and scavengers of hydroxyl radicals (KI, 5 mM; catalase, 4 units) were added to the samples prior to the photolysis. To confirm the presence of singlet oxygen as the effective ROS, D_2O (4 μL) was also used as an additive where singlet oxygen lifetime is more. The final sample volume consisting most active complex **3** and different additives were made up to 20 μL using Tris-HCl/NaCl buffer. UVITEC Gel Documentation software was used to process and analyze the raw images and data of agarose gel electrophoresis experiments. The errors of calculations were found to be within 3−5% with respect to the band intensities for all experiments.

Singlet oxygen generation studies:

The qualitative and quantitative detection of singlet oxygen formed by the ligands L^2-L^3 and complexes **2**-**3** on photo irradiation were done using 400-700 nm visible light Luzchem Photoreactor (Model LZC-1, Ontario, Canada, fluence rate = 2.4 mW cm^{-2}, dose = 10 *J* cm^{-2}) and the intensity of the light source was kept constant throughout all experiments. For qualitative studies, the gradual decay in the absorption maxima of singlet oxygen scavenger diphenylisobenzofuran (DPBF) dye was monitored in presence of consant concentration of the

complexes **2** and **3** after photoirradiation for 5 sec each time.[S15] While the quantitative detection of singlet oxygen was done via titrating DPBF with a known standard Rose Bengal (RB) and ligands L^2-L^3 and complexes **2-3** separately where each photo exposure lasted for 10 sec.[S15] DPBF was used as convenient acceptor because of its ability not only to absorb in a region of dye transparency but also due to its potential for rapid scavenging of singlet oxygen to produce colourless products. This reaction happens with little or no physical quenching. For quantum yield studies, all UV-vis spectra were recorded at very low dye concentrations (optical density: 0.1–0.2 at irradiation wavelengths >500 nm) to minimize the possibility of singlet oxygen quenching by the dyes. In each measurement, the photooxidation of DPBF was monitored between 10 sec to 60 sec. No thermal recovery of DPBF (from a possible decomposition of the endoperoxide product) was observed under these experimental conditions. The quantum yields of singlet oxygen generation ($\Phi[^1O_2]$ or Φ_Δ) were calculated using the indirect method by comparing the quantum yield of the photooxidation of DPBF that was sensitized by the compound of interest to the quantum yield of Rose Bengal (RB) (Φ_Δ = 0.76 in DMSO) as a reference compound according to equation (1), where subscripts "c" and "RB" denote ligands L^2-L^3 or complexes **2-3** and Rose Bengal, respectively, Φ_Δ is the quantum yield of singlet oxygen, "m" is the slope of a plot with a difference in the change in the absorbance of DPBF (at 417 nm) with the irradiation time, and "F" is the absorption correction factor, which is given by $F=1–10^{-OD}$, where OD is the optical density at the irradiation wavelength.

$$\Phi\Delta_c = \Phi\Delta_{RB} \times (m_c/m_{RB}) \times (F_{RB}/F_c) \qquad \ldots \text{eq. (1)}$$

Schemes

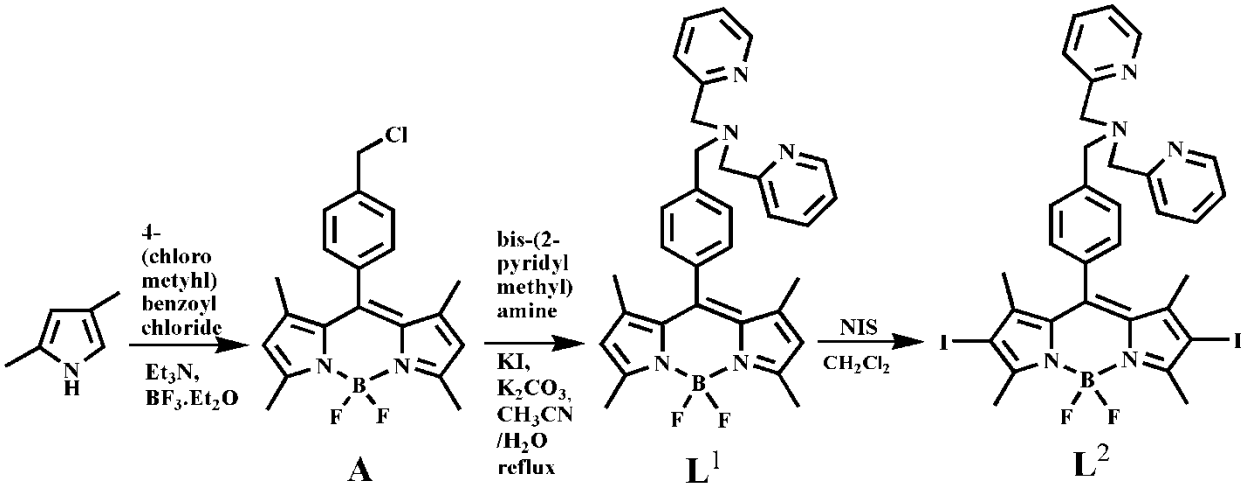

Scheme S1 Synthetic scheme for the preparation of BODIPY ligands L^2 and L^3.

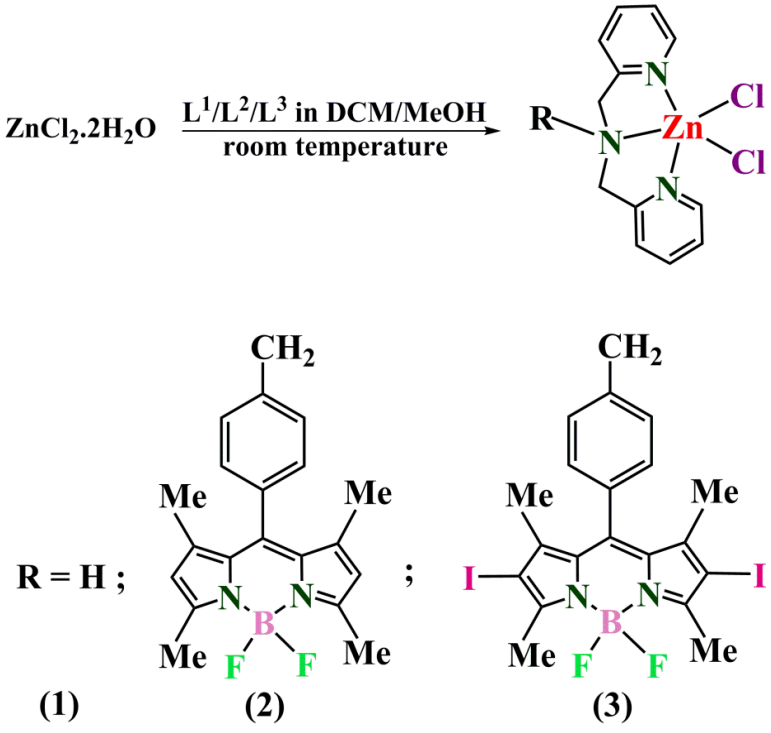

Scheme S2 General synthetic scheme for the preparation of complexes **1**-**3**.

Figures

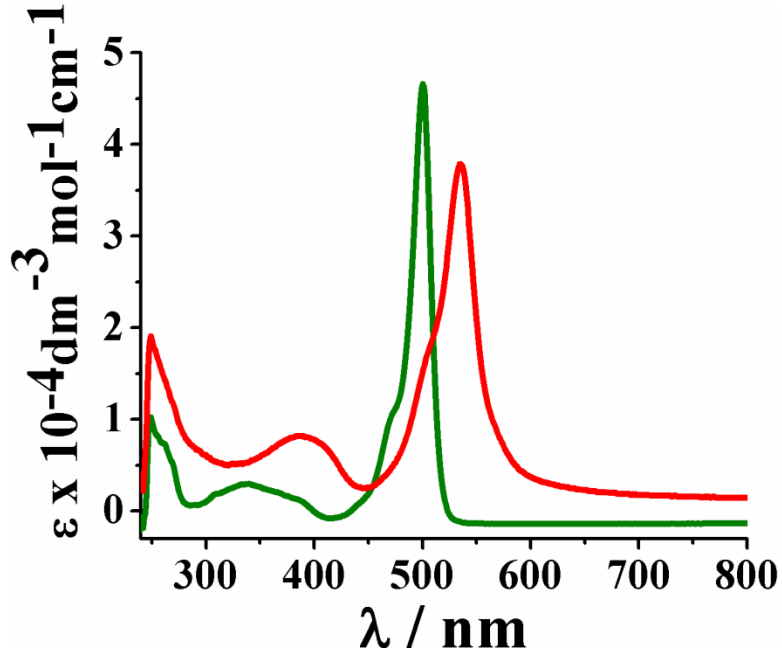

Figure S1 UV-vis absorption spectra of ligands L^2 and L^3 in 10% DMSO-DBPS buffer (pH = 7.4). Colour codes used: green, L^2 and red, L^3.

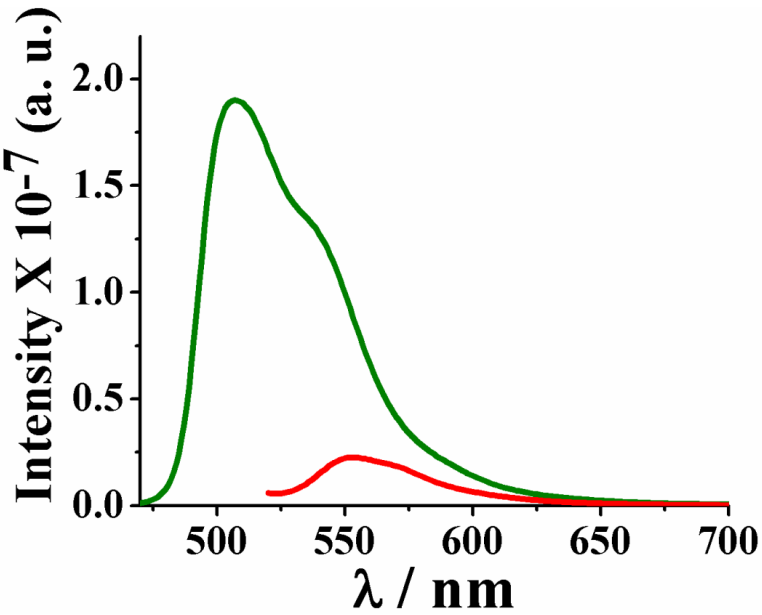

Figure S2 Emission spectra of ligands L^2 and L^3 in 10% DMSO-DPBS buffer (pH = 7.4). Colour codes used: green, L^2 and red, L^3. λ_{ex} for L^2 = 450 nm and for L^3 = 500 nm, where λ_{ex} is the excitation wavelength used for emission studies.

(a)

Ligand L^1

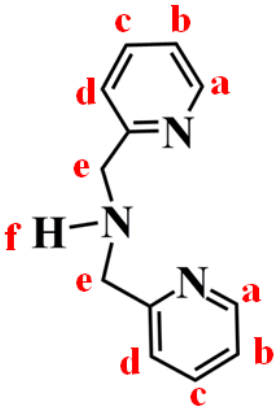

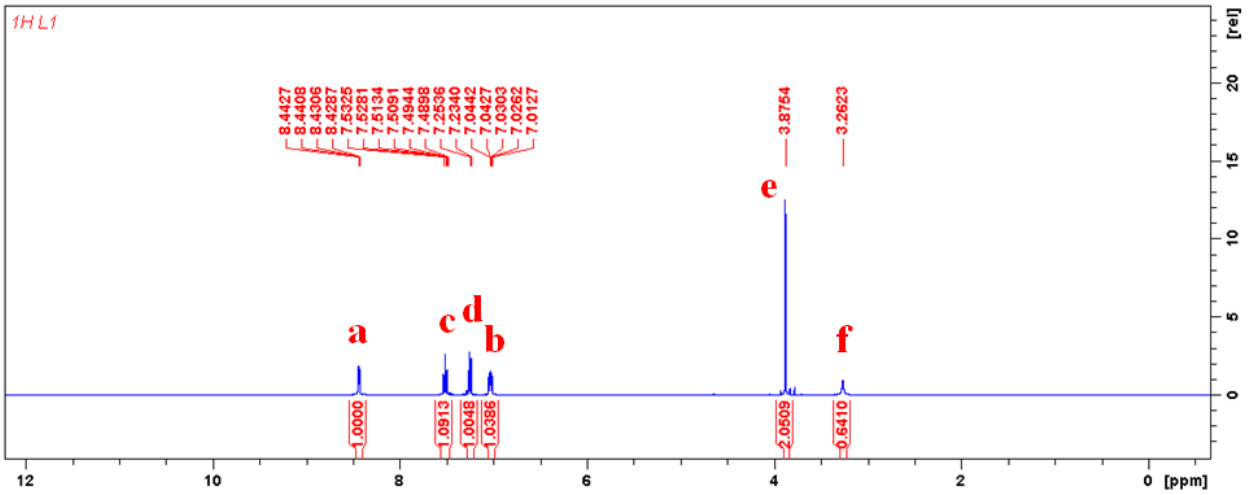

(b)

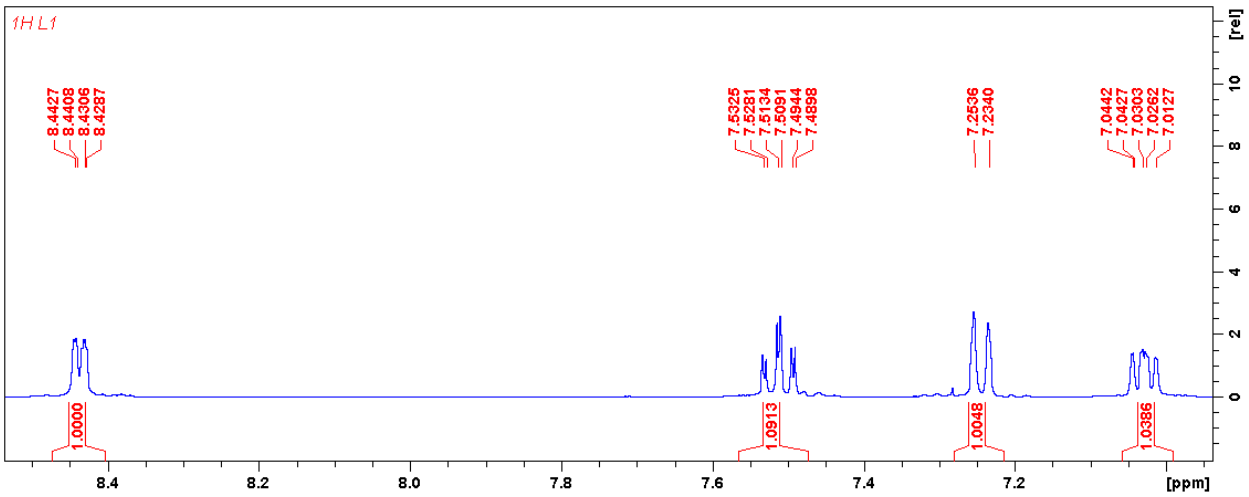

Figure S3 (a) ^{1}H NMR spectrum of ligand L^1 in $CDCl_3$ and **(b)** showing the expanded aromatic region.

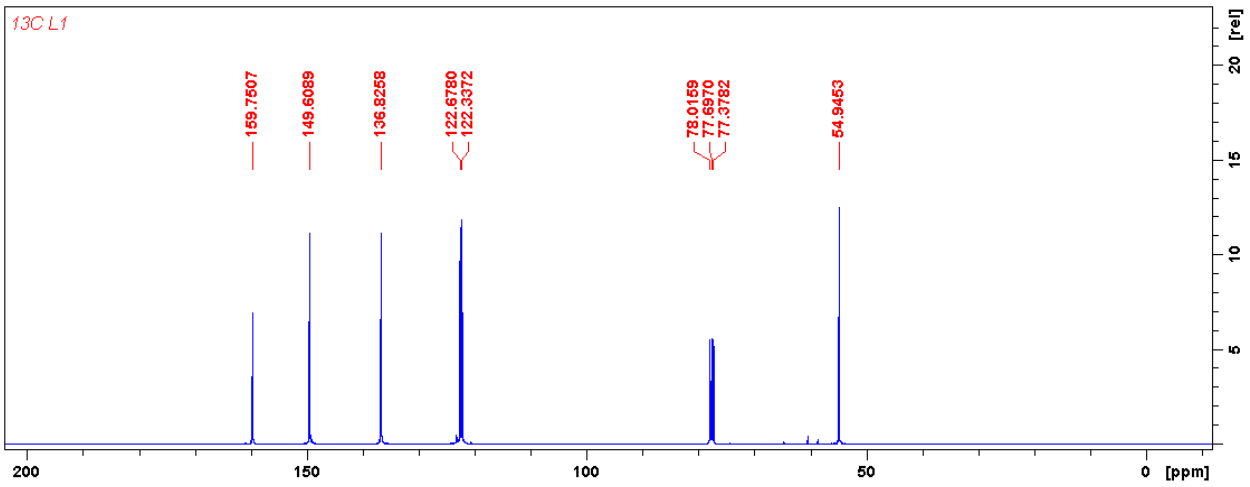

Figure S4. ^{13}C NMR spectrum of ligand L^1 in $CDCl_3$.

(a)

Ligand L^2

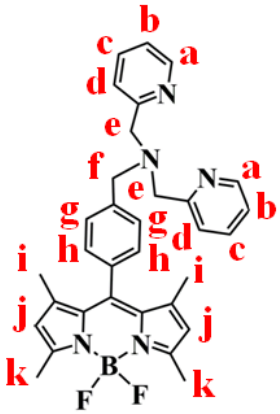

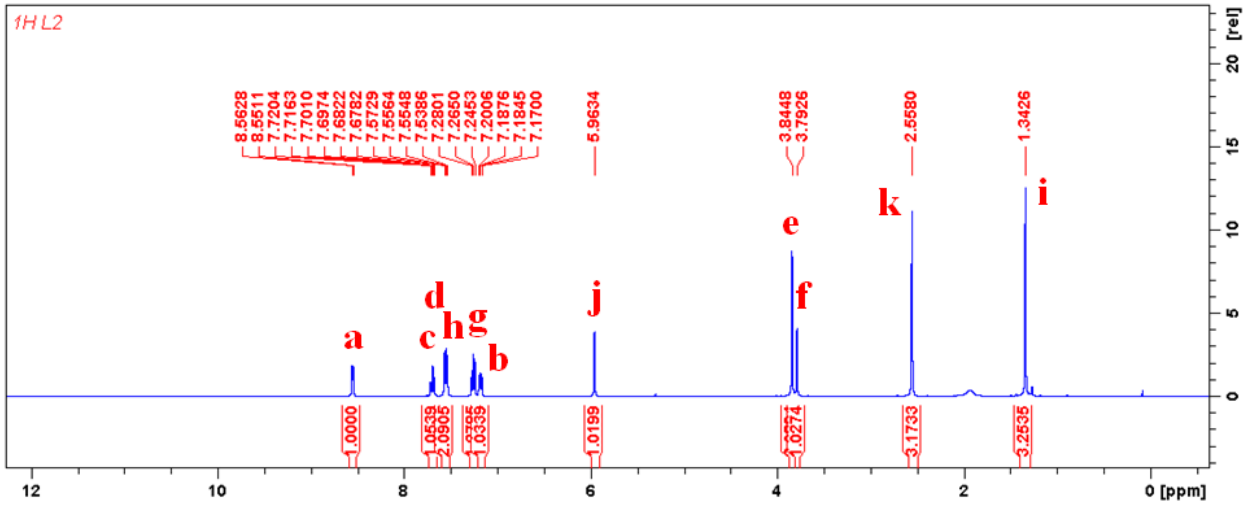

(b)

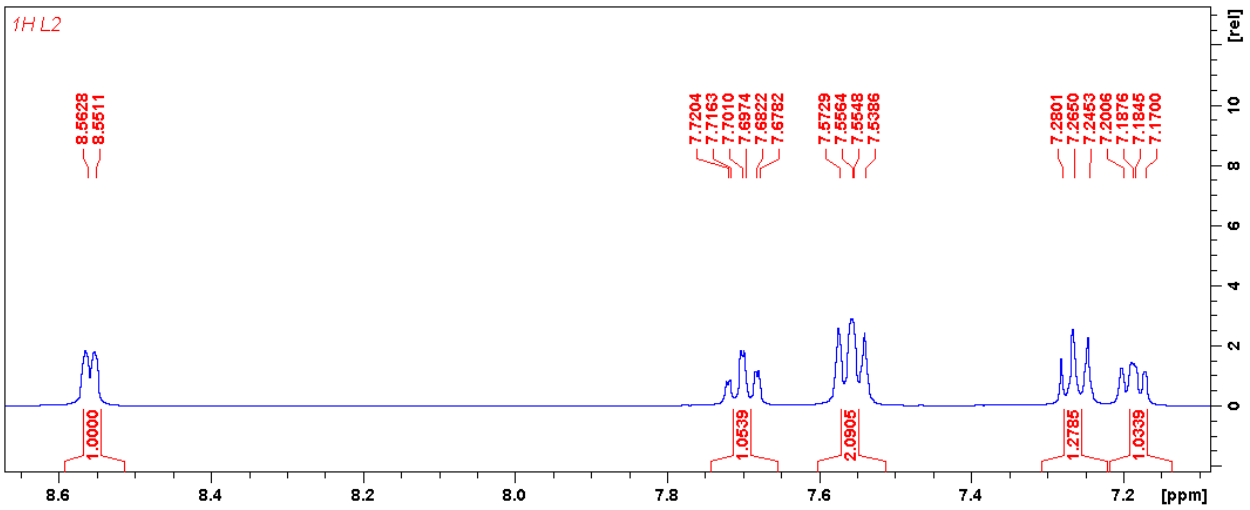

Figure S5 (a) ^{1}H NMR spectrum of ligand L^{2} in $CDCl_3$ and **(b)** showing the expanded aromatic region.

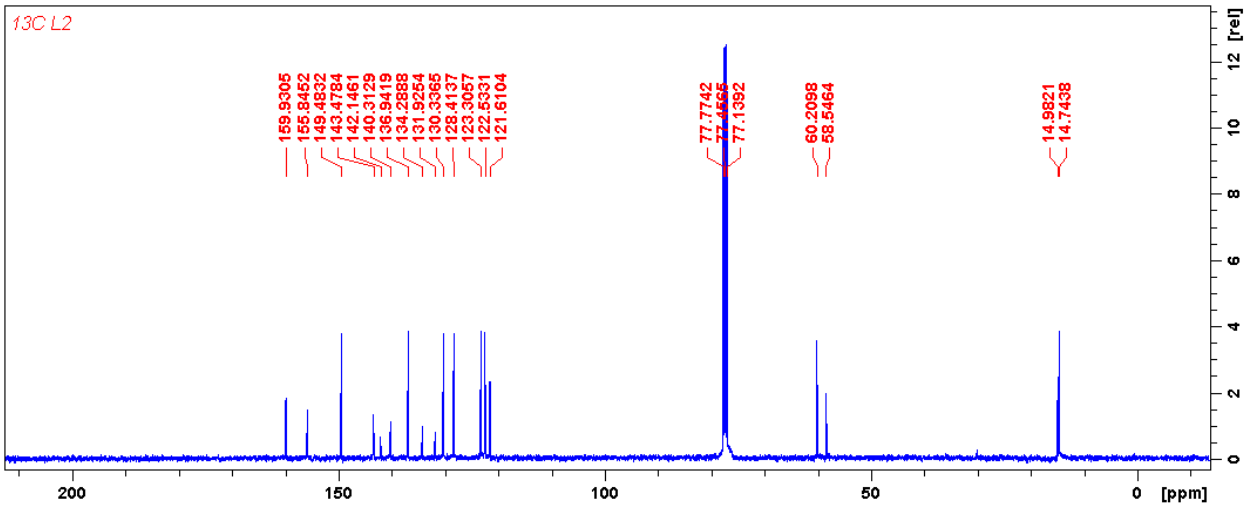

Figure S6 ^{13}C NMR spectrum of ligand L^{2} in $CDCl_3$.

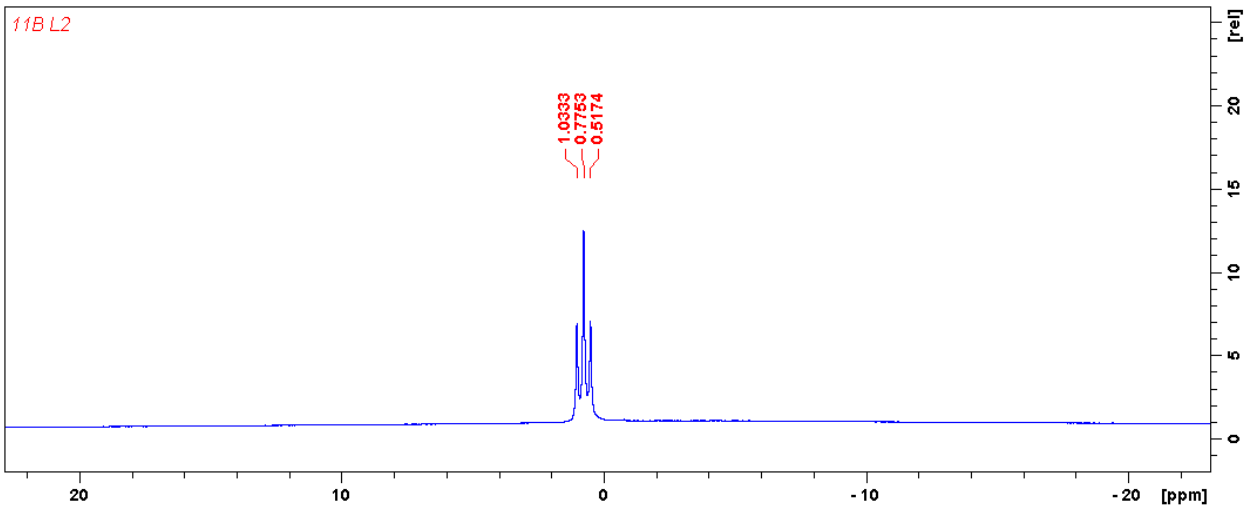

Figure S7 ^{11}B NMR spectrum of ligand L^2 in $CDCl_3$.

(a)

Ligand L^3

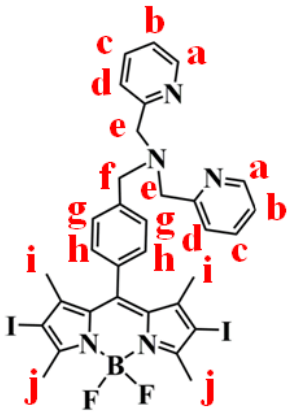

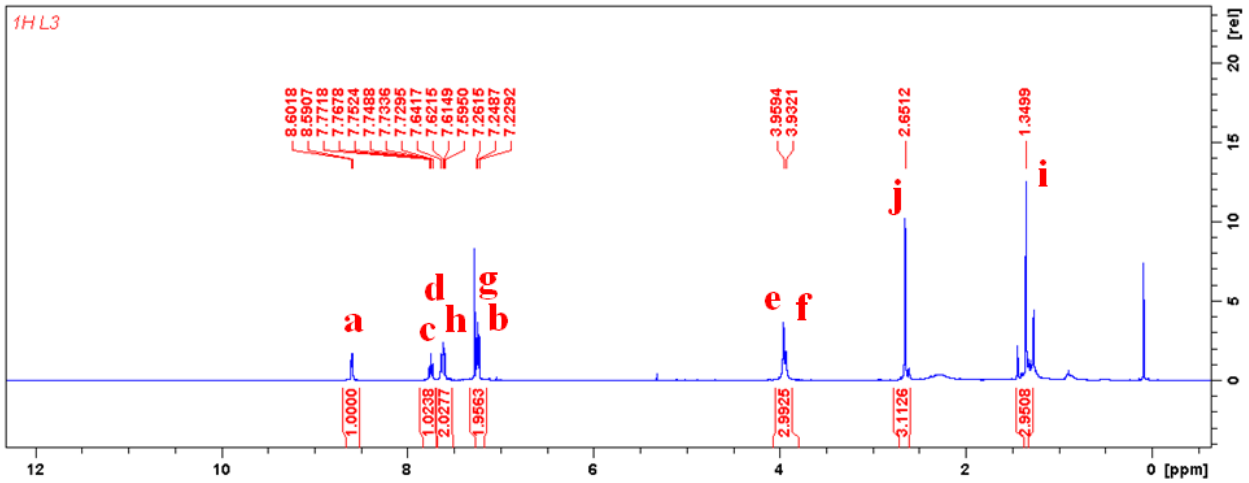

(b)

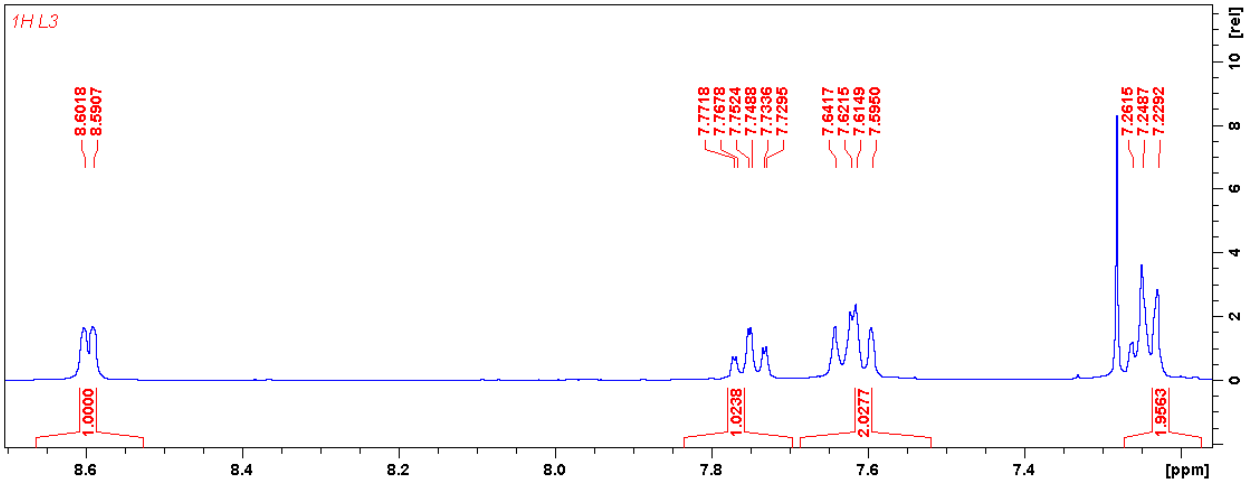

Figure S8 (a) ^{1}H NMR spectrum of ligand L^{3} in $CDCl_3$ and **(b)** showing the expanded aromatic region.

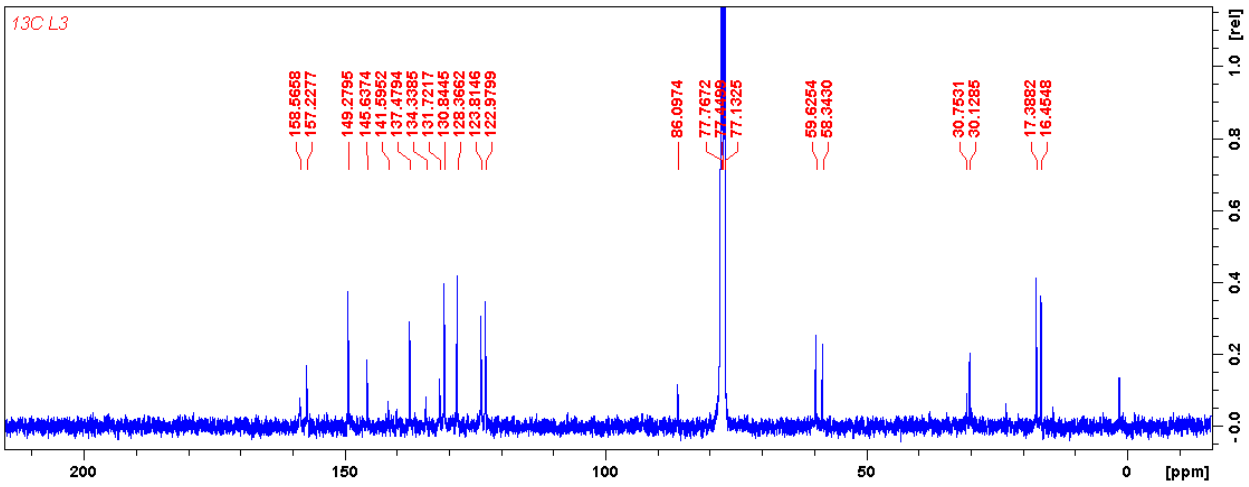

Figure S9 ^{13}C NMR spectrum of ligand L^{3} in $CDCl_3$.

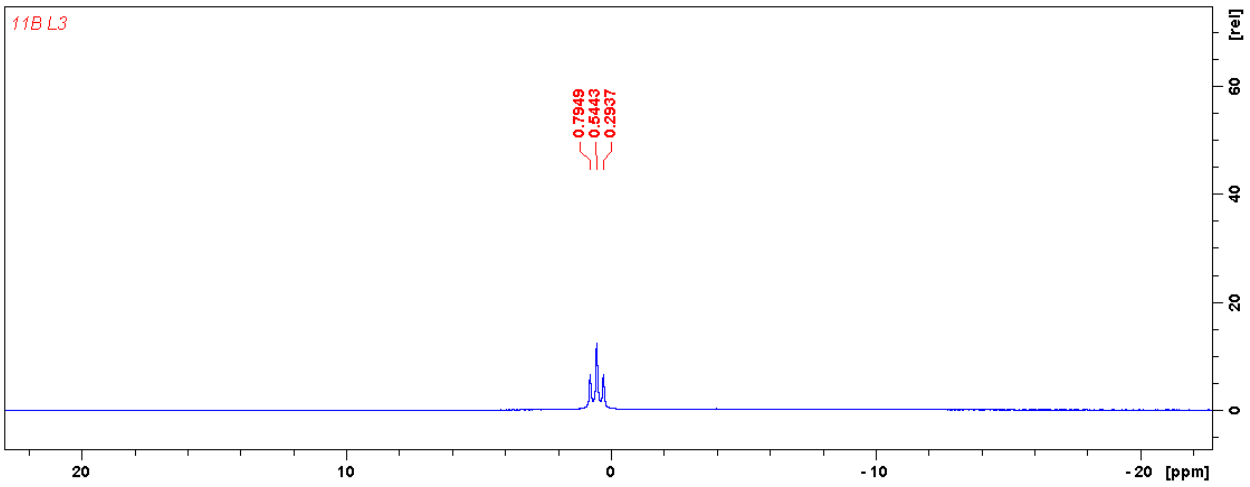

Figure S10 ^{11}B NMR spectrum of ligand L^3 in $CDCl_3$.

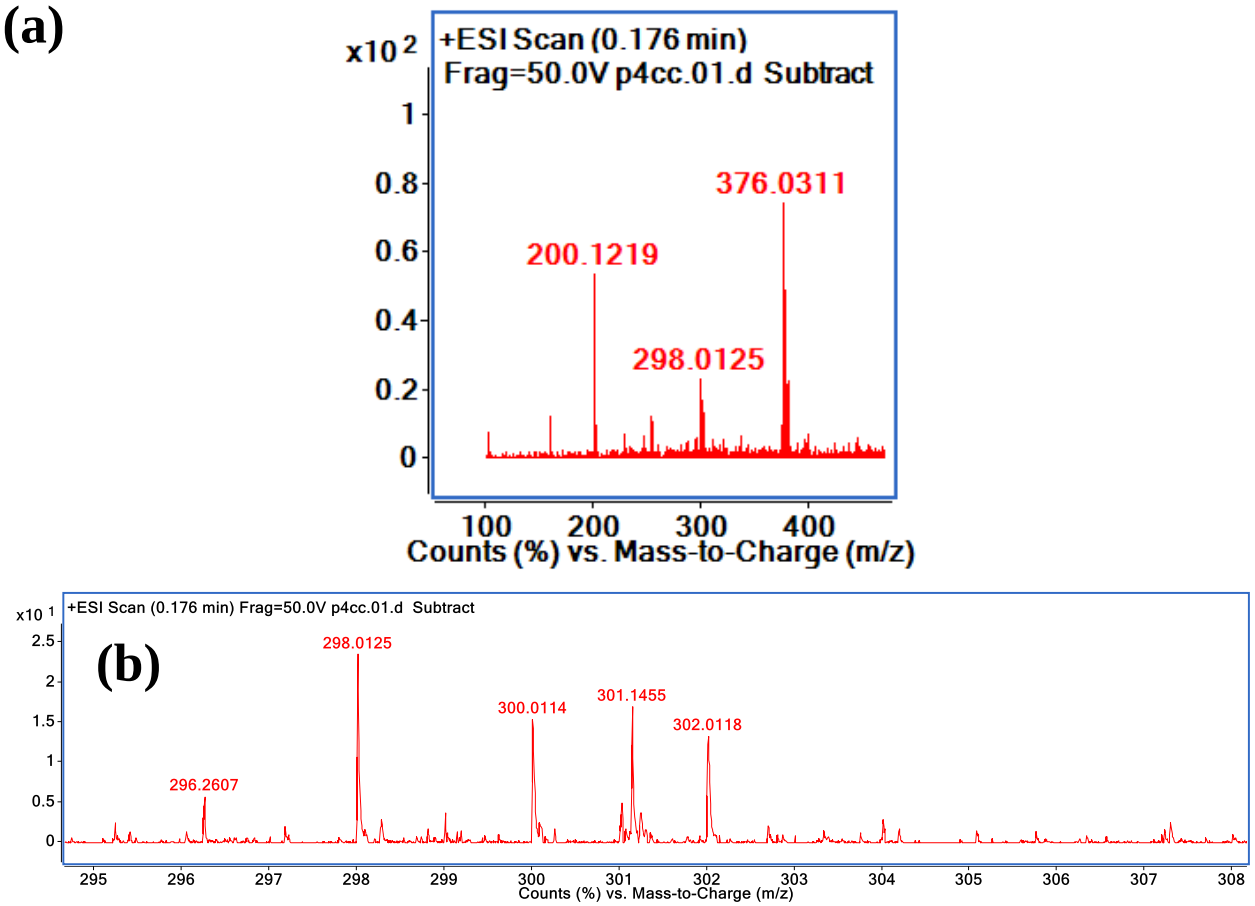

Figure S11 (a) ESI-MS spectrum of complex **1** recorded in acetonitrile (major peaks appeared at m/z 298.0125 for $[\mathbf{1} - Cl]^+$, at m/z 200.1219 for $[L^1 + H]^+$ and at m/z 376.0311 for $[\mathbf{1} + CH_3CN]^+$) and **(b)** showing the isotopic distribution pattern.

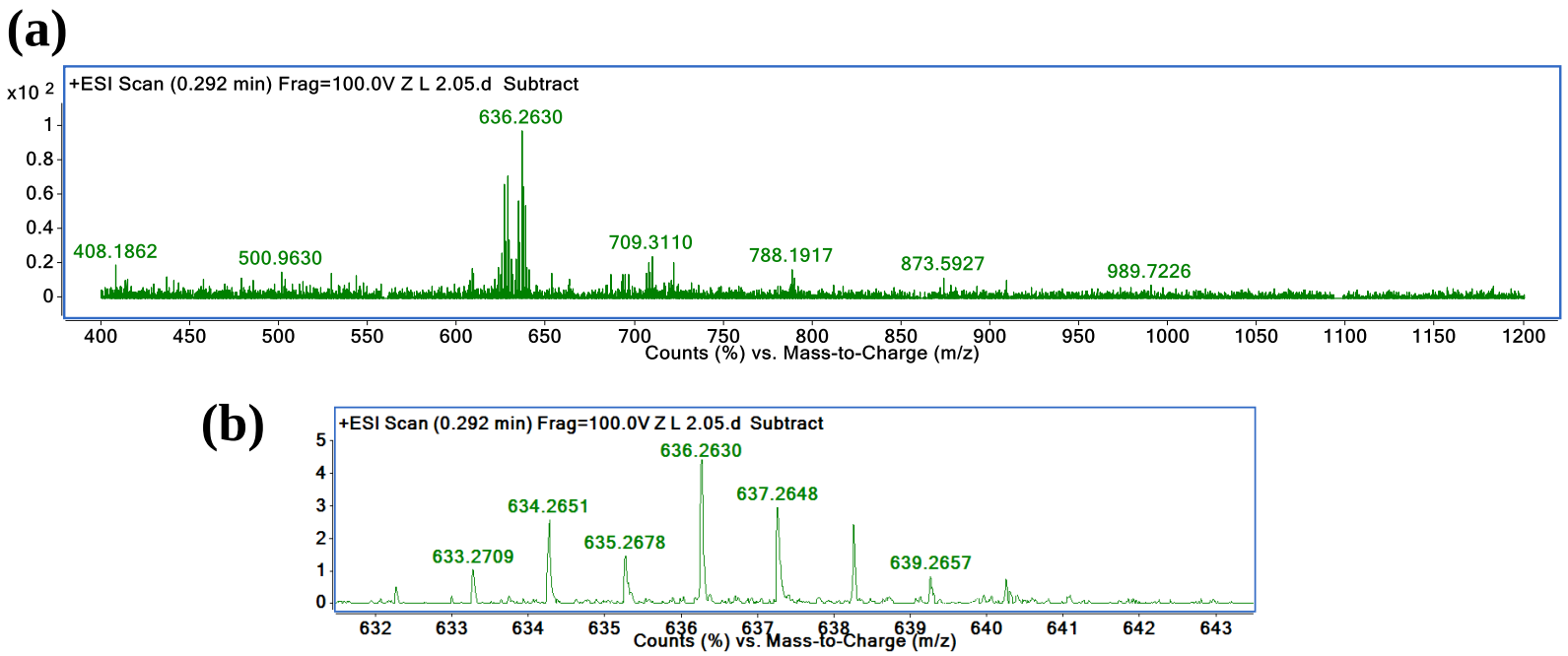

Figure S12 (a) ESI-MS spectrum of complex **2** recorded in acetonitrile (Base peak appeared at m/z 636.2630 for $[\mathbf{2} - Cl]^{+}$) and **(b)** showing the isotopic distribution pattern.

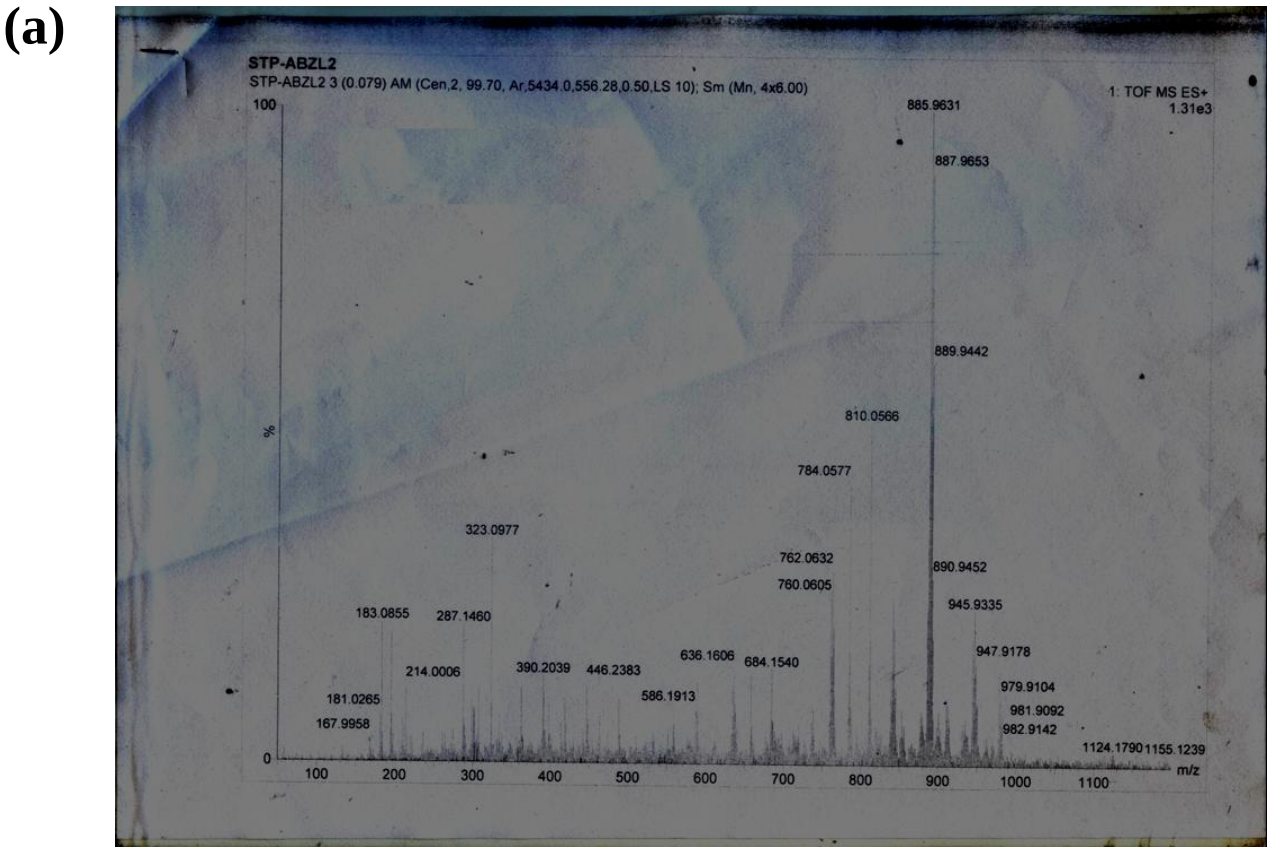

(b)

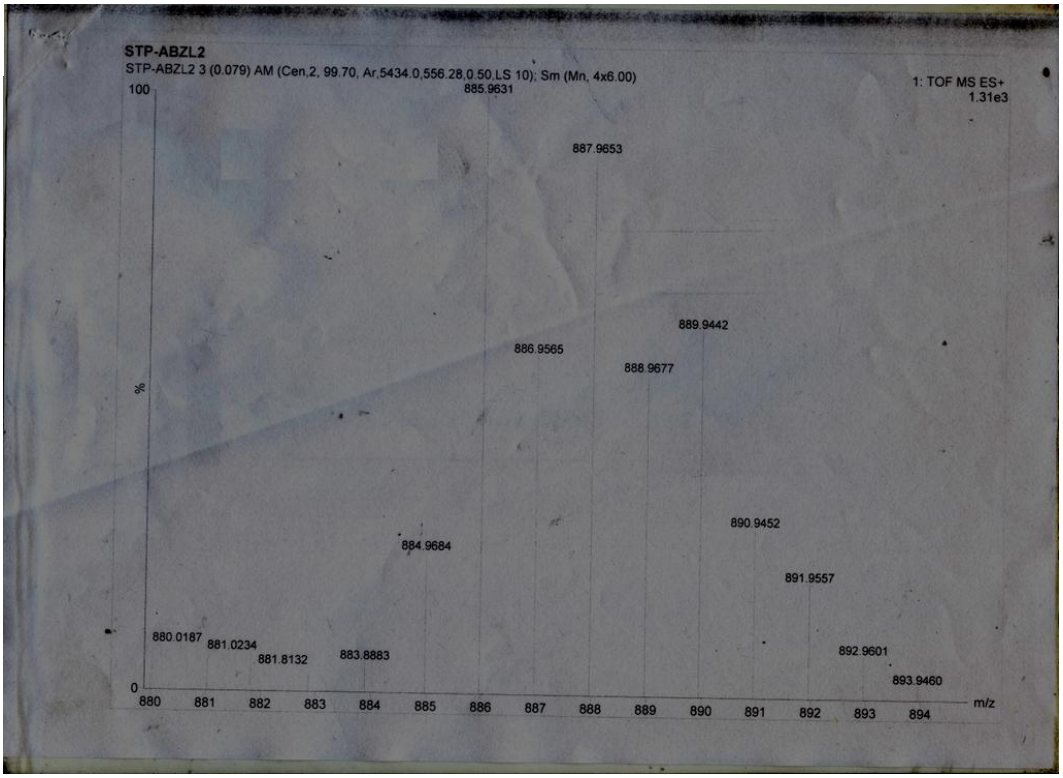

Figure S13 (a) ESI-MS spectrum of complex **3** recorded in MeOH (base peak appeared at m/z 885.9631 for [**3** – Cl]$^{+}$) and **(b)** showing the isotopic distribution pattern (major peaks appeared at m/z 884.9684, 885.9631, 886.9565, 887.9653, 888.9677, 889.9442, 890.9452, 891.9557 etc.)

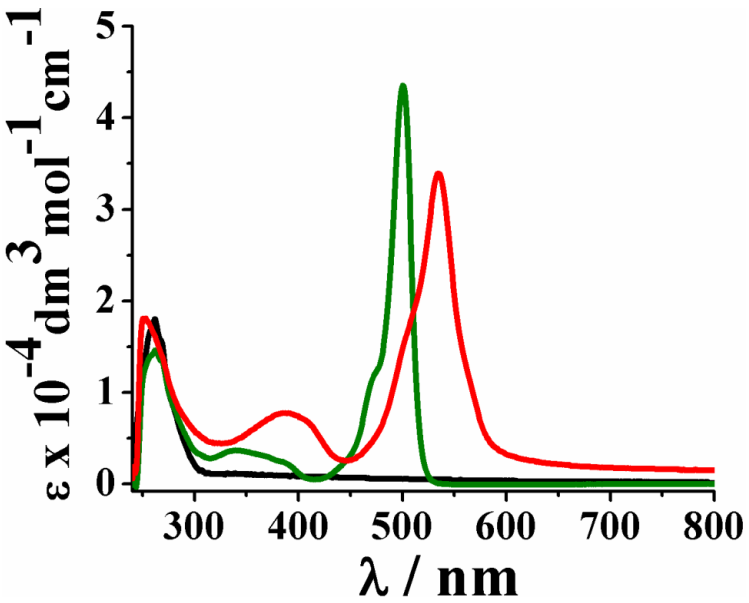

Figure S14 UV-vis absorption spectra of complexes **1**-**3** in 1.0% DMSO-DBPS buffer (pH = 7.4). Colour codes used: black, complex **1**, green, complex **2** and red, complex **3**.

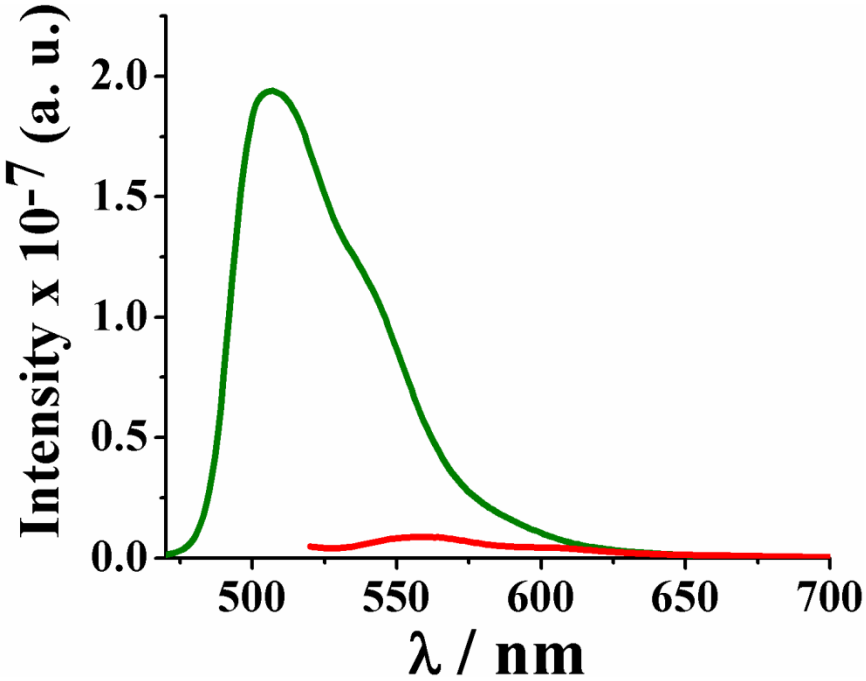

Figure S15 Emission spectra of complexes **2**, **3** in 1.0% DMSO-DPBS buffer (pH = 7.4). Colour codes used: green, complex **2** and red, complex **3** [λ_{ex} for complex **2** = 450 nm and for complex **3** = 500 nm; λ_{ex}, the excitation wavelength used for emission studies].

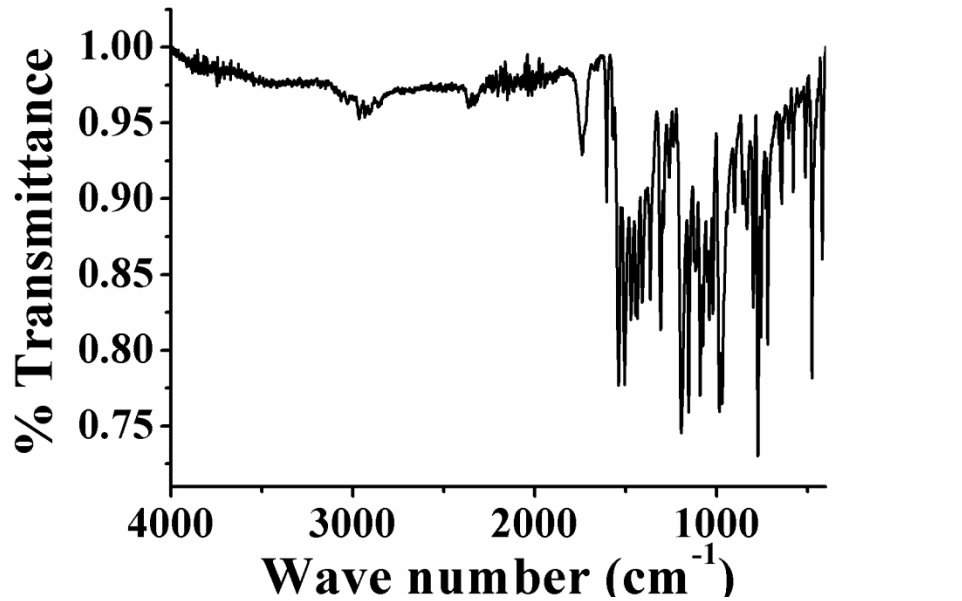

Figure S16 FTIR spectrum of complex **2**.

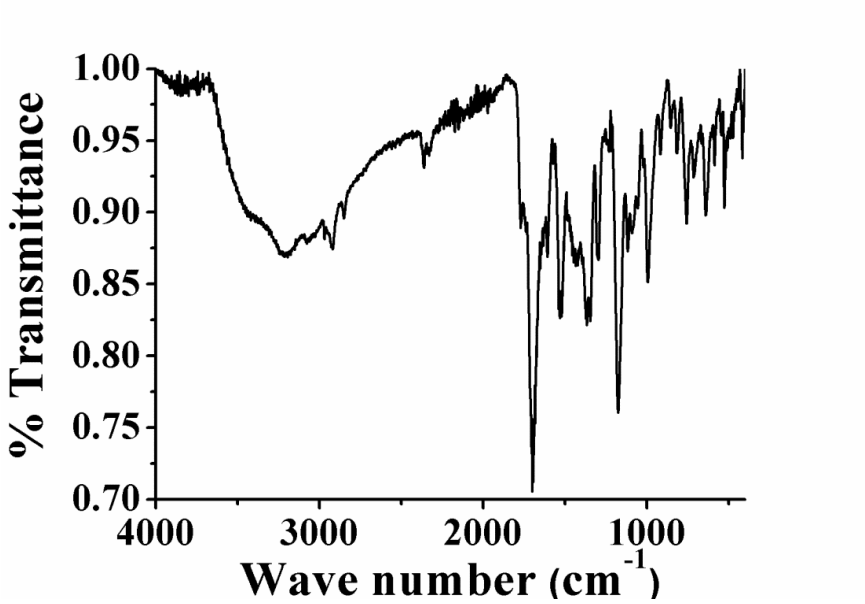

Figure S17 FTIR spectrum of complex **3**.

(a)

Complex 1

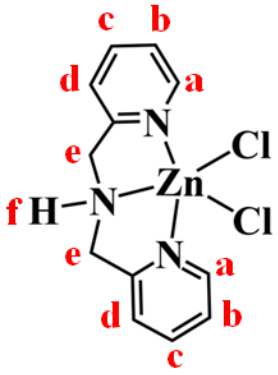

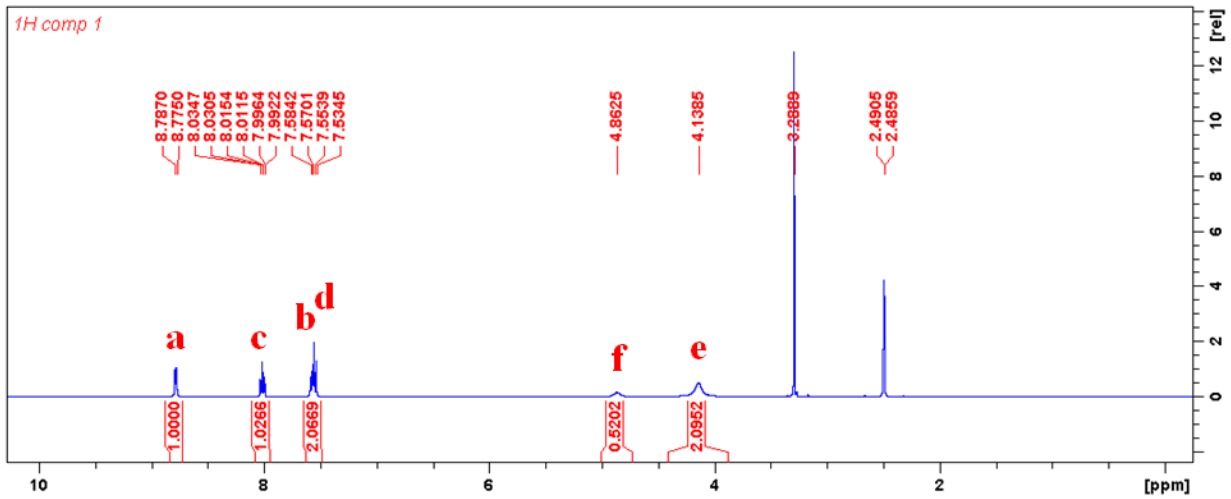

(b)

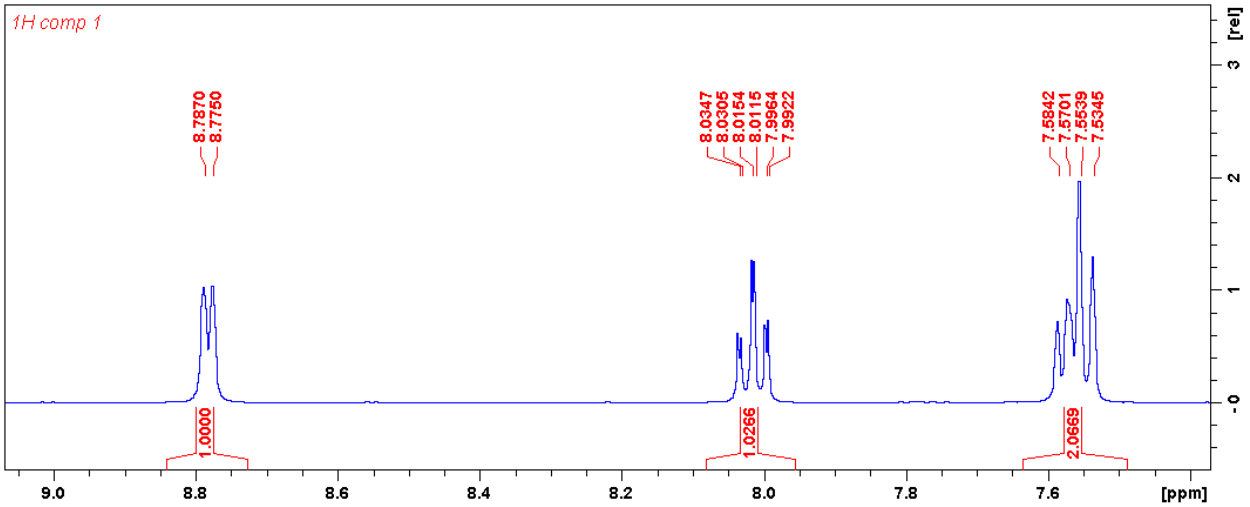

Figure S18 (a) ^{1}H NMR spectrum of complex **1** in DMSO-D_6 and (b) showing the expanded aromatic region.

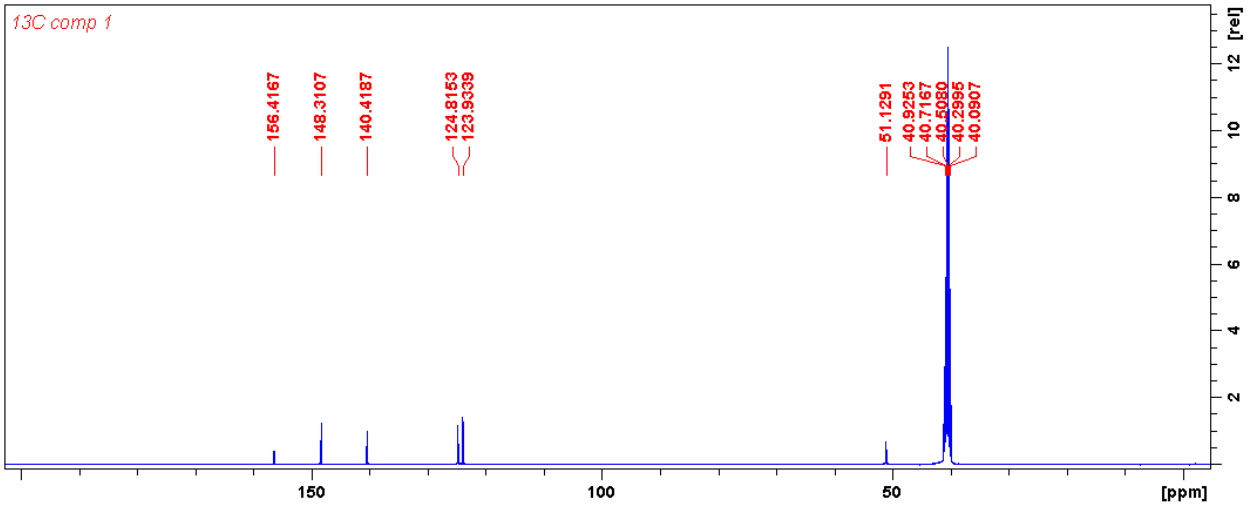

Figure S19 ^{13}C NMR spectrum of complex **1** in DMSO-D_6.

(a)

Complex 2

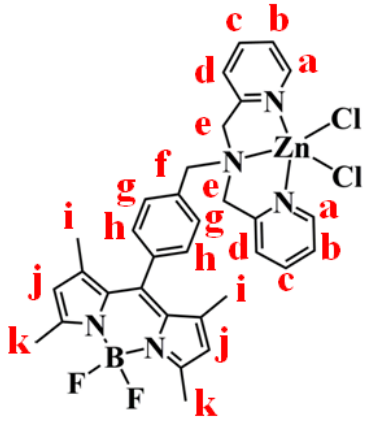

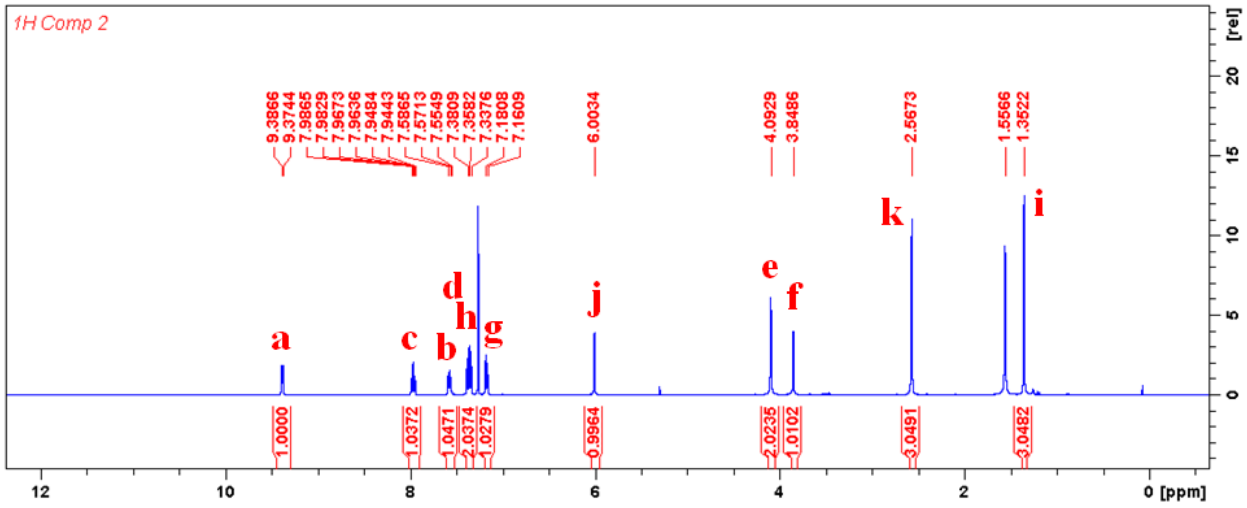

(b)

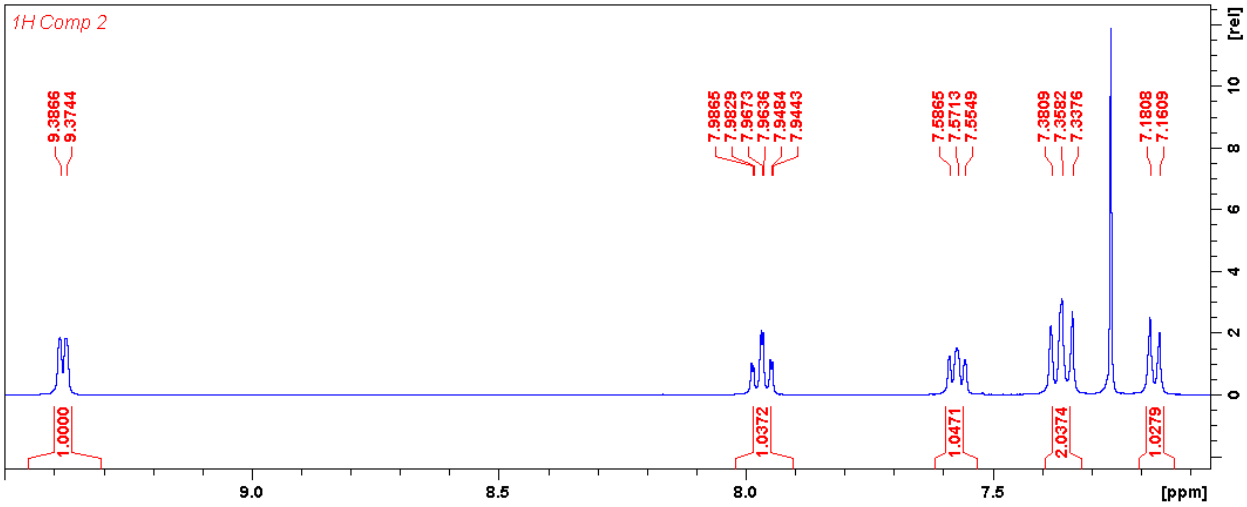

Figure S20 (a) ^{1}H NMR spectrum of complex **2** in $CDCl_3$ and **(b)** showing the expanded aromatic region.

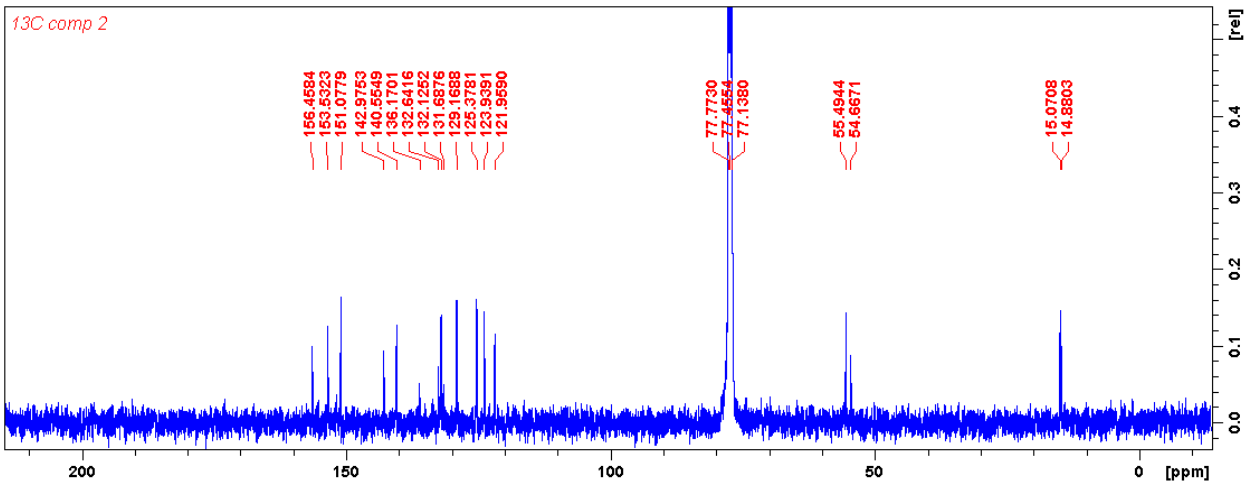

Figure S21 ^{13}C NMR spectrum of complex **2** in $CDCl_3$.

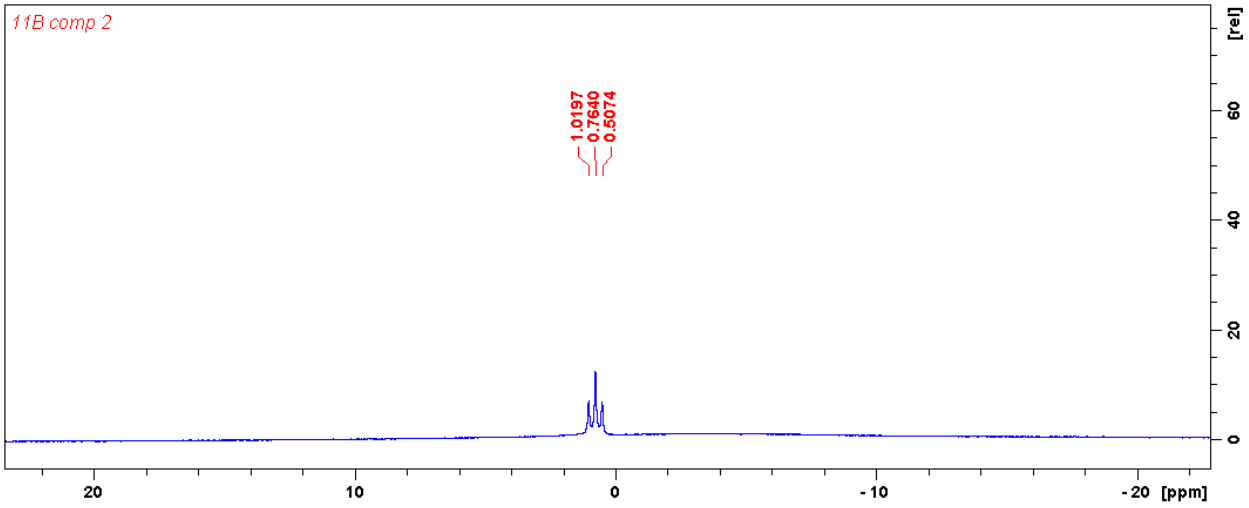

Figure S22 ^{11}B NMR spectrum of complex **2** in $CDCl_3$.

(a)

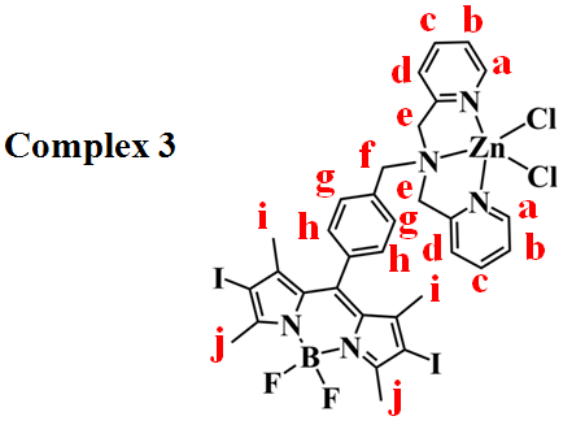

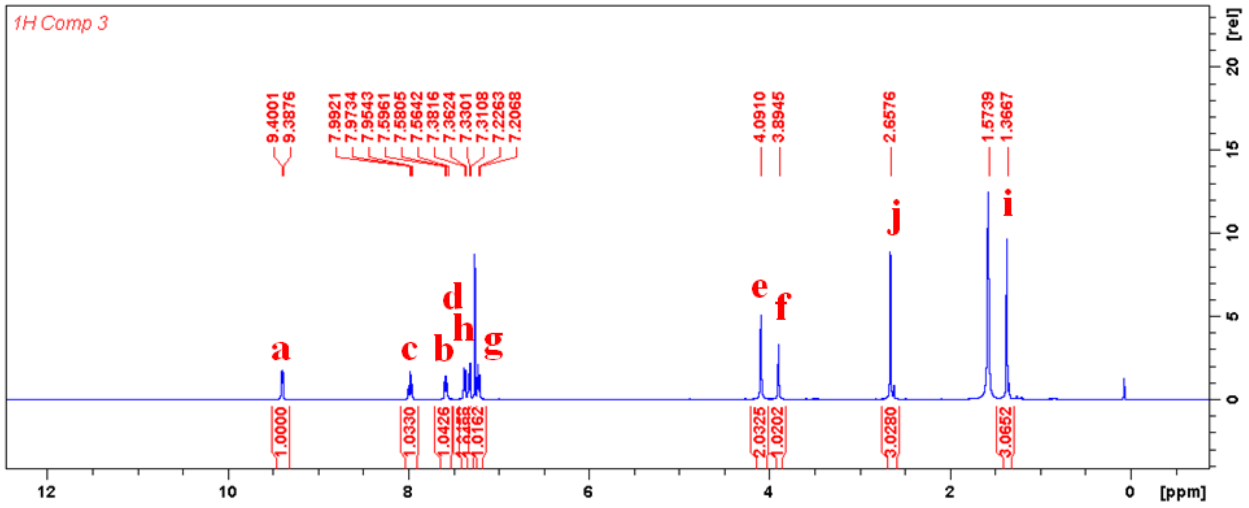

(b)

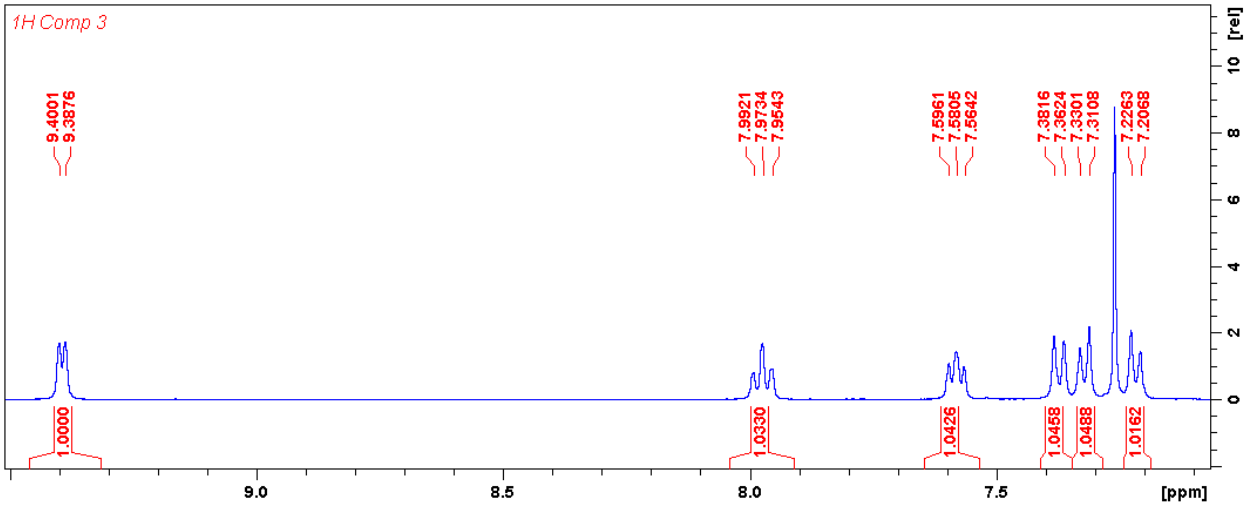

Figure S23 (a) ^{1}H NMR spectrum of complex **3** in $CDCl_3$ and **(b)** showing the expanded aromatic region.

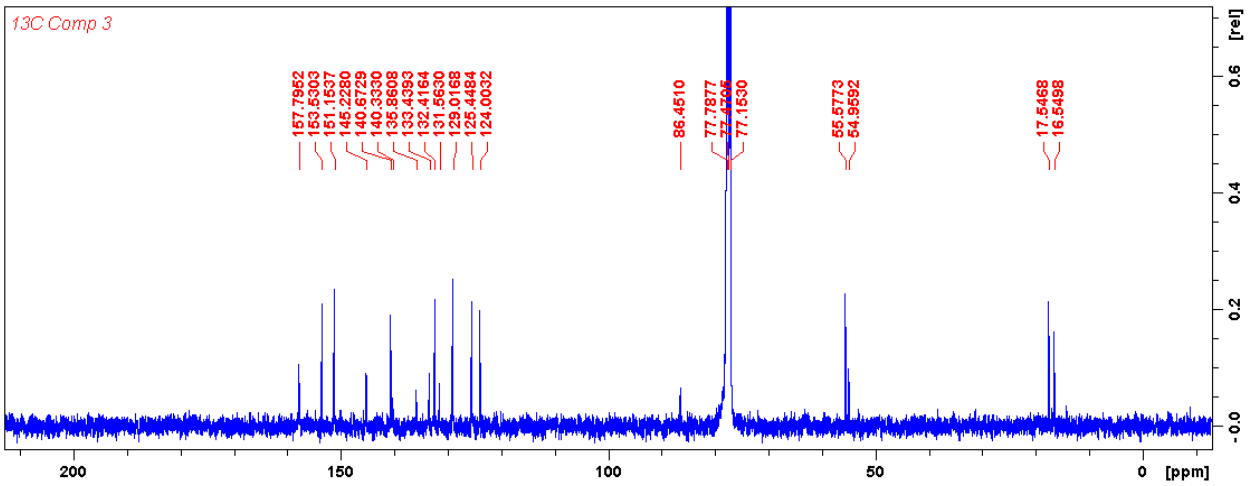

Figure S24 ^{13}C NMR spectrum of complex **3** in $CDCl_3$.

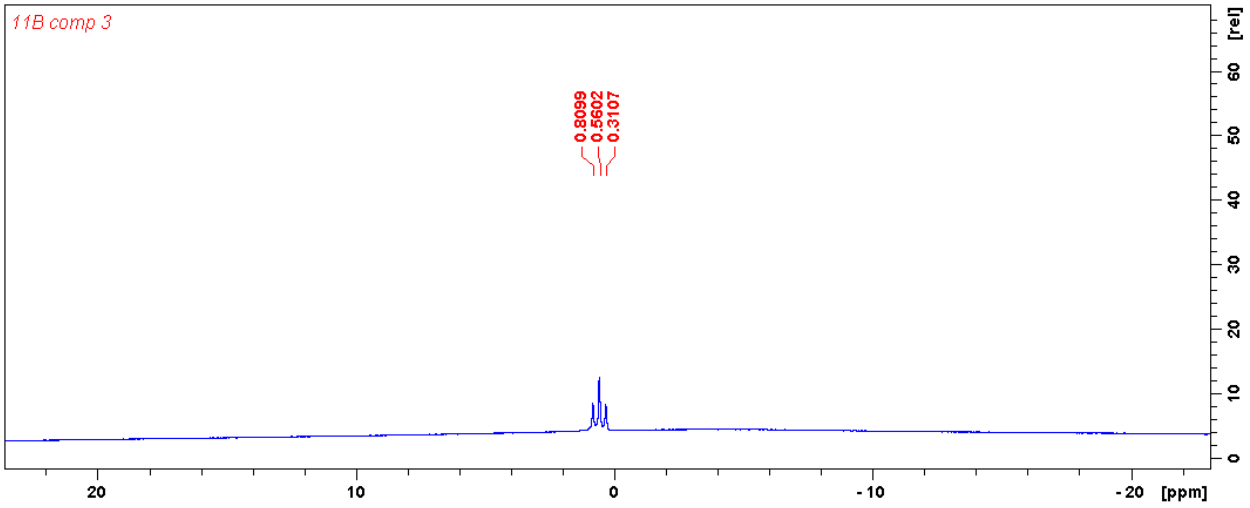

Figure S25 ^{11}B NMR spectrum of complex **3** in $CDCl_3$.

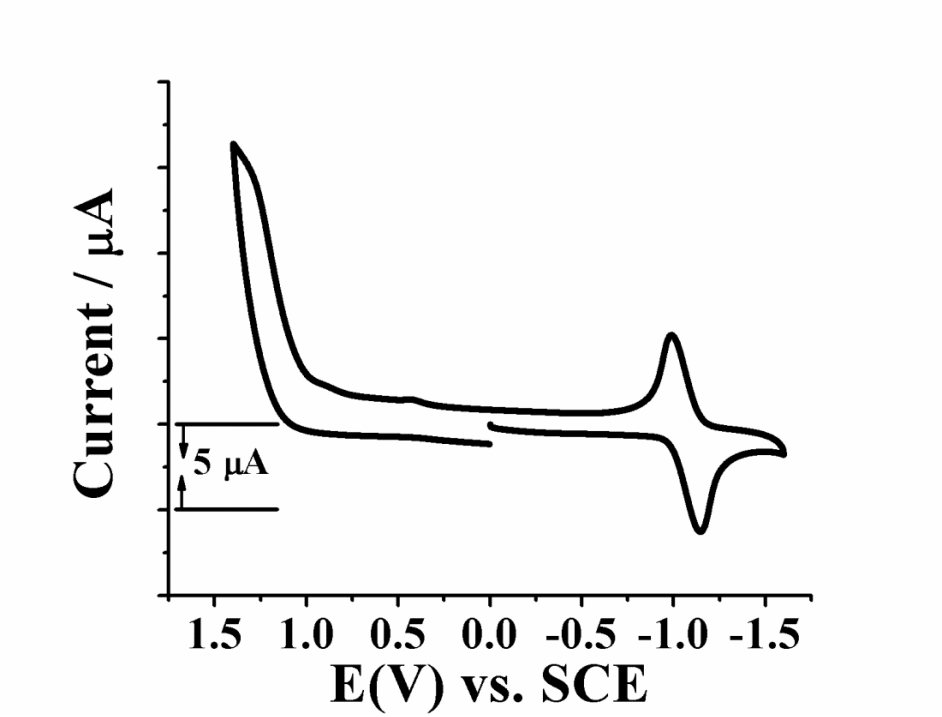

Figure S26 Cyclic voltammogram of complex **2** recorded in DMF-0.1M TBAP. Sample concentration = 2.0 mmol, scan rate = 50 mV s^{-1}, scan direction was cathodic.

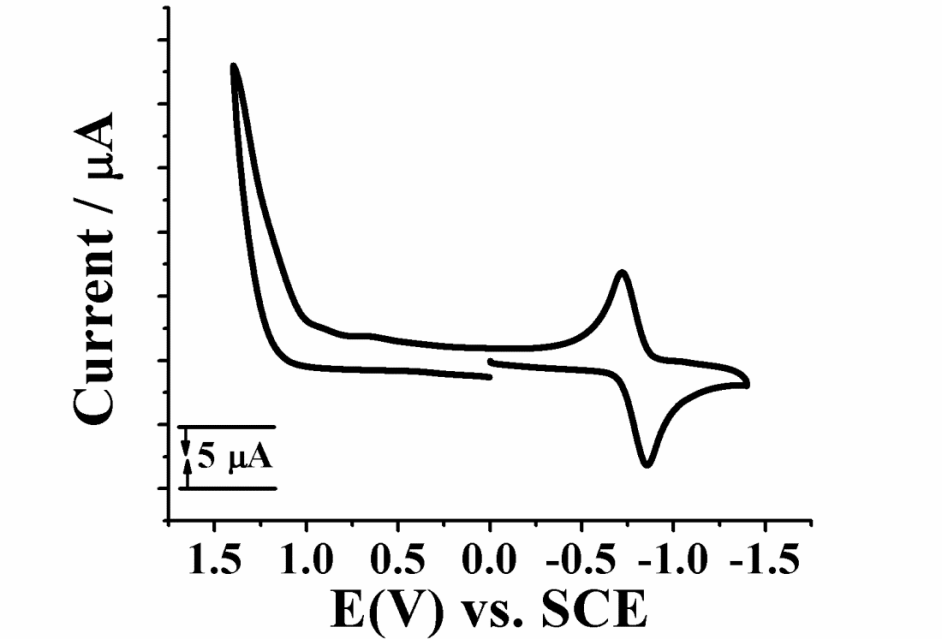

Figure S27 Cyclic voltammogram of complex **3** recorded in DMF-0.1M TBAP. Sample concentration = 2.0 mmol, scan rate = 50 mV s^{-1}, scan direction was cathodic.

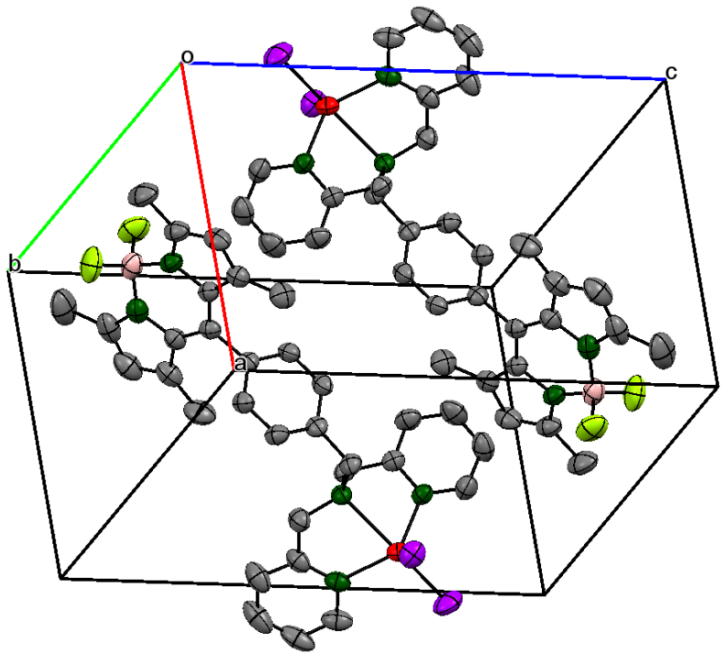

Figure S28 Unit cell packing diagram of complex **2**. Hydrogen atoms are not shown for clarity. Color codes used: red, zinc; deep green, nitrogen; violet, chlorine; gray, carbon; pink, boron, and light green, fluorine.

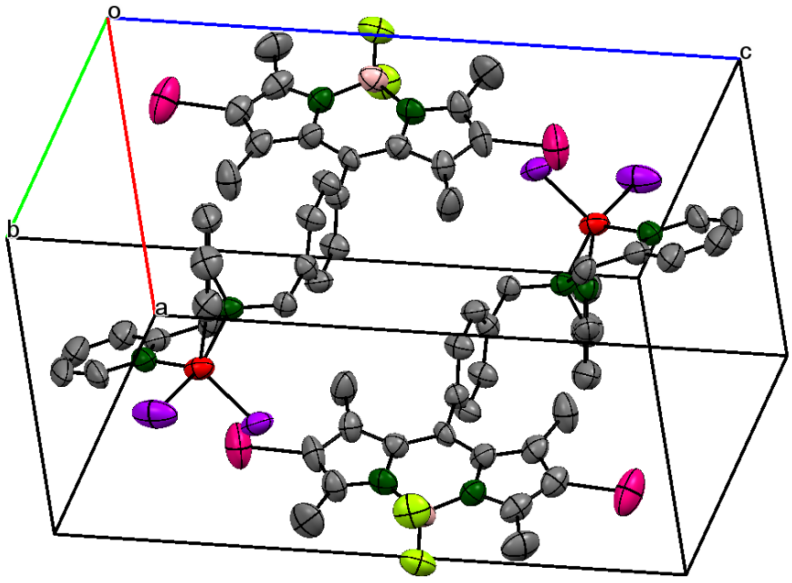

Figure S29 Unit cell packing diagram of complex **3**. Hydrogen atoms are not shown for clarity. Color codes used: red, zinc; deep green, nitrogen; violet, chlorine; gray, carbon; pink, boron, light green, fluorine and purple, iodine.

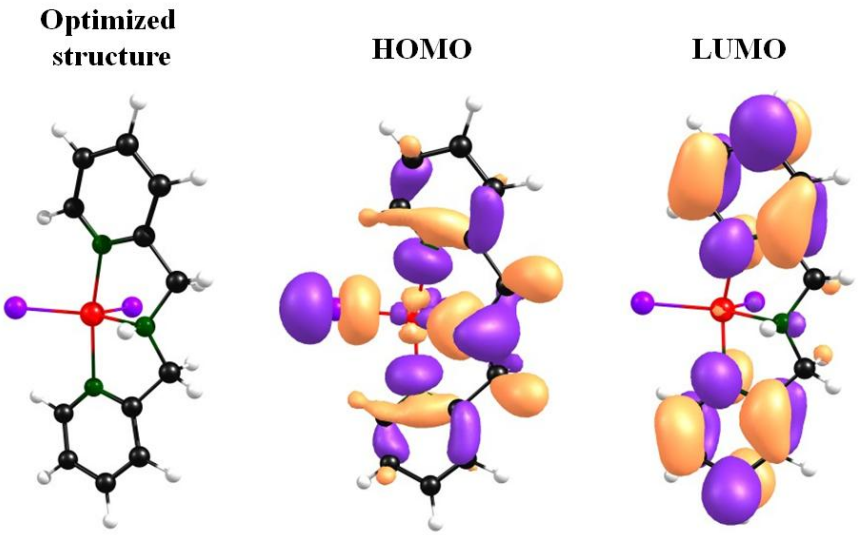

Figure S30 Optimized structure of control complex **1** and their frontier molecular orbitals Colour codes used: red, zinc; deep green, nitrogen; violet, chlorine; black, carbon and light gray, hydrogen.

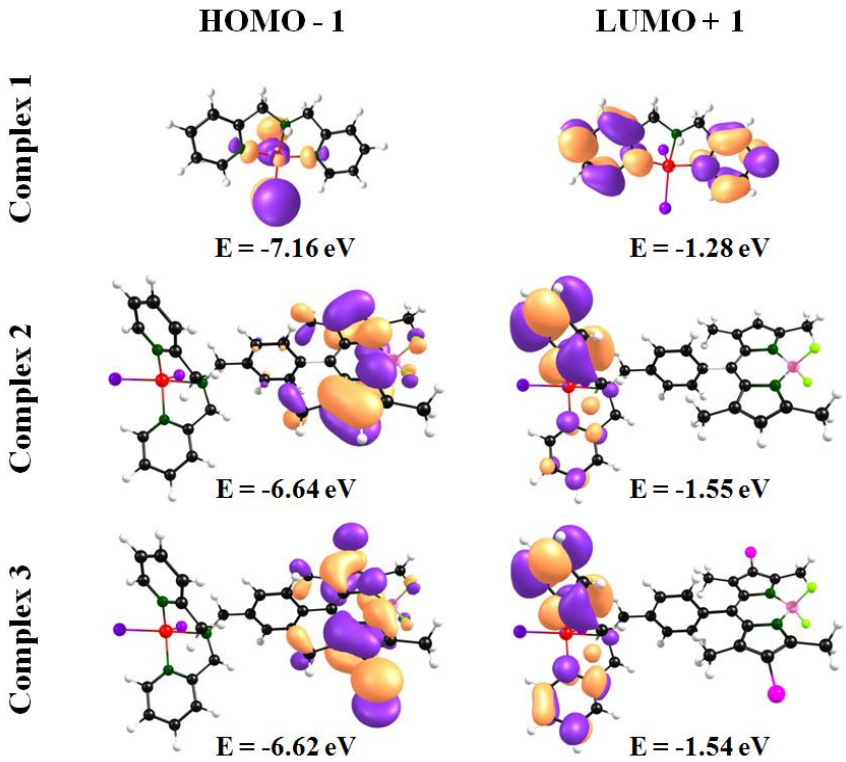

Figure S31 Optimized structures of complexes **1-3** showing the HOMO–1 and LUMO+1 molecular orbitals. Colour codes used: red, zinc; deep green, nitrogen; violet, chlorine; black, carbon; pink, boron; light green, fluorine; purple, iodine and light gray, hydrogen.

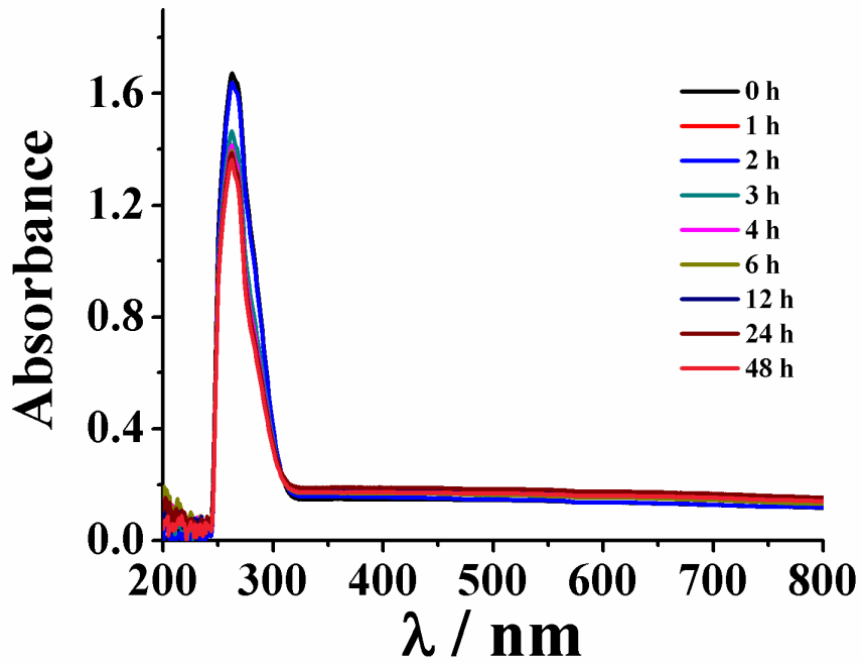

Figure S32 Time dependent absorption spectra of complex **1** in 10% DMSO-DPBS buffer (pH = 7.4) measured up to 48 h at 37 ° C to verify the stability of the complex in biological media under dark conditions.

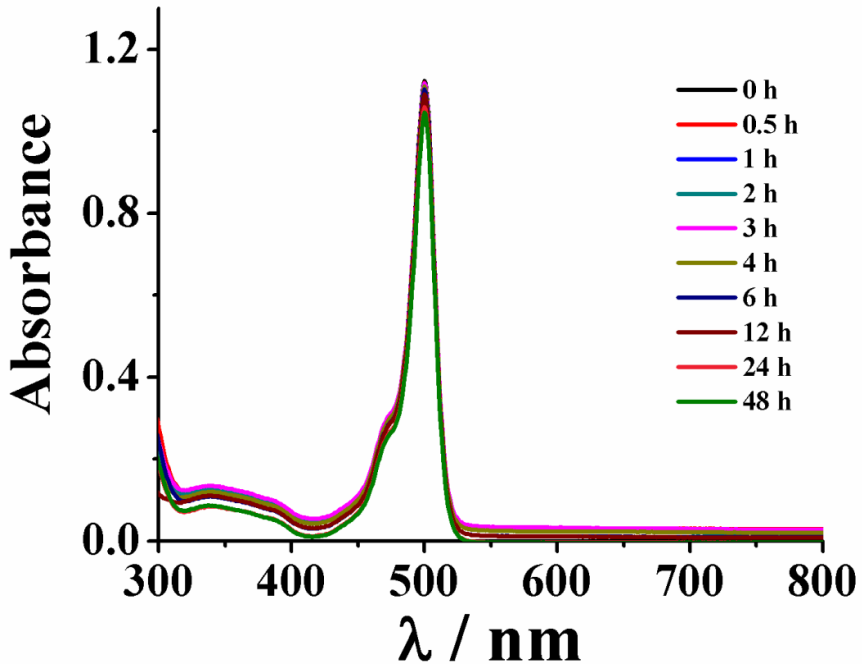

Figure S33 Time dependent absorption spectra of complex **2** in 10% DMSO-DPBS buffer (pH = 7.4) measured up to 48 h at 37° C to verify the stability of the complex in biological media under dark conditions.

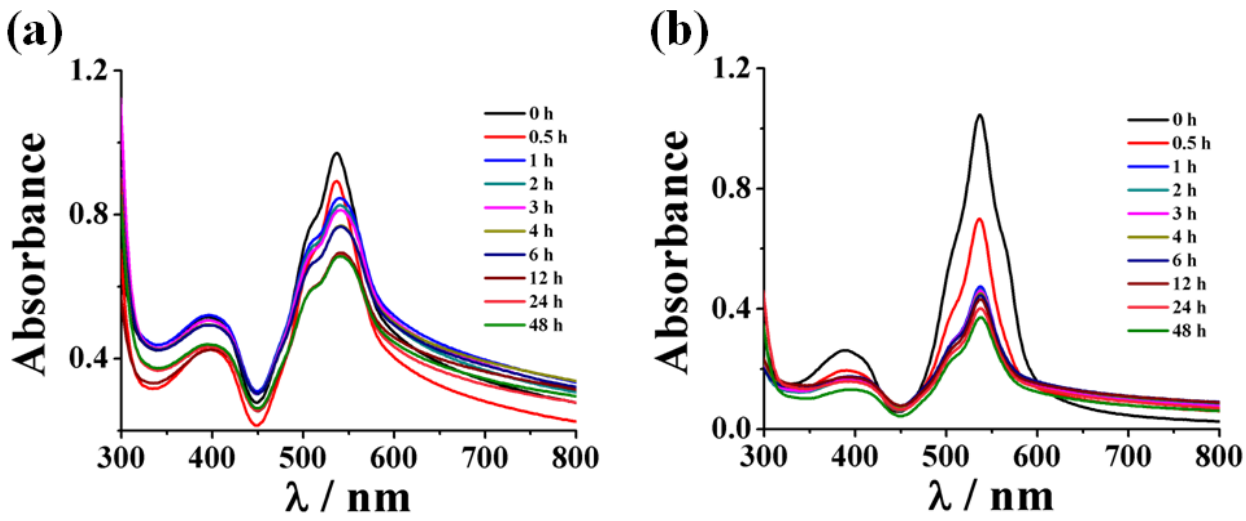

Figure S34 Time dependent absorption spectra of complex **3** (a) and free ligand L^3 (b) in 10% DMSO-DPBS buffer (pH = 7.4) measured up to 48 h at 37 ° C to verify the comparative stability of the complex and the free ligand in biological media under dark conditions. Plots suggest significantly better stability of complex **3** compared to the free organic ligand.

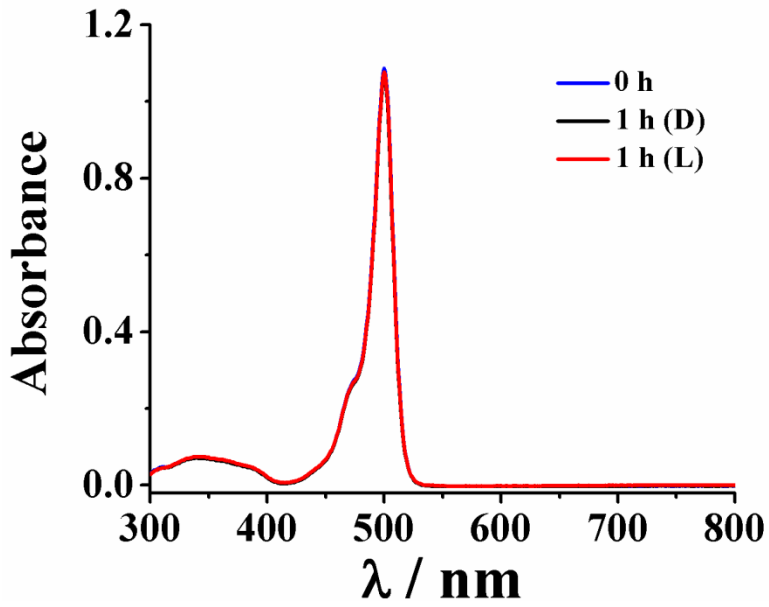

Figure S35 UV-vis absorption spectra of complex **2** in 10% DMSO-DPBS buffer (pH = 7.4) to verify the photostability of the complex in biological media. Colour codes: blue, the spectra of complex **2** before light irradiation; red, the spectra of complex **2** after photo-irradiation with 400-700 cm visible light source (10 *J* cm^{-2}, 1 h) and black, the spectra of complex **2** measured after keeping the sample in dark for 1 h at 37 ° C used as control. Plots suggest photo-exposure had no apparent effect on the stability of complex **2** in biological media.

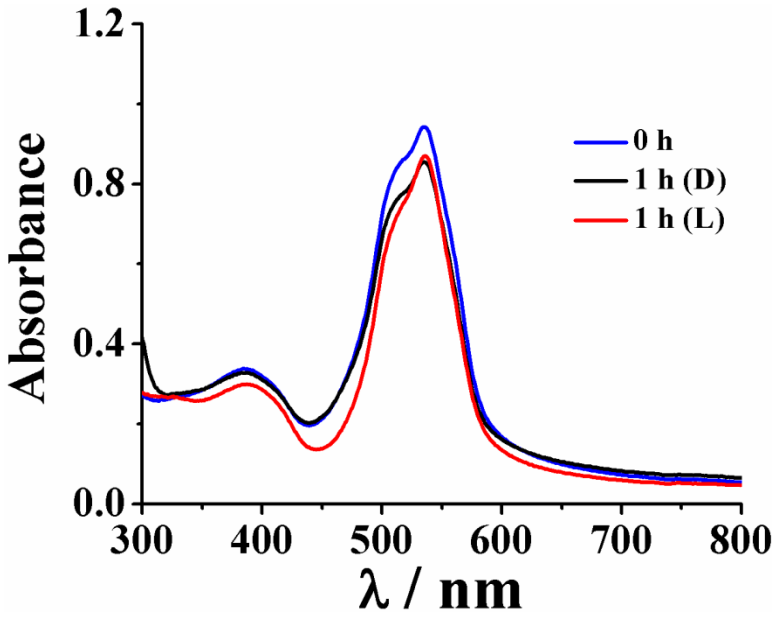

Figure S36 UV-vis absorption spectra of complex **3** in 10% DMSO-DPBS buffer (pH = 7.4) to verify the photostability of the complex in biological media. Colour codes: blue, the spectra of complex **3** before light irradiation; red, the spectra of complex **3** after photo-irradiation with 400-700 cm visible light source (10 *J* cm^{-2}, 1 h) and black, the spectra of complex **3** measured after keeping the sample in dark for 1 h at 37 ° C used as control. Plots suggest photo-exposure had no significant effect on the stability of complex **3** in biological media.

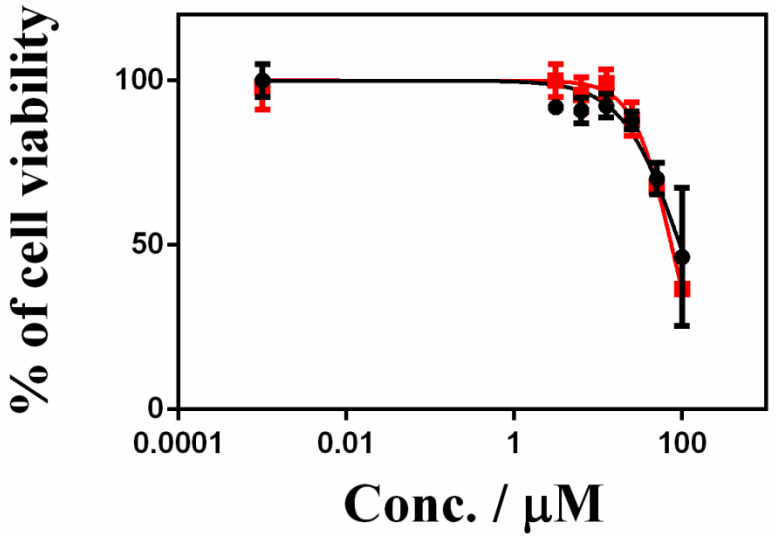

Figure S37 Cell viability plots as obtained from the MTT assay in HeLa cells treated with the complex **1** for 4 h, followed by 1 h incubation in the dark (black) or exposure to visible light (red, 400-700 nm, 10 *J* cm^{-2}).

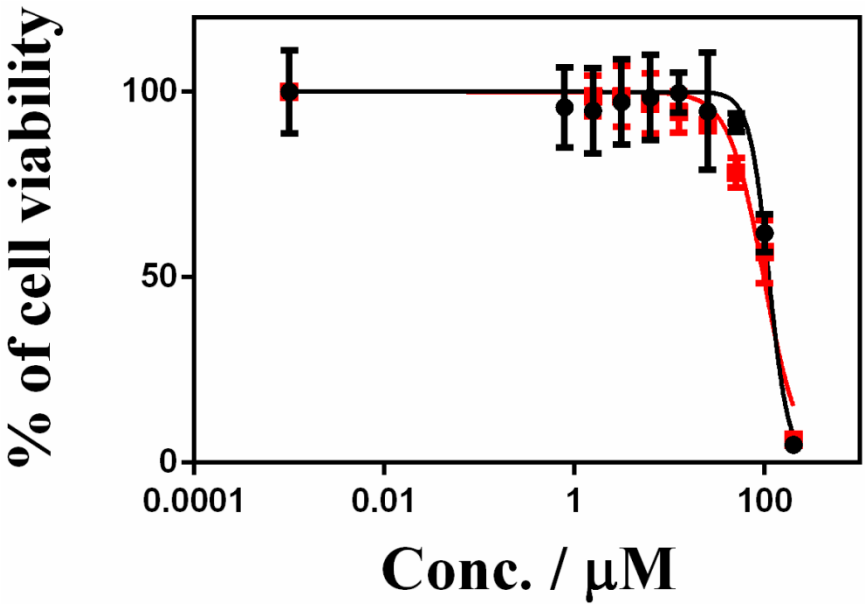

Figure S38 Cell viability plots as obtained from the MTT assay in MCF-7 cells treated with the complex **1** for 4 h, followed by 1 h incubation in the dark (black) or exposure to visible light (red, 400-700 nm, 10 *J* cm^{-2}).

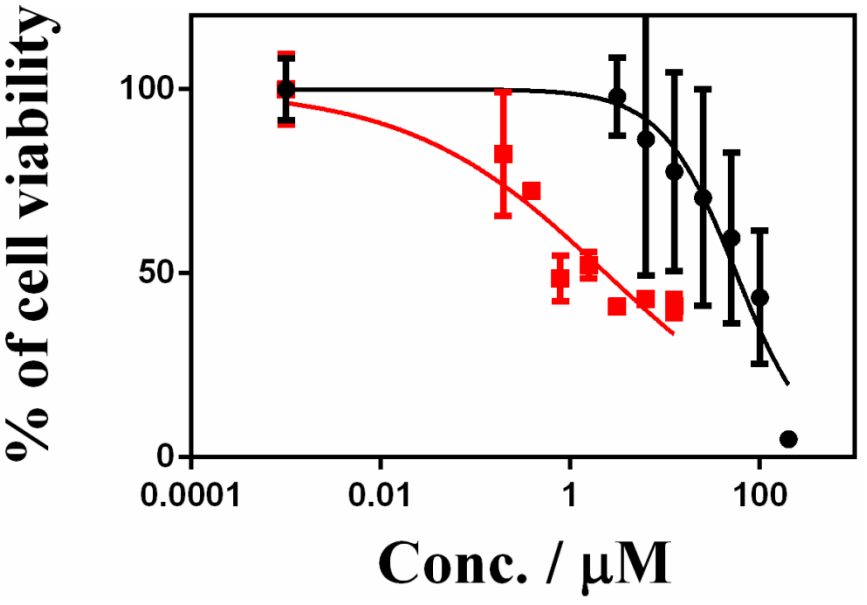

Figure S39 Cell viability plots as obtained from the MTT assay in HeLa cells treated with the complex **2** for 4 h, followed by 1 h incubation in the dark (black) or exposure to visible light (red, 400-700 nm, 10 *J* cm^{-2}).

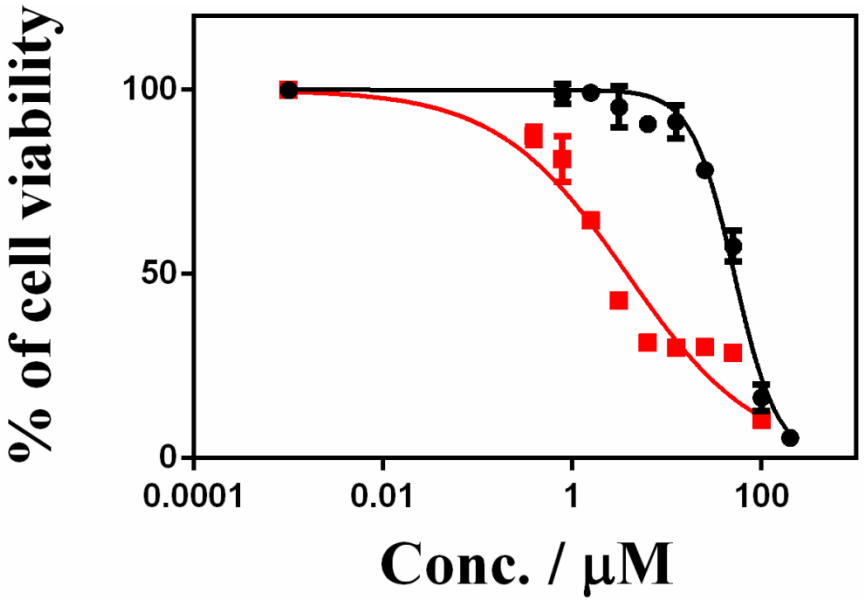

Figure S40 Cell viability plots as obtained from the MTT assay in MCF-7 cells treated with the complex **2** for 4 h, followed by 1 h incubation in the dark (black) or exposure to visible light (red, 400-700 nm, 10 *J* cm^{-2}).

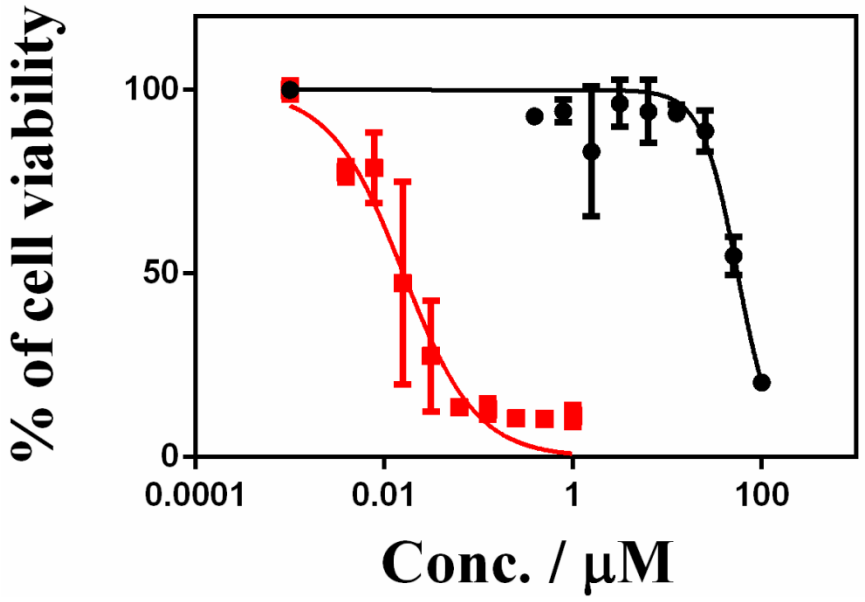

Figure S41 Cell viability plots as obtained from the MTT assay in HeLa cells treated with the complex **3** for 4 h, followed by 1 h incubation in the dark (black) or exposure to visible light (red, 400-700 nm, 10 *J* cm^{-2}).

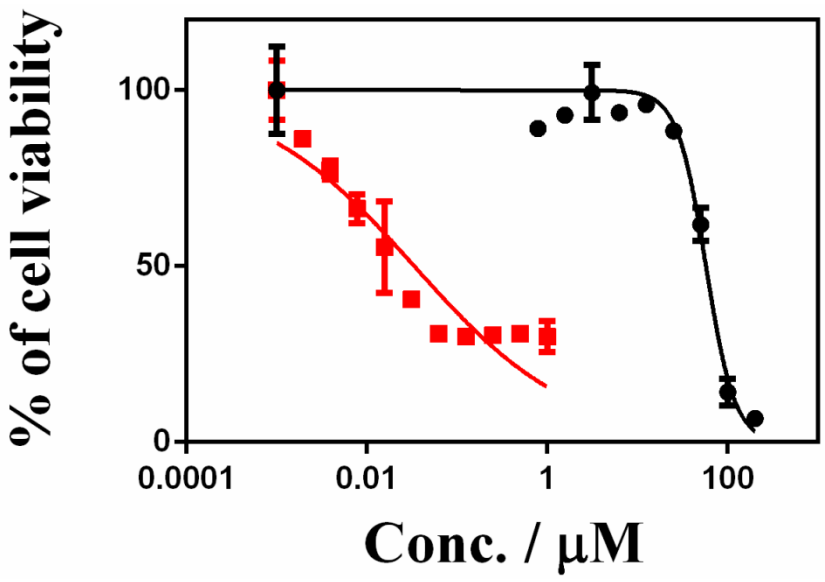

Figure S42 Cell viability plots as obtained from the MTT assay in MCF-7 cells treated with the complex **3** for 4 h, followed by 1 h incubation in the dark (black) or exposure to visible light (red, 400-700 nm, 10 *J* cm^{-2}).

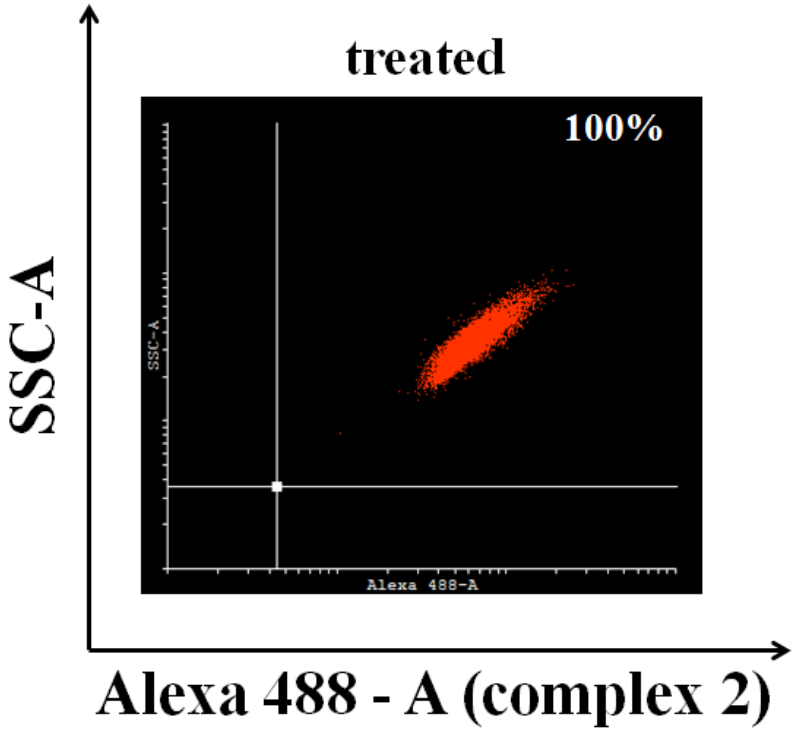

Figure S43 Cellular uptake data of complex **2** (1.0 µM) in HeLa cells using FACS analysis. The dot plot shows 100% accumulation of the complex inside HeLa cells on 4 h incubation. The control experiments are referred to reference S11.

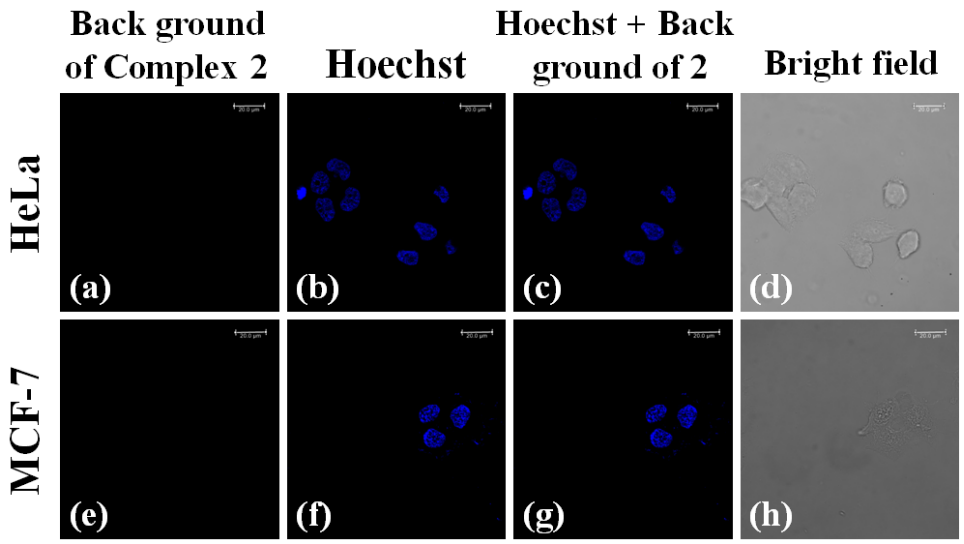

Figure S44 Confocal microscopy images of HeLa and MCF-7 cancer cells taken after 4 h without the treatment of complex **2**. These images are taken as controls. Panels (b) and (f) indicate blue fluorescence of nuclear targeting Hoechst 33258 dye (5 μg ml^{-1}); panels (a) and (e) exhibit background green emission without **2**; panels (c) and (g) are the merged images of background green emission and Hoechst dye and panels (d) and (h) are the bright field images. Scale bar = 20 μm.

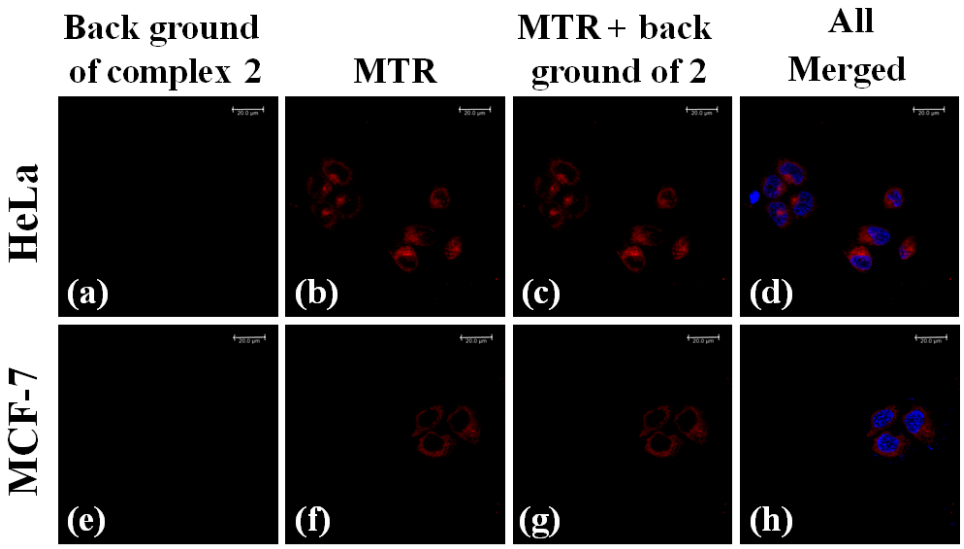

Figure S45 Confocal microscopy images of HeLa and MCF-7 cells taken after 4 h with MitoTracker Red (MTR, 0.1 μM) and without the treatment of complex **2.** These images were taken as controls. Panels (a) and (e) show the back ground green fluorescence without complex **2**, panels (b) and (f) display the red fluorescence of MTR; panels (c) and (g) are the merged images of MTR and the back ground emission of complex **2** and panels (d) and (h) are the merged pictures of Hoechst 33258 dye and MTR red with the back ground of **2**. Scale bar = 20 μm.

(a)

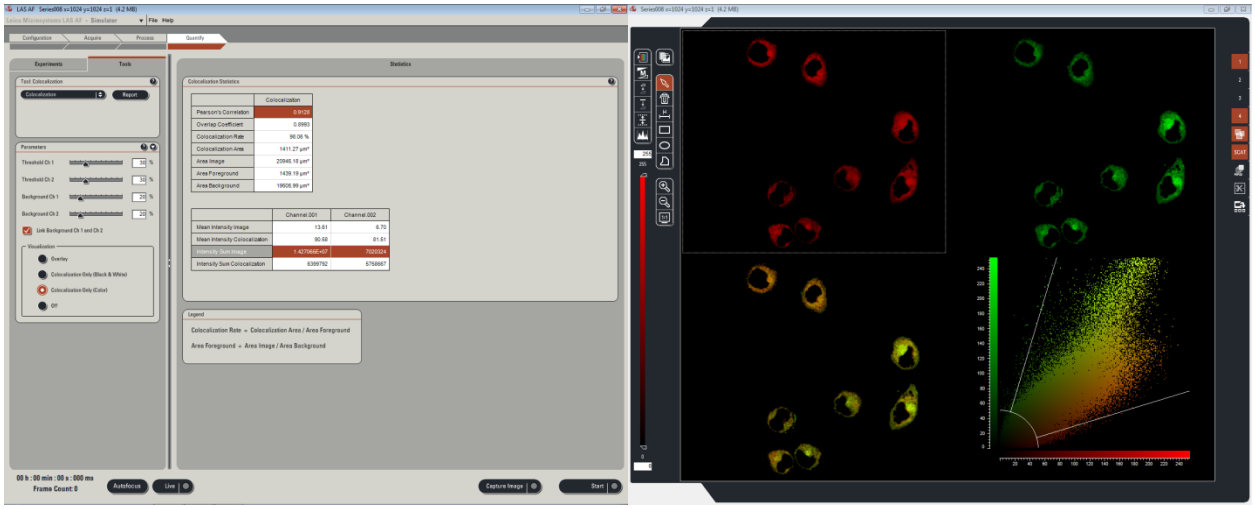

(b)

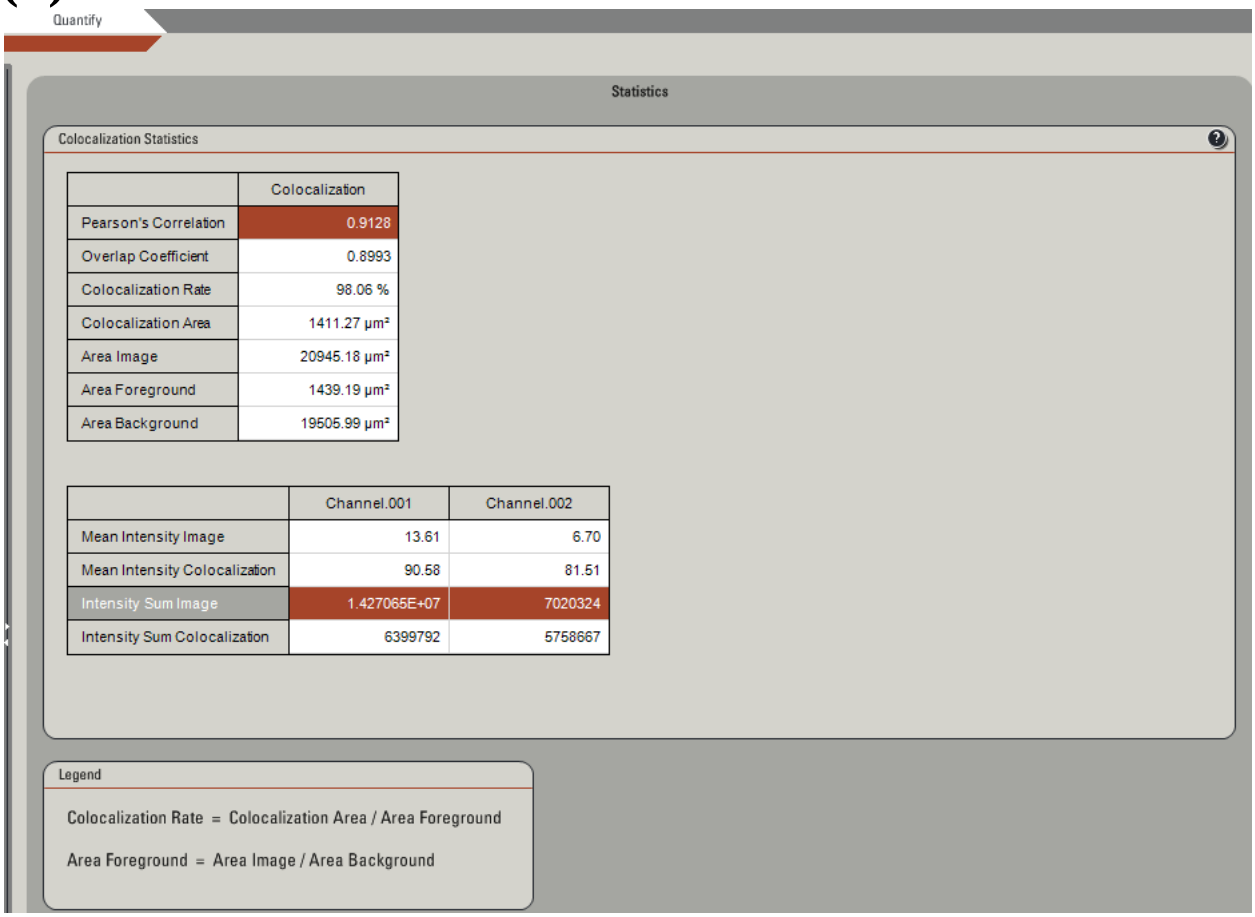

Figure S46 (a, b) Calculations and plots for the determination of Pearson correlation coefficient (PCC) and overlap coefficient (OC) of complex **2** inside the mitochondria of the HeLa cells.

(a)

(b)

Quantify

Statistics

Colocalization Statistics

	Colocalization
Pearson's Correlation	0.8827
Overlap Coefficient	0.9093
Colocalization Rate	89.12 %
Colocalization Area	5415.81 µm²
Area Image	20945.18 µm²
Area Foreground	6077.32 µm²
Area Background	14867.86 µm²

	Channel.001	Channel.002
Mean Intensity Image	44.77	21.05
Mean Intensity Colocalization	115.56	70.04
Intensity Sum Image	4.69411E+07	2.207739E+07
Intensity Sum Colocalization	3.133147E+07	1.899042E+07

Legend

Colocalization Rate = Colocalization Area / Area Foreground

Area Foreground = Area Image / Area Background

Figure S47 (a, b) Calculations and plots for the determination of Pearson correlation coefficient (PCC) and overlap coefficient (OC) of complex **2** inside the mitochondria of the MCF-7 cells.

(a)

Cell control

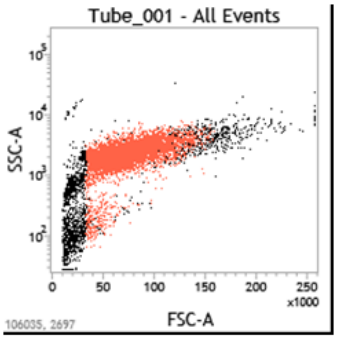

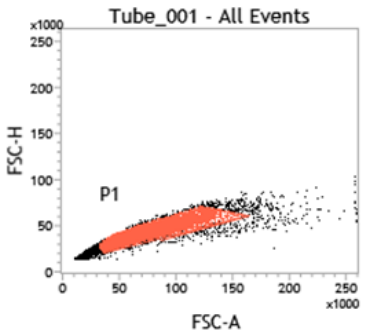

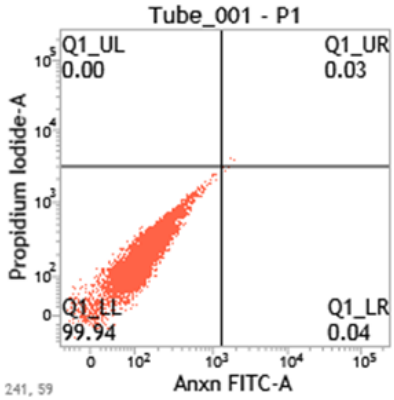

Annexin control

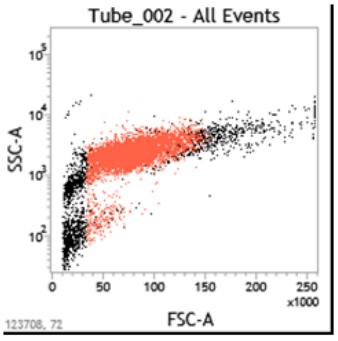

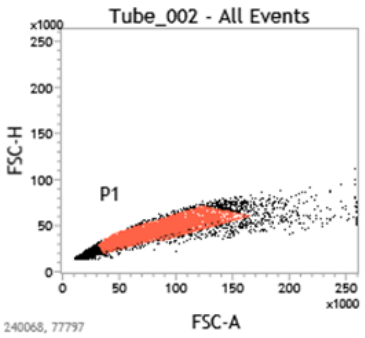

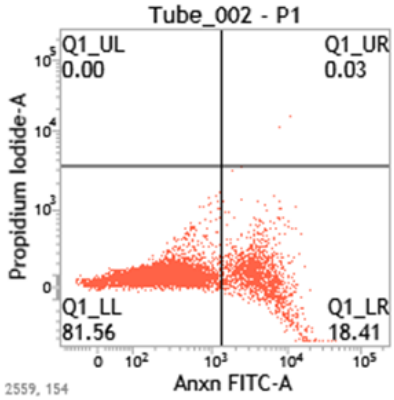

PI control

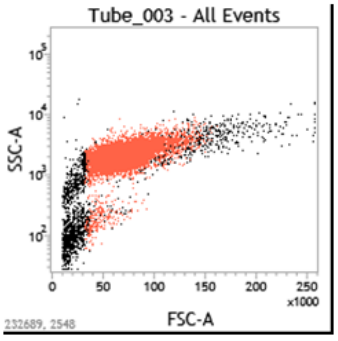

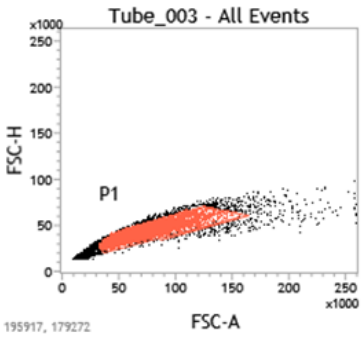

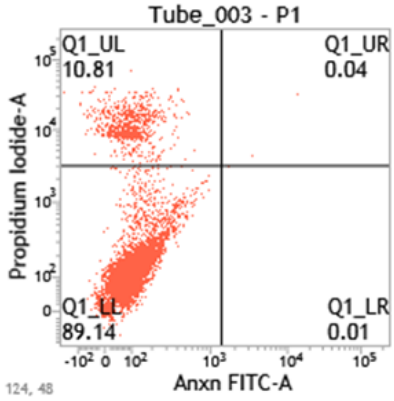

(b)

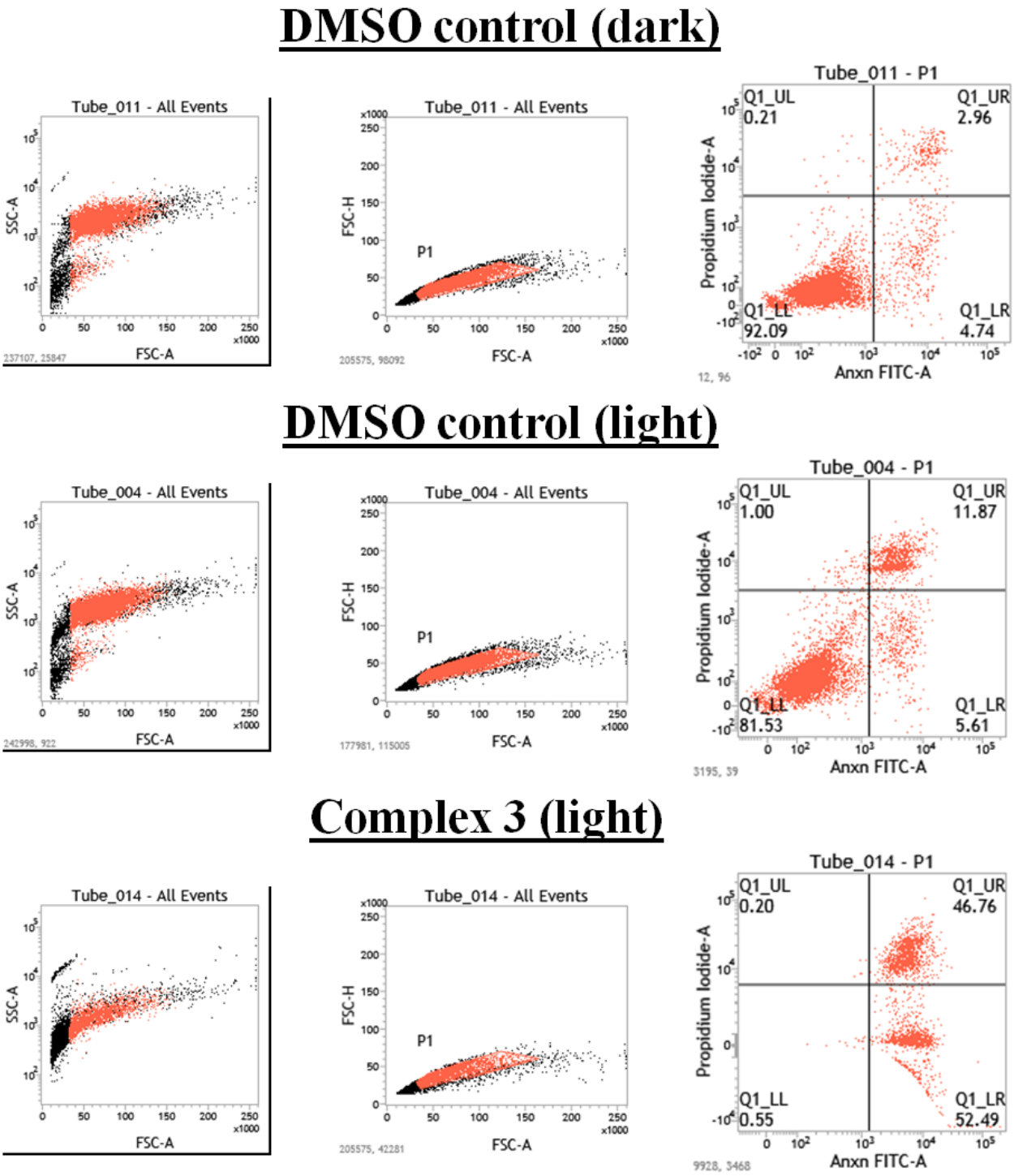

Figure S48 (a) FACS analysis data showing cell control, Annexin control and PI control experiments used for the Annexin V-FITC/PI assay of complex **3** in HeLa cells. **(b)** FACS analysis data showing DMSO control and complex **3** plots for the Annexin V-FITC/PI assay in HeLa cells.

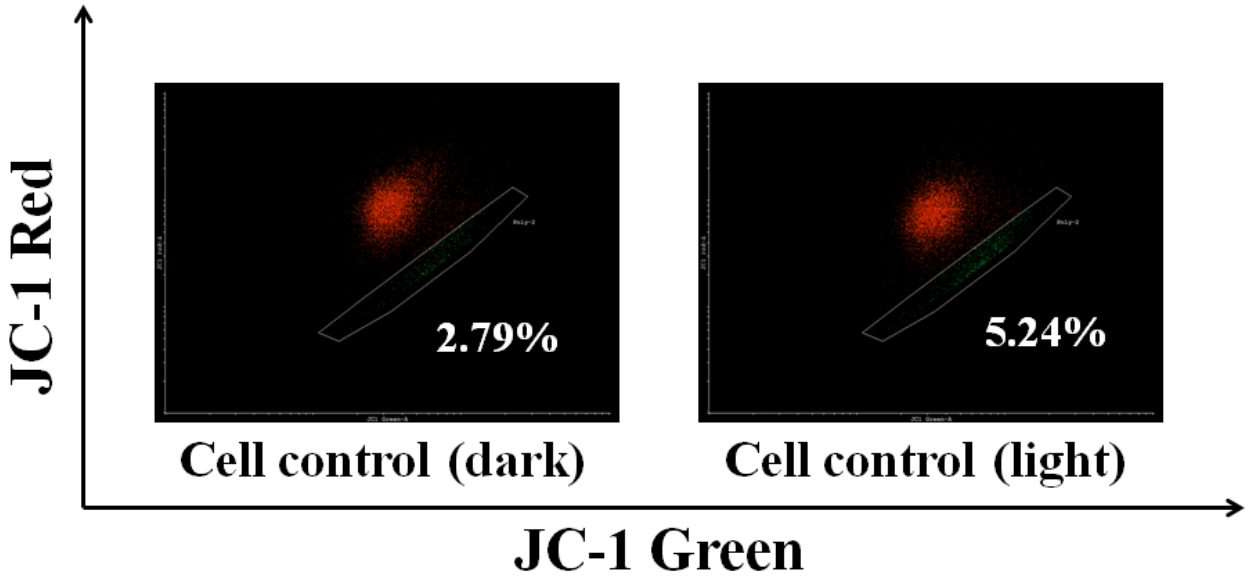

Figure S49. Plots show the control experiments used for JC-1 assay of complex **3** in HeLa cells using FACS analysis. Left side panel indicates HeLa cells treated with JC-1 dye alone kept in dark condition and right side panel shows HeLa cells with JC-1 dye alone after visible light irradiation (400-700 nm, 10 J cm^{-2}, 1 h). Digits indicate the percentage of cells exhibiting green fluorescence of JC-1 dye originating due to the change in the mitochondrial membrane potential.

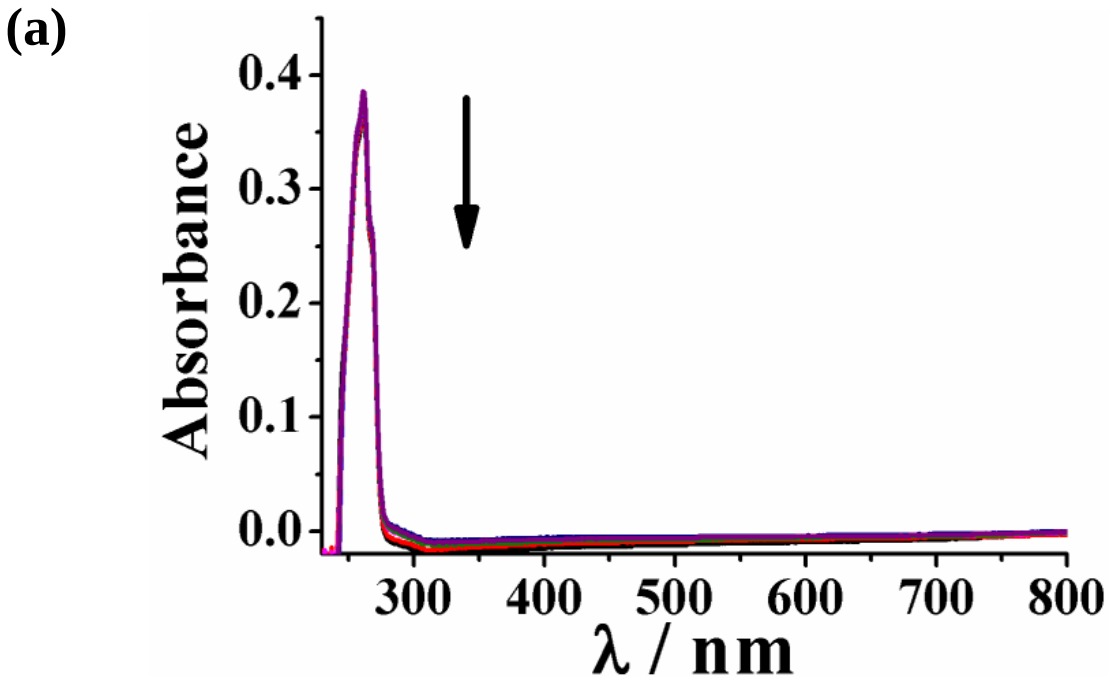

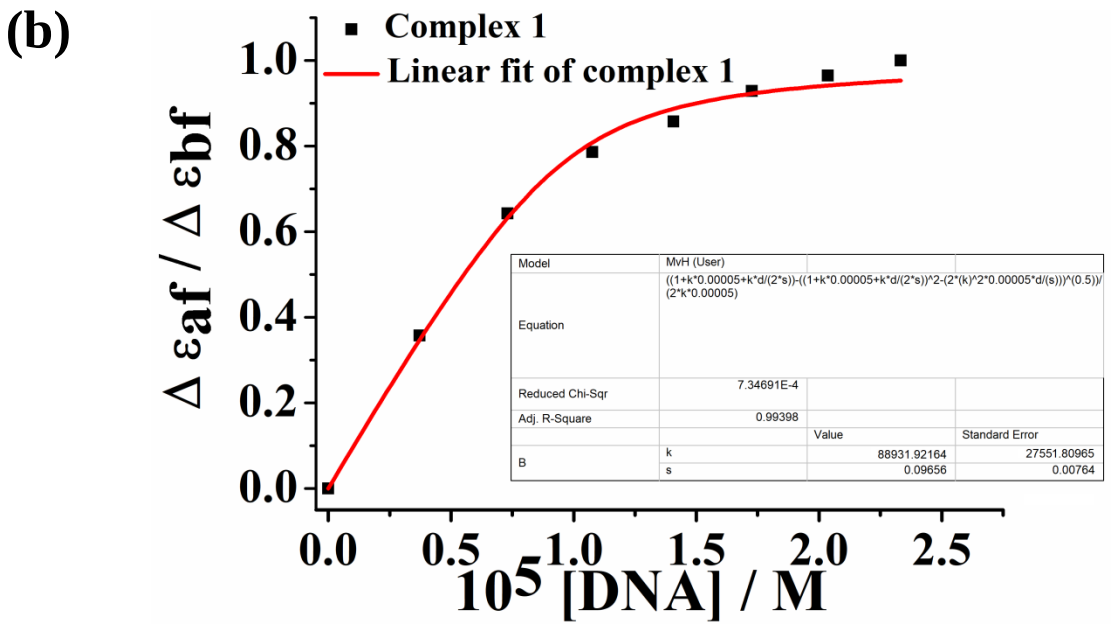

Figure S50 (a) Absorption spectral traces of complex **1** in Tris-HCl/NaCl buffer (pH = 7.2) on increasing the concentration of calf thymus (ct) DNA showing a gradual decrease in the absorption maxima. **(b)** The least-squares fit of $\Delta\varepsilon_{af}$ / $\Delta\varepsilon_{bf}$ vs. [DNA] for complex **1** using McGhee-von Hippel (MvH) method to determine the DNA binding constant (K_b) and fitting parameter (s).

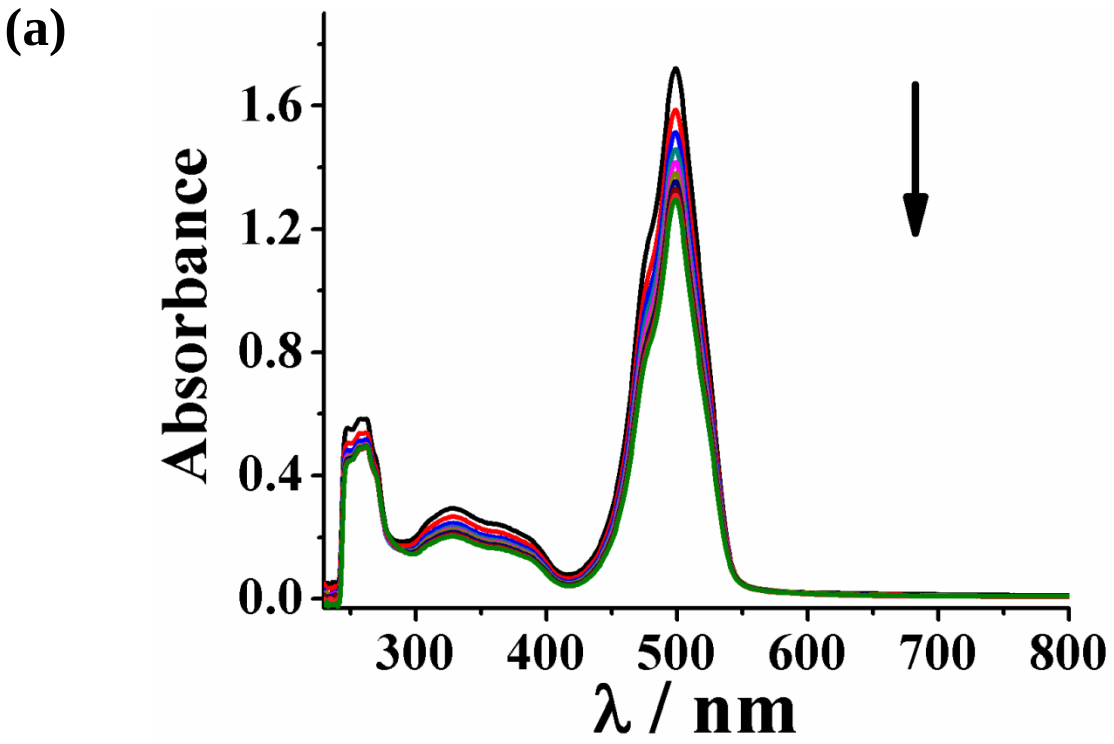

(b)

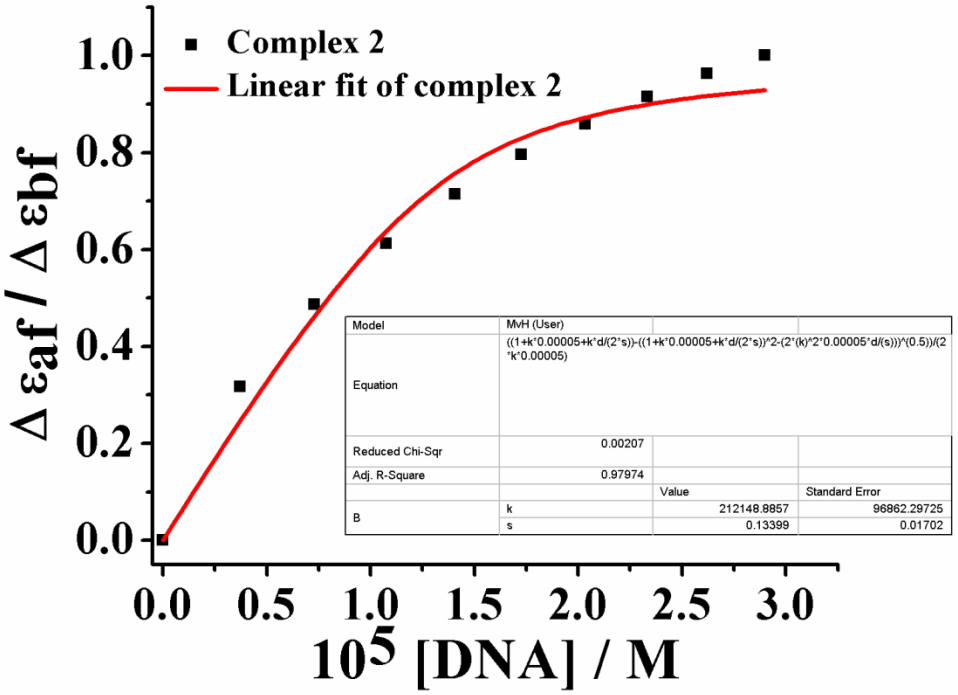

Figure S51 (a) Absorption spectral traces of complex **2** in Tris-HCl/NaCl buffer (pH = 7.2) on increasing the concentration of calf thymus (ct) DNA showing a gradual decrease in the absorption maxima. **(b)** The least-squares fit of $\Delta\varepsilon_{af}$ / $\Delta\varepsilon_{bf}$ vs. [DNA] for complex **2** using McGhee-von Hippel (MvH) method to determine the DNA binding constant (K_b) and fitting parameter (s).

(a)

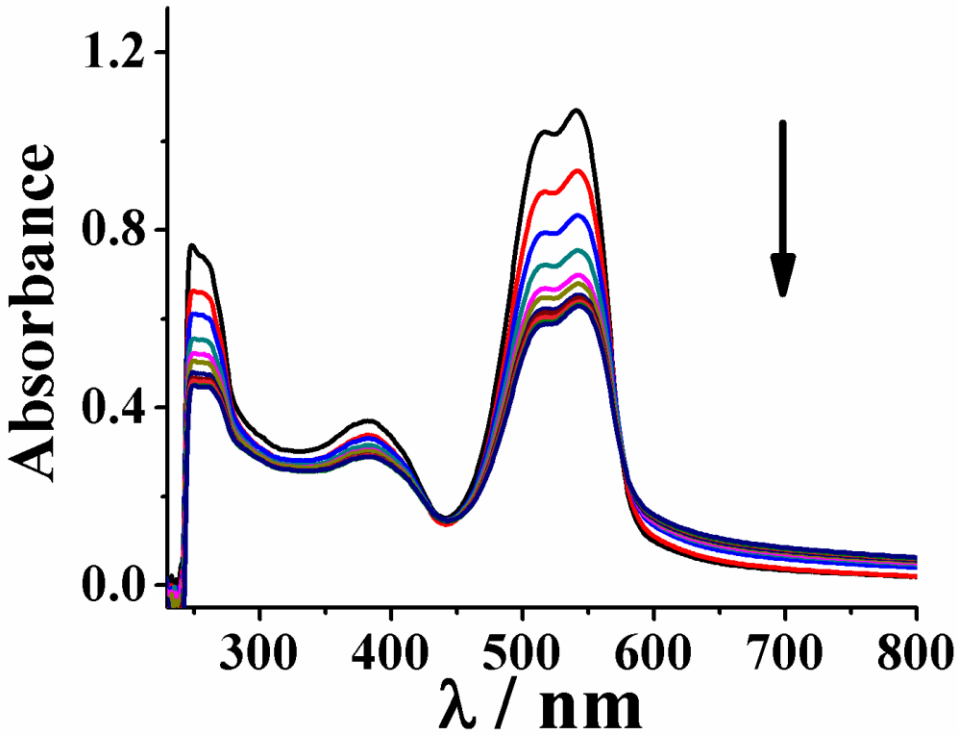

.

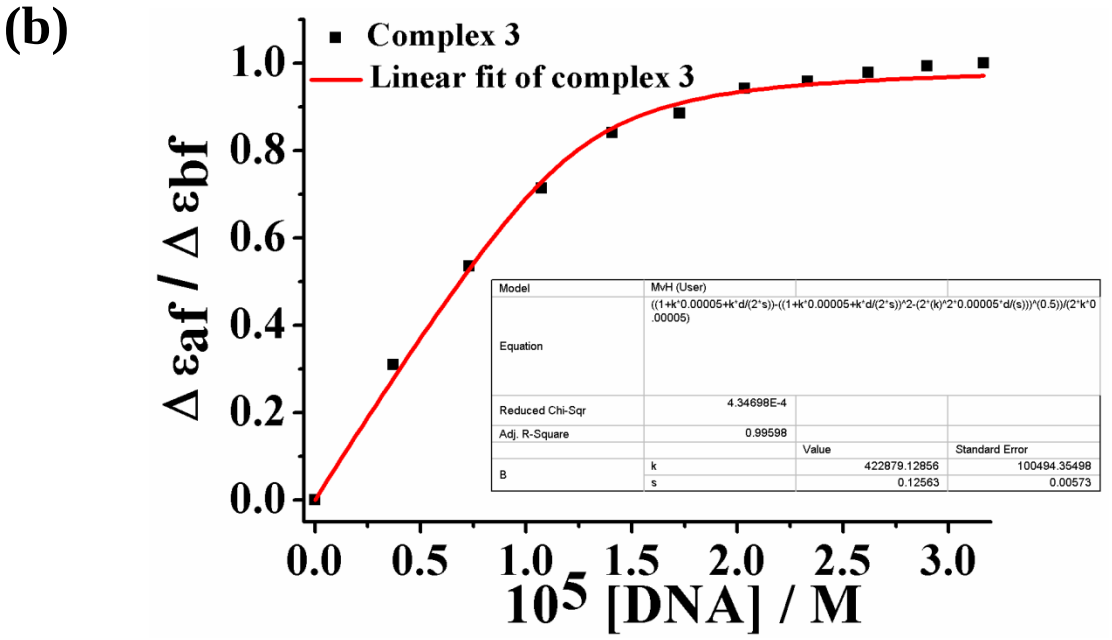

Figure S52 (a) Absorption spectral traces of complex **3** in Tris-HCl/NaCl buffer (pH = 7.2) on increasing the concentration of calf thymus (ct) DNA showing a gradual decrease in the absorption maxima **(b)** The least-squares fit of $\Delta\varepsilon_{af}$ / $\Delta\varepsilon_{bf}$ vs. [DNA] for complex **3** using McGhee-von Hippel (MvH) method to determine the DNA binding constant (K_b) and fitting parameter (s).

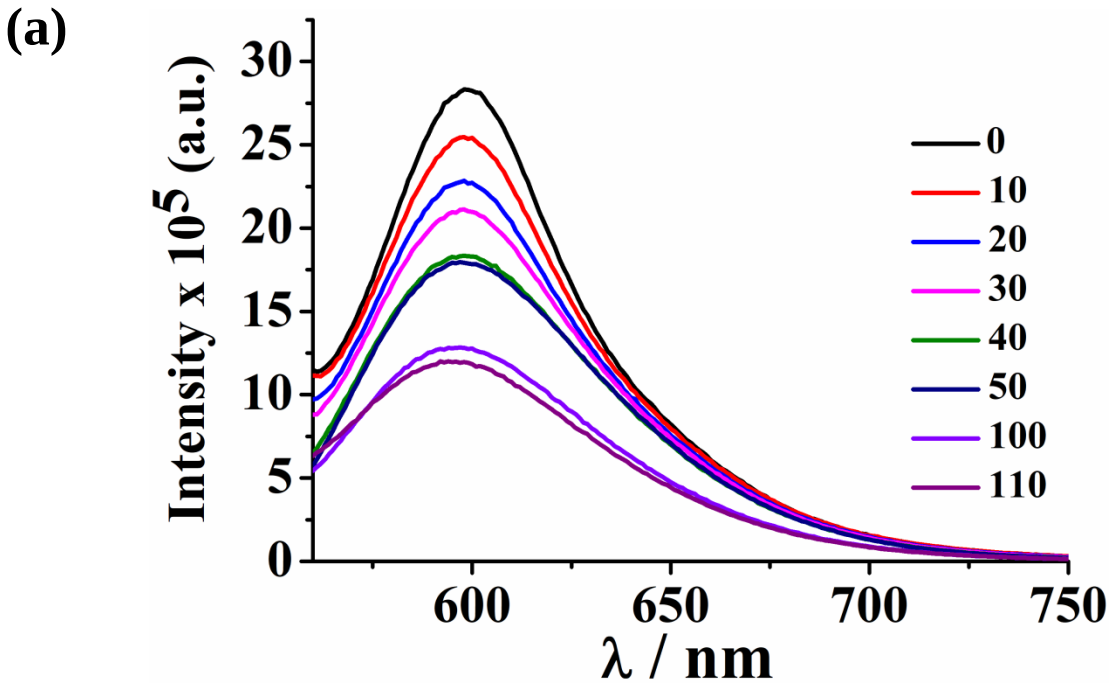

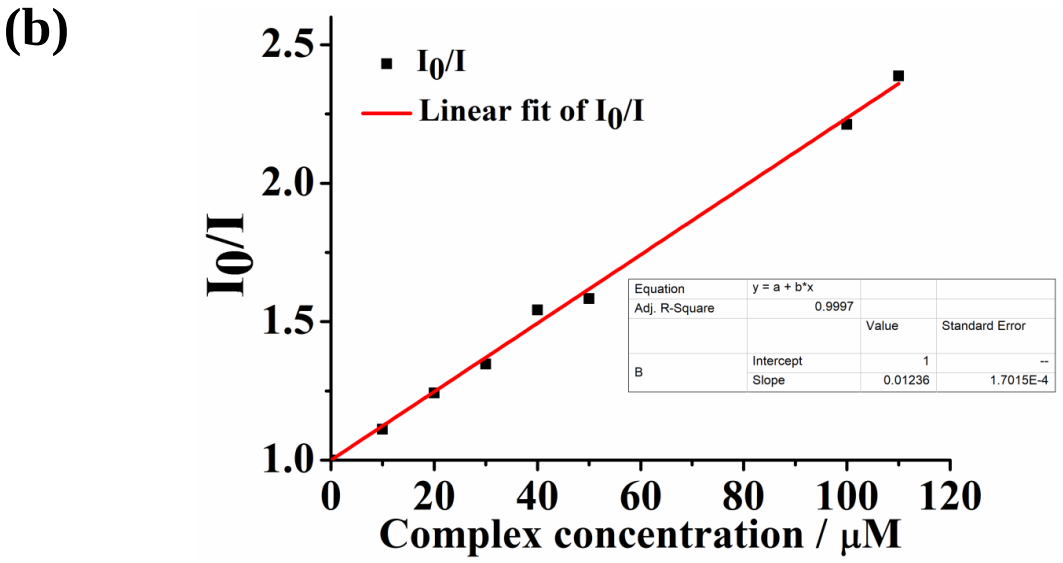

Figure S53 (a) Emission spectral traces of ethidium bromide (EB) bound to ct-DNA in Tris-HCl/NaCl buffer (pH = 7.2) on increasing the concentration of complex **1** (0-110 μM) showing a gradual decrease in the emission intensity. Digits in the figure indicate the micromolar concentration of complex **1** added in each instance. **(b)** Linear fitting plot of I_0/I versus complex concentration for the determination of quenching rate constant (K_q) and apparent DNA binding constant (K_{app}) of complex **1** using ethidium bromide (EB) displacement assay. I_0 represents the emission intensity of EB bound to ct-DNA in the absence of complex **1** while I indicate the emission intensities of EB bound to ct-DNA in the presence of different concentrations of complex **1**.

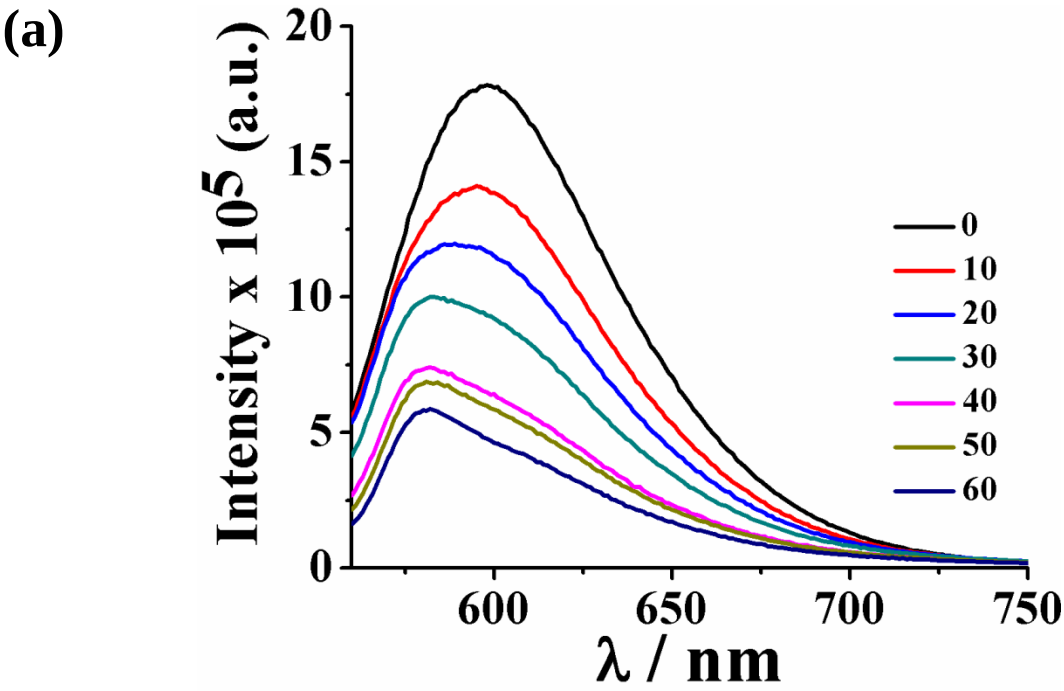

(b)

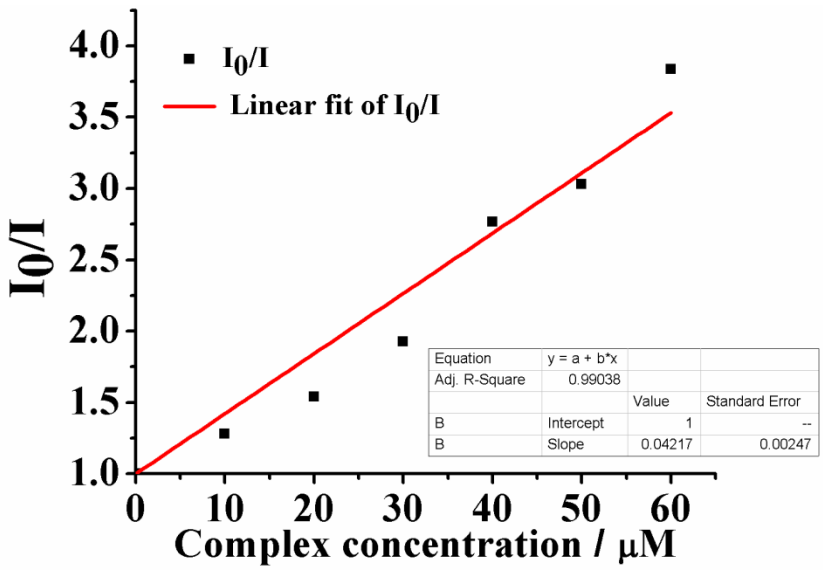

Figure S54 (a) Emission spectral traces of ethidium bromide (EB) bound to ct-DNA in Tris-HCl/NaCl buffer (pH = 7.2) on increasing the concentration of complex **2** (0-60 μM) showing a gradual decrease in the emission intensity. Digits in the figure indicate the micromolar concentration of complex **2** added in each instance.

(b) Linear fitting plot of I_0/I versus complex concentration for the determination of quenching rate constant (K_q) and apparent DNA binding constant (K_{app}) of complex **2** using ethidium bromide (EB) displacement assay. I_0 represents the emission intensity of EB bound to ct-DNA in the absence of complex **2**, while I indicate the emission intensities of EB bound to ct-DNA in the presence of different concentrations of complex **2**.

(a)

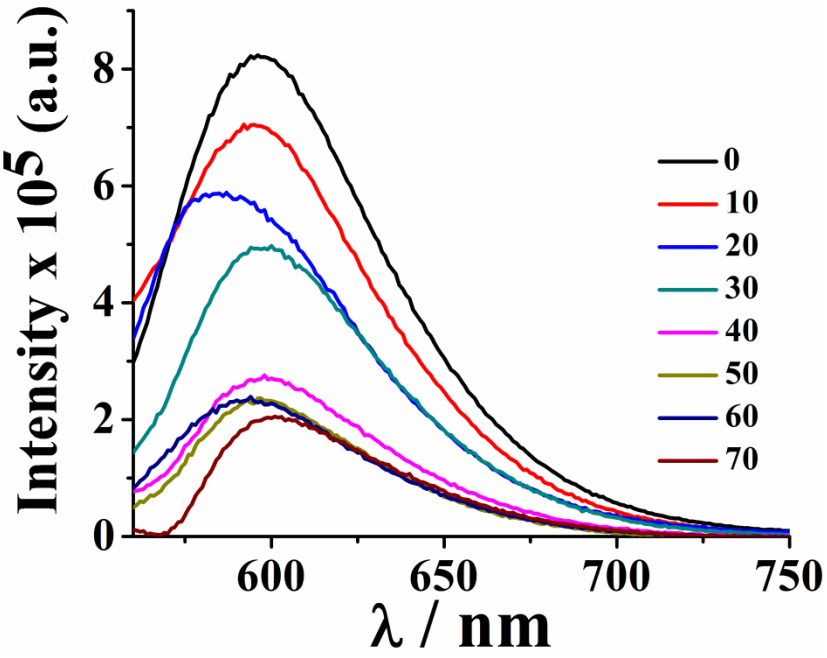

(b)

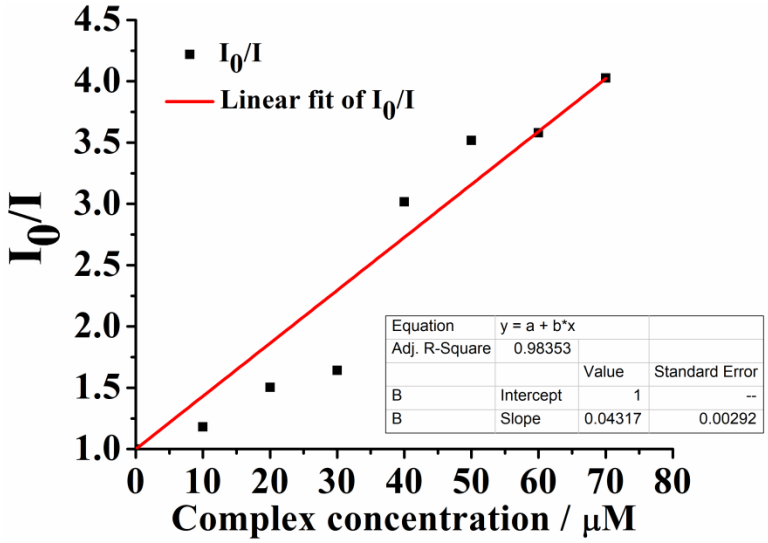

Figure S55 (a) Emission spectral traces of ethidium bromide (EB) bound to ct-DNA in Tris-HCl/NaCl buffer (pH = 7.2) on increasing the concentration of complex **3** (0-70 μM) showing a gradual decrease in the emission intensity. Digits in the figure indicate the micromolar concentration of complex **3** added in each instance.

(b) Linear fitting plot of I_0/I versus complex concentration for the determination of quenching rate constant (K_q) and apparent DNA binding constant (K_{app}) of complex **3** using ethidium bromide (EB) displacement assay. I_0 represents the emission intensity of EB bound to ct-DNA in the absence of complex **3**, while I indicate the emission intensities of EB bound to ct-DNA in the presence of different concentrations of complex **3**.

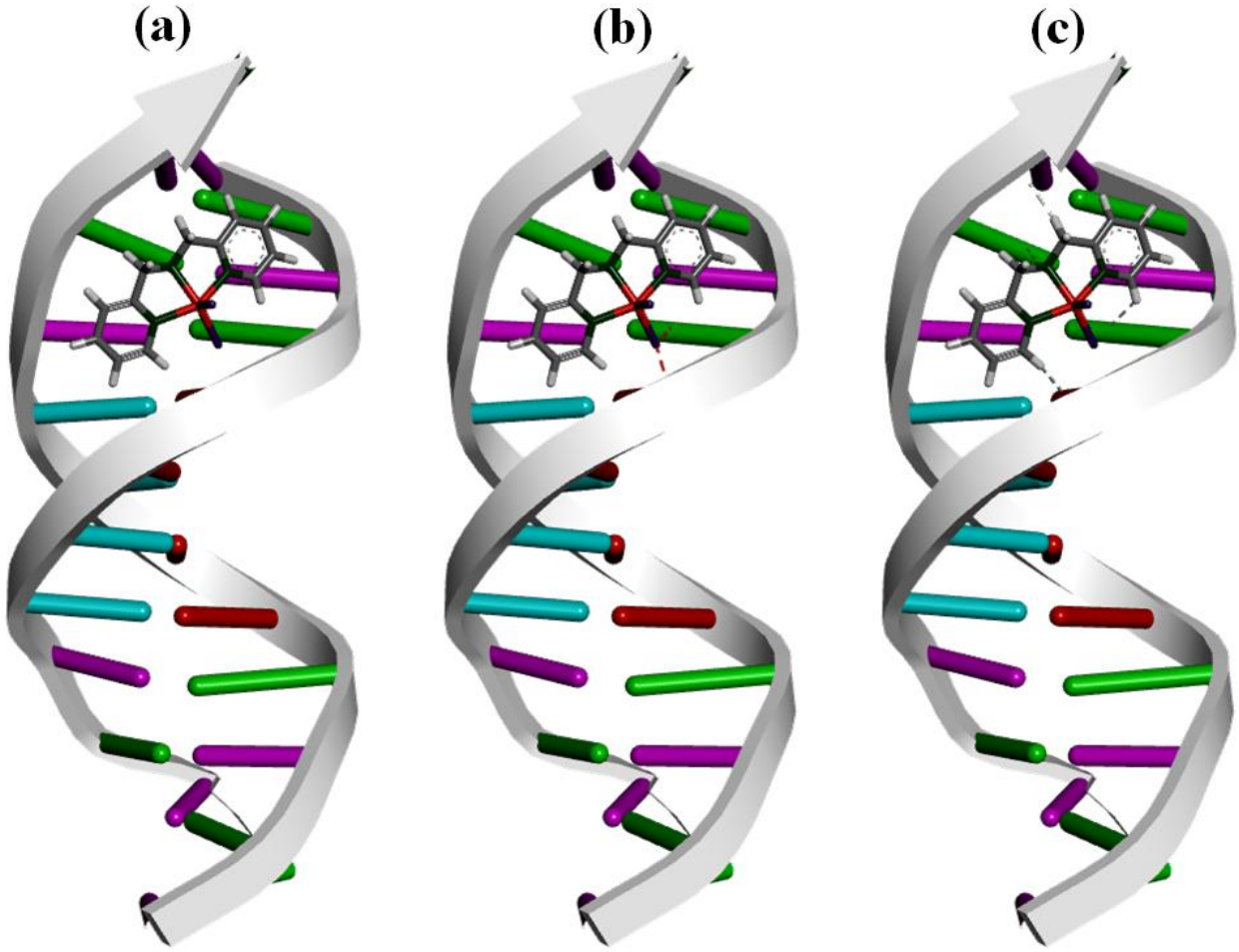

Figure S56 Docked structure of complex **1** with DNA [(a), PDB ID: 1BNA] showing electrostatic (b) and hydrogen bonding (c) interactions of complex **1** with the DNA double strand.

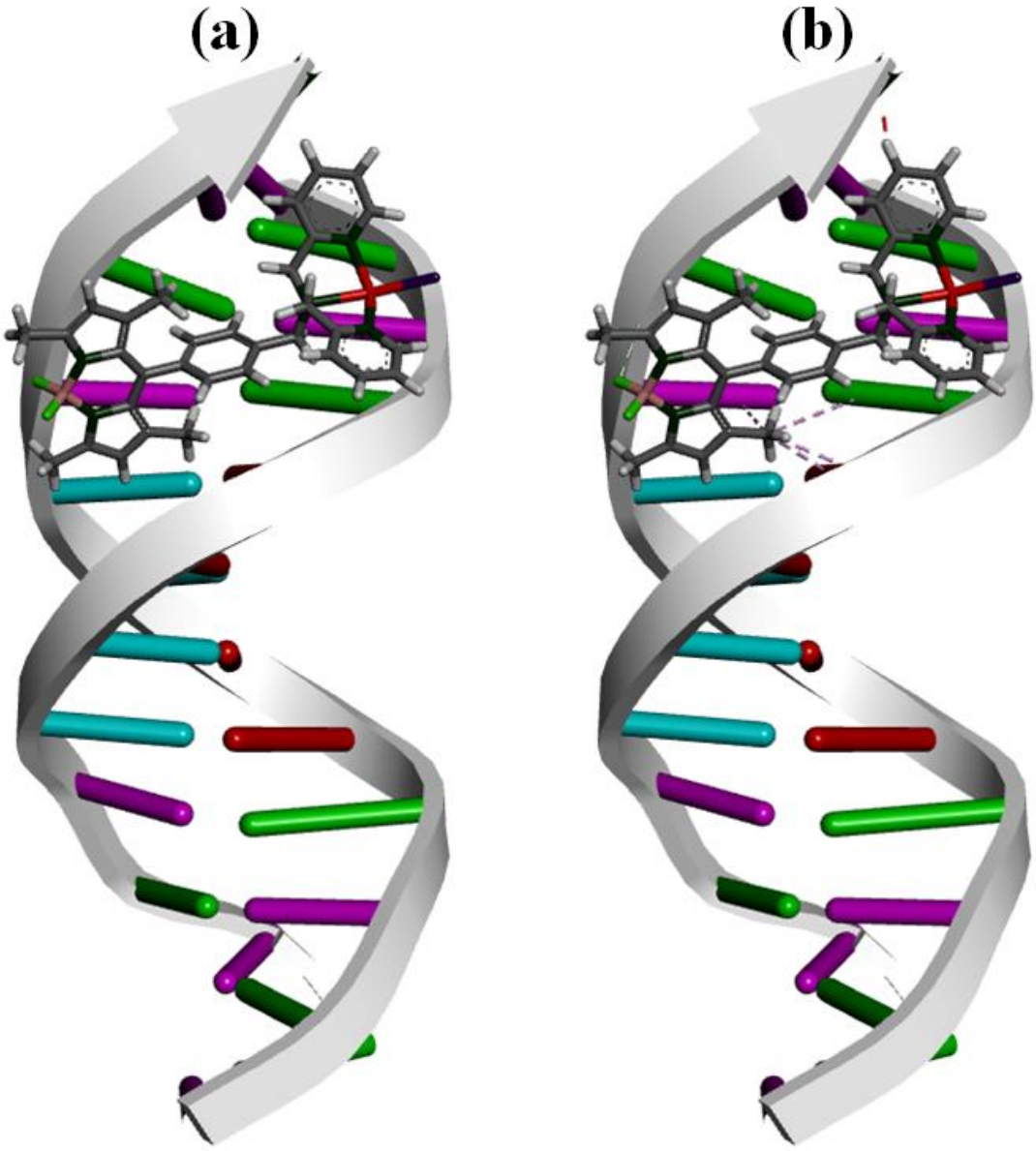

Figure S57 Docked structure of complex **2** with DNA [(a), PDB ID: 1BNA] showing different stabilizing interactions of complex **2** with the DNA double strand (b).

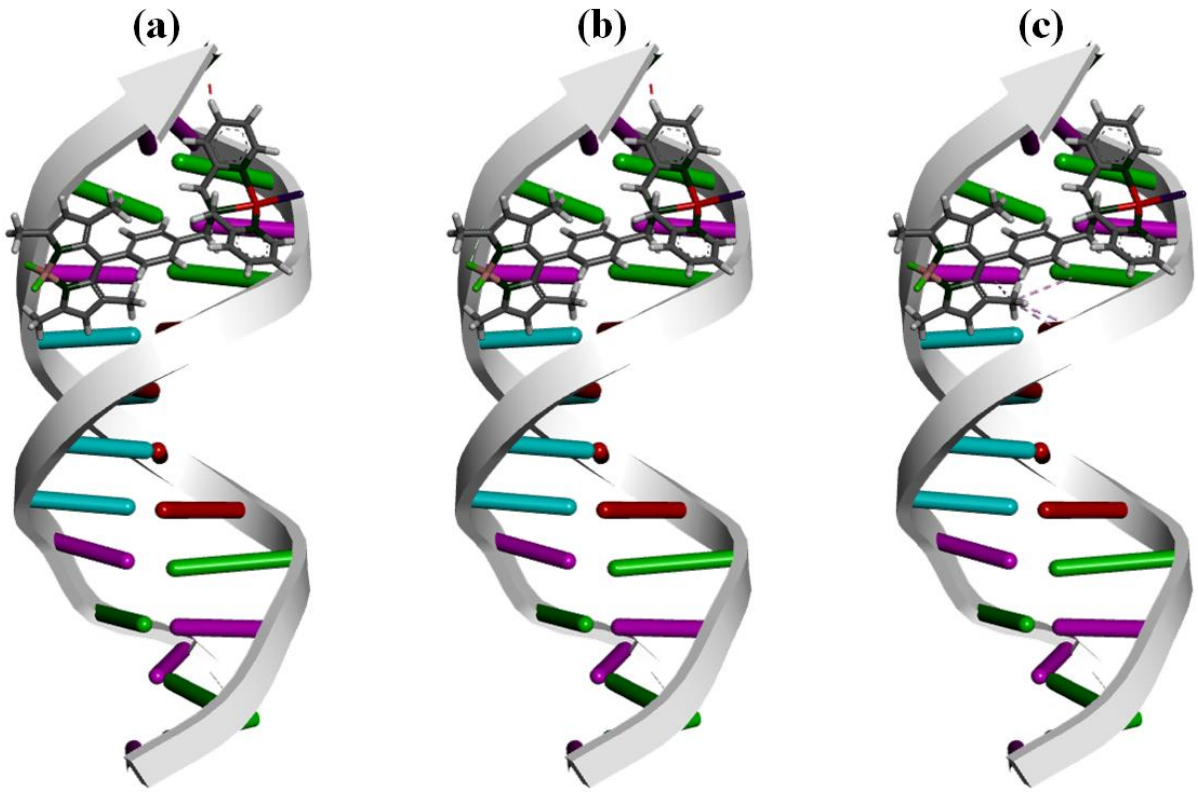

Figure S58 Docked structure of complex **2** with DNA [PDB ID: 1BNA] showing electrostatic (a), hydrogen bonding (b) and hydrophobic interactions (c) of complex **2** with the DNA double strand.

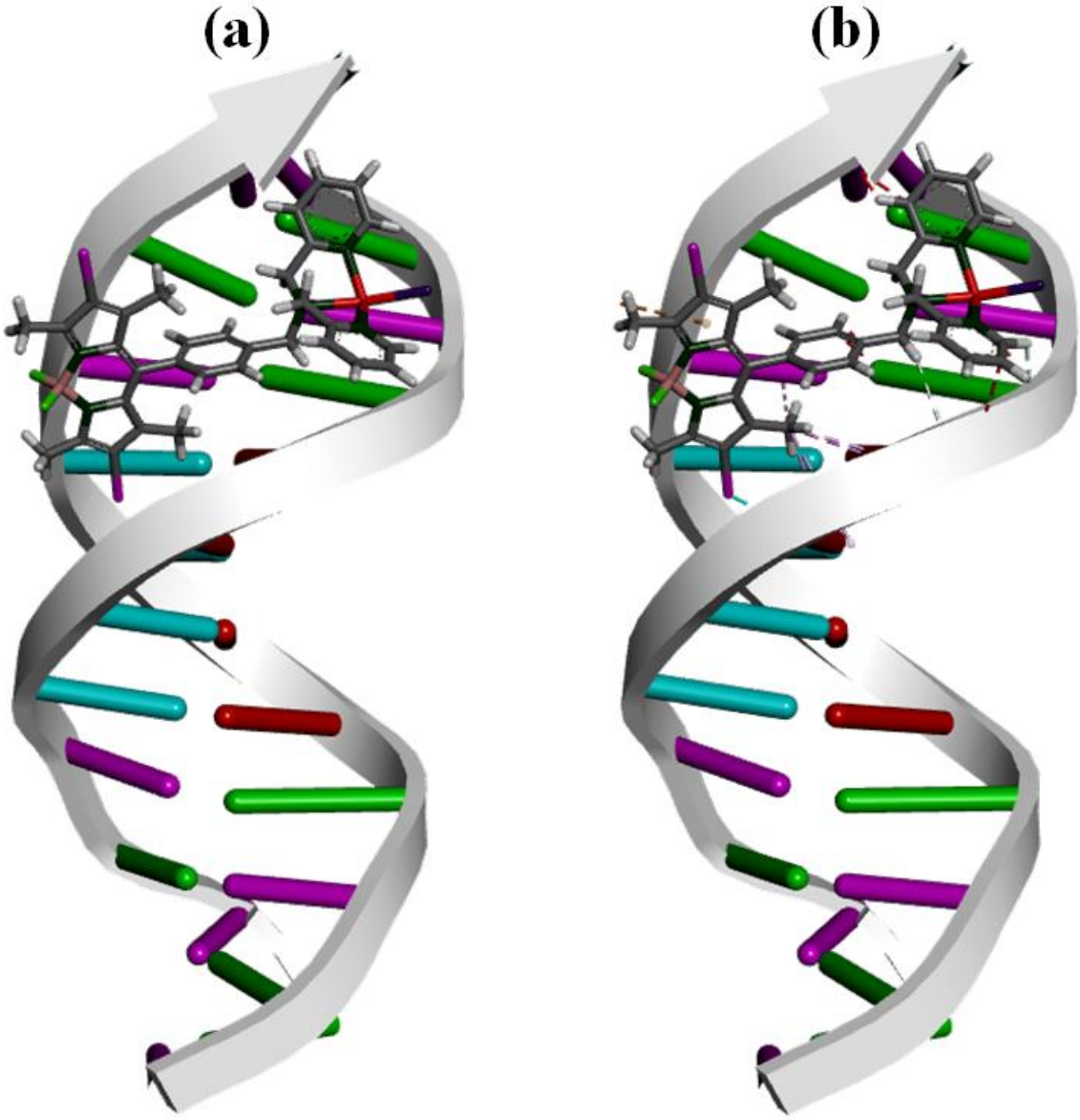

Figure S59 Docked structure of complex **3** with DNA [(a), PDB ID: 1BNA] showing different stabilizing interactions of complex **3** with the DNA double strand (b).

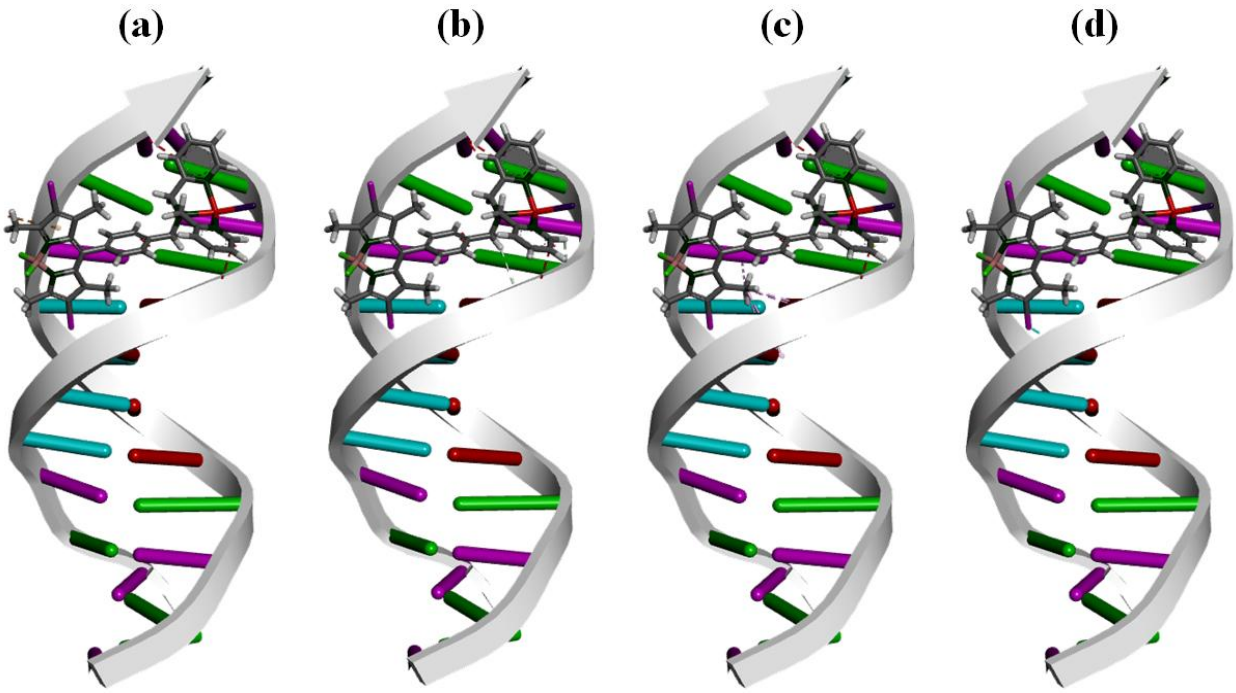

Figure S60 Docked structure of complex **3** with DNA [PDB ID: 1BNA] showing electrostatic (a), hydrogen bonding (b), hydrophobic (c) interactions and other non-bonding interactions through iodine atoms (d) of complex **3** with the DNA double strand.

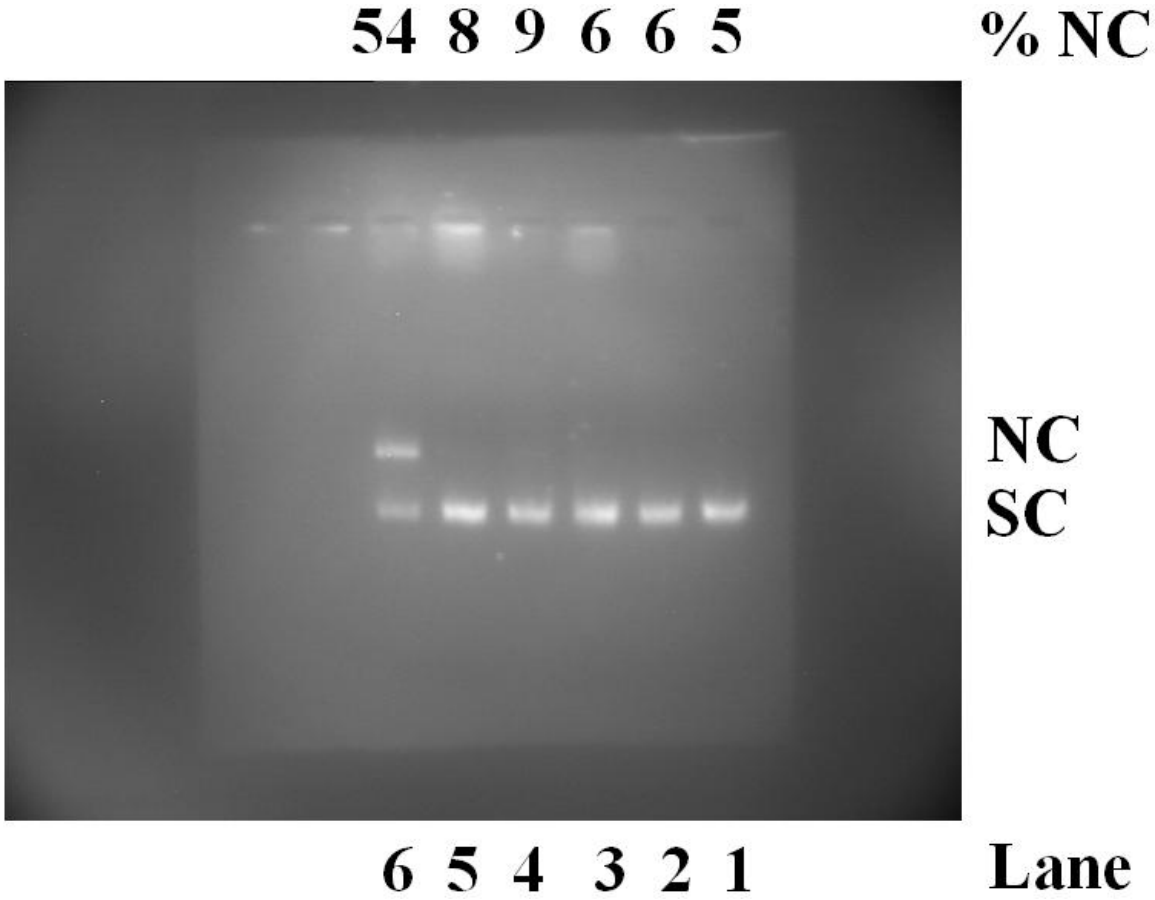

Figure S61 Gel diagram showing the extent of SC pUC19 DNA (0.2 μg, 30 μM base pair) cleavage on agarose gel eletrophoresis using complexes **1**-**2** in dark and in presence of green laser light source (532 nm, 100 mW, 1 h exposure). Lane 1: DNA control in dark; Lane 2: DNA control in light; Lane 3: DNA + Comp **1** (50 μM) in dark; Lane 4: DNA + Comp **1** (50 μM) in light; Lane 5: DNA + Comp **2** (20 μM) in dark and Lane 6: DNA + Comp **2** (20 μM) in light. Sample composition: 1 μL DNA + 1 μL NaCl (50 mM) + 8 μL Tris-HCl Buffer (50 mM, pH = 7.2) + 10 μL stock solution of complex **1** or **2** (total volume of samples = 20 μL); SC = supercoiled and NC = nicked circular DNA.

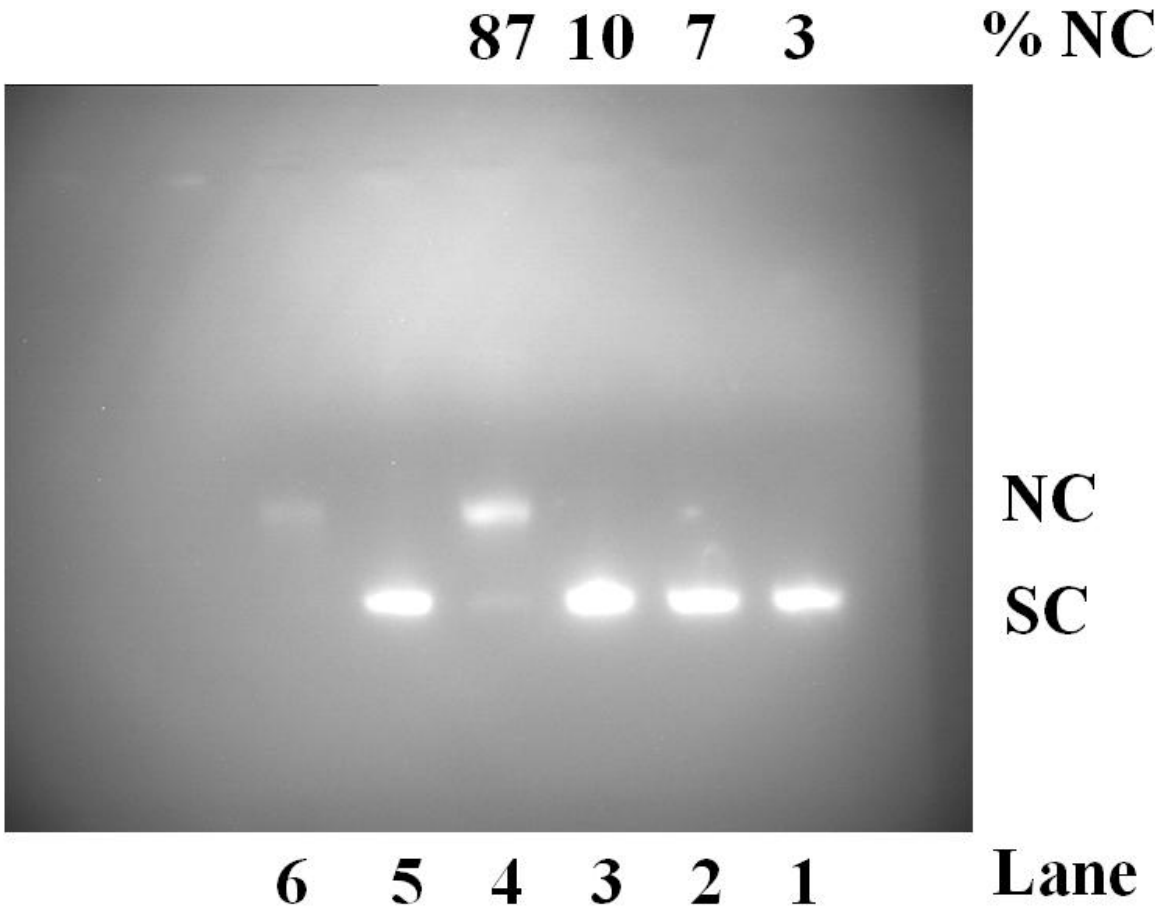

Figure S62 Gel diagram showing the extent of SC pUC19 DNA (0.2 μg, 30 μM base pair) cleavage on agarose gel eletrophoresis using complex **3** in dark and in presence of green diode laser light source (532 nm, 100 mW, 1 h exposure). Lane 1: DNA control in dark; Lane 2: DNA control in light; Lane 3: DNA + **3** (10 µM) in dark; Lane 4: DNA + **3** (10 µM) in light. Lanes 5 and 6 were not used for calculations. Sample composition: 1 µL DNA + 1 µL NaCl (50 mM) + 8 µL Tris-HCl Buffer (50 mM, pH = 7.2) + 10 µL complex **3** (total volume of samples = 20 µL); SC = supercoiled and NC = nicked circular DNA.

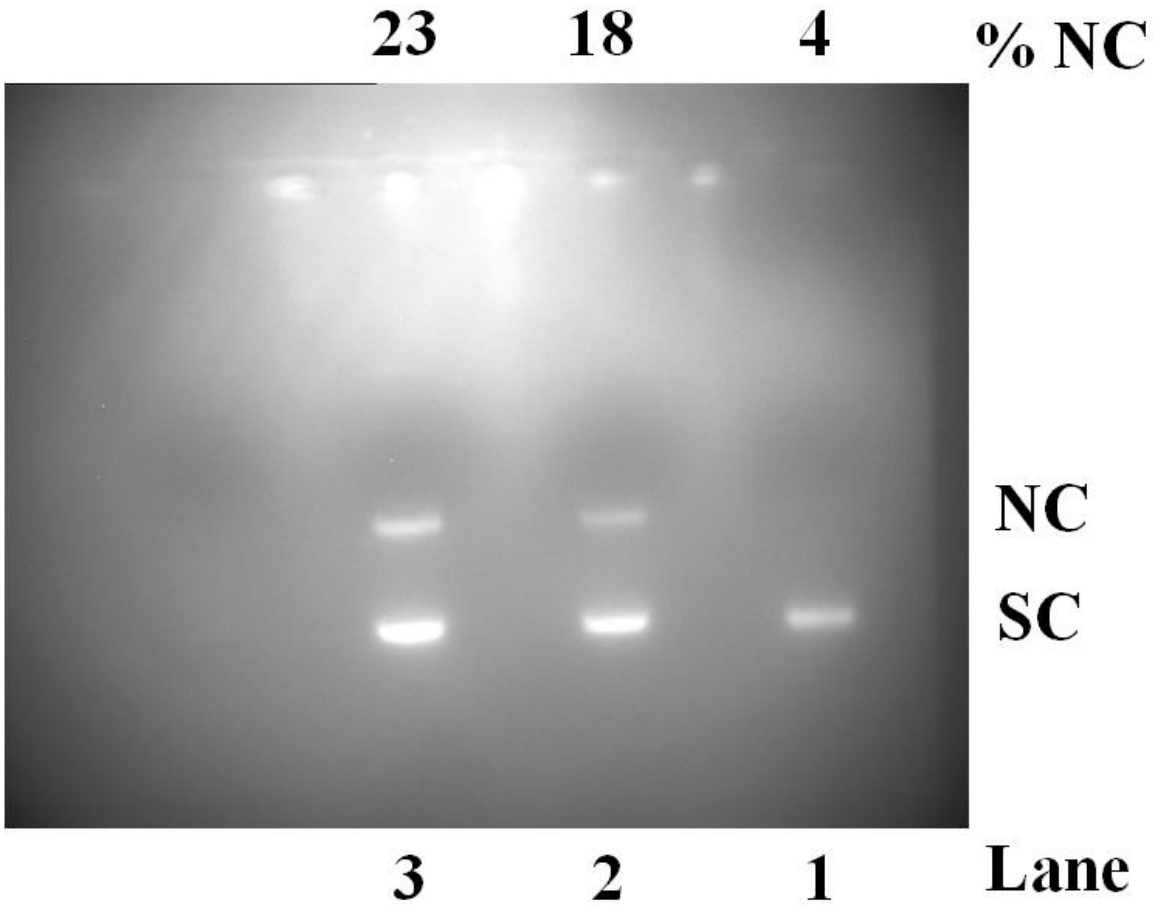

Figure S63 Gel diagram showing the extent of SC pUC19 DNA (0.2 μg, 30 μM base pair) cleavage on agarose gel eletrophoresis using the most active complex **3** in presence of green diode laser light source (532 nm, 100 mW, 1 h exposure) upon addition of singlet oxygen quenchers TEMP and NaN_3. Lane 1: DNA control in light; Lane 2: DNA + **3** (10 μM) + TEMP (5 mM) in light and Lane 3: DNA + **3** (10 μM) + NaN_3 (5 mM) in light. Sample composition: 1 μL DNA + 1 μL NaCl (50 mM) + 4 μL Tris-HCl Buffer (50 mM, pH = 7.2) + 10 μL complex + 4 μL TEMP or NaN_3 (5 mM) (total volume of samples = 20 μL); SC = supercoiled and NC = nicked circular DNA.

(a)

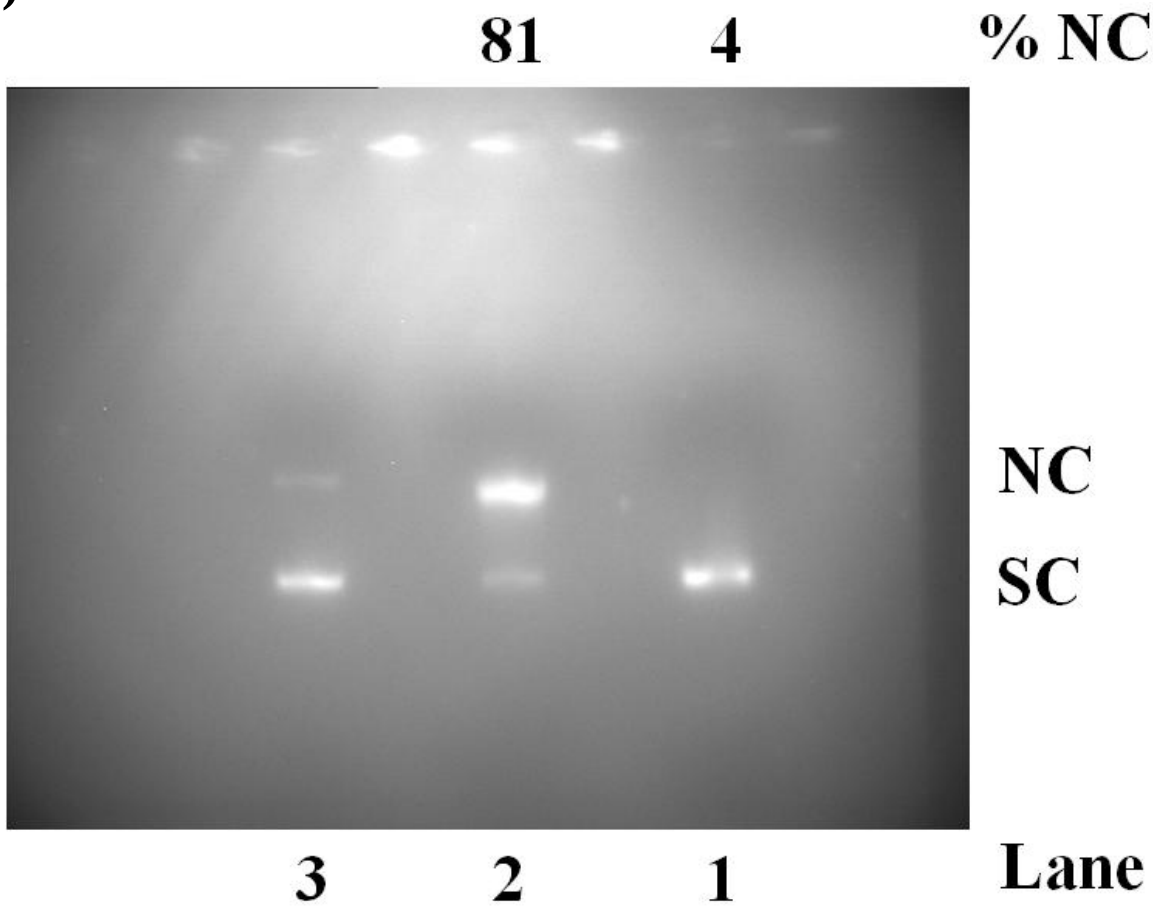

(b)

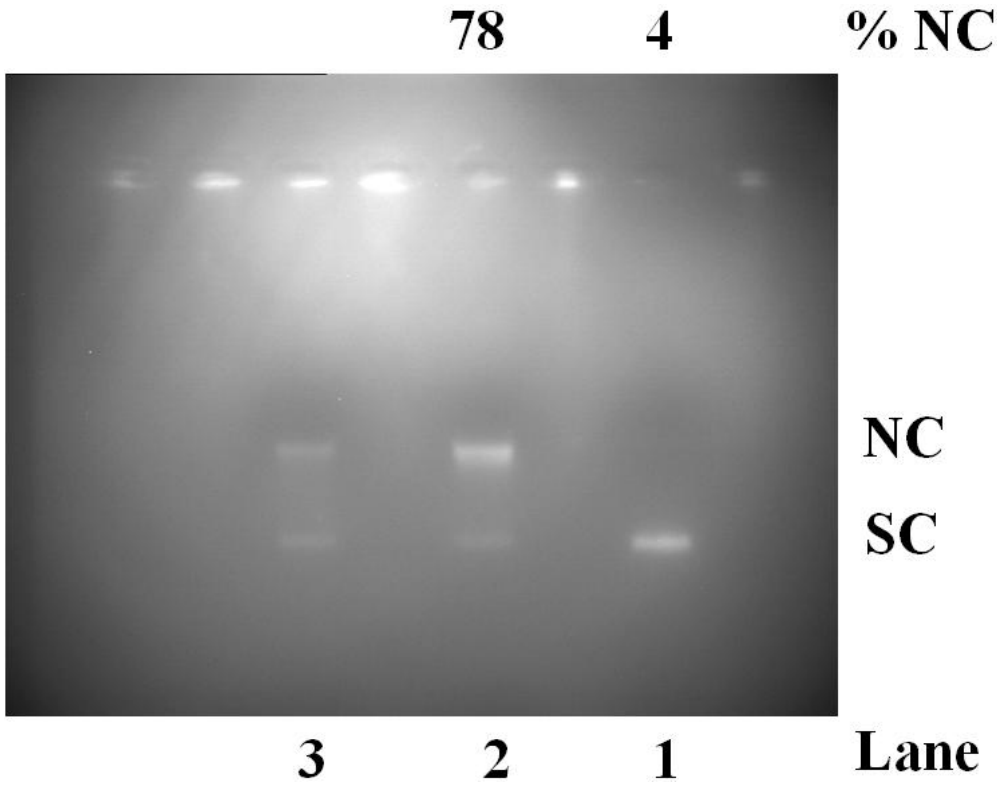

Figure S64 (a) Gel diagram showing the extent of SC pUC19 DNA (0.2 μg, 30 μM base pair) cleavage on agarose gel eletrophoresis using the most active complex **3** in presence of green laser light source (532 nm, 100 mW, 1 h exposure) upon addition of hydroxyl radical scavenger KI. Lane 1: DNA control in light; Lane 2: DNA + **3** (10 μM) + KI (5 mM) in light. Lane 3 was not used for calculations. Sample composition: 1 μL DNA + 1 μL NaCl (50 mM) + 4 μL Tris-HCl Buffer (50 mM, pH = 7.2) + 10 μL complex + 4 μL KI (5 mM) (total volume of samples = 20 μL); SC = super coiled and NC = nicked circular DNA.

(b) Gel diagram showing the extent of SC pUC19 DNA (0.2 μg, 30 μM base pair) cleavage on agarose gel eletrophoresis using the most active complex **3** in presence of green diode laser light source (532 nm, 100 mW, 1 h exposure) upon addition of hydroxyl radical scavenger catalase. Lane 1: DNA control in light; Lane 2: DNA + Comp **3** (10 μM) + catalase (4 unit) in light. Lane 3 was not used for the calculations. Sample composition: 1 μL DNA + 1 μL NaCl (50 mM) + 4 μL Tris-HCl Buffer (50 mM, pH = 7.2) + 10 μL complex + 4 μL catalase (4 units) (total volume of samples = 20 μL); SC = supercoiled and NC = nicked circular DNA.

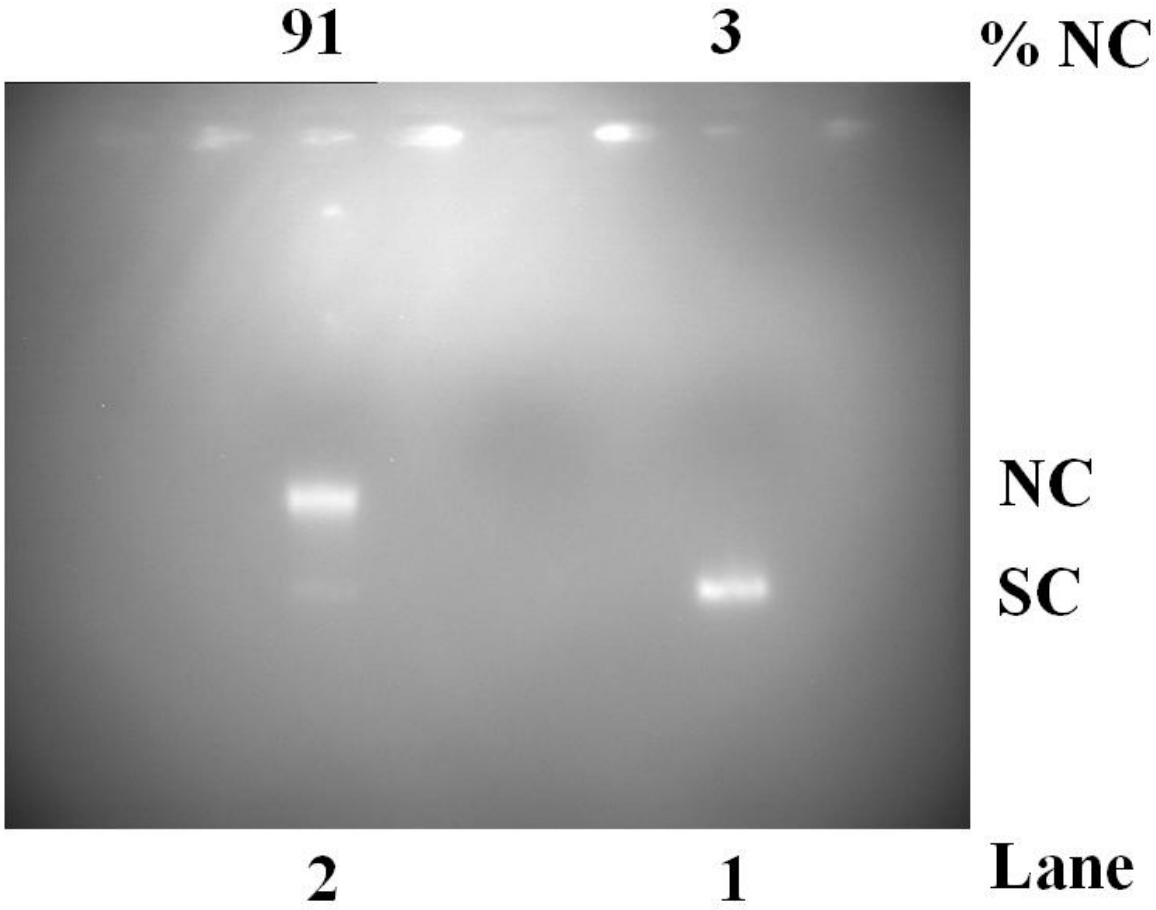

Figure S65 Gel diagram showing the extent of SC pUC19 DNA (0.2 μg, 30 μM base pair) cleavage on agarose gel eletrophoresis using the most active complex **3** in presence of green diode laser light source (532 nm, 100 mW, 1 h exposure) upon addition of D_2O. Lane 1: DNA control in light; Lane 2: DNA + **3** (10 μM) + D_2O (4 μL) in light. Sample composition: 1 μL DNA + 1 μL NaCl (50 mM) + 4 μL Tris-HCl Buffer (50 mM, pH = 7.2) + 10 μL complex + 4 μL D_2O (4 units) (total volume of samples = 20 μL); SC = supercoiled and NC = nicked circular DNA.

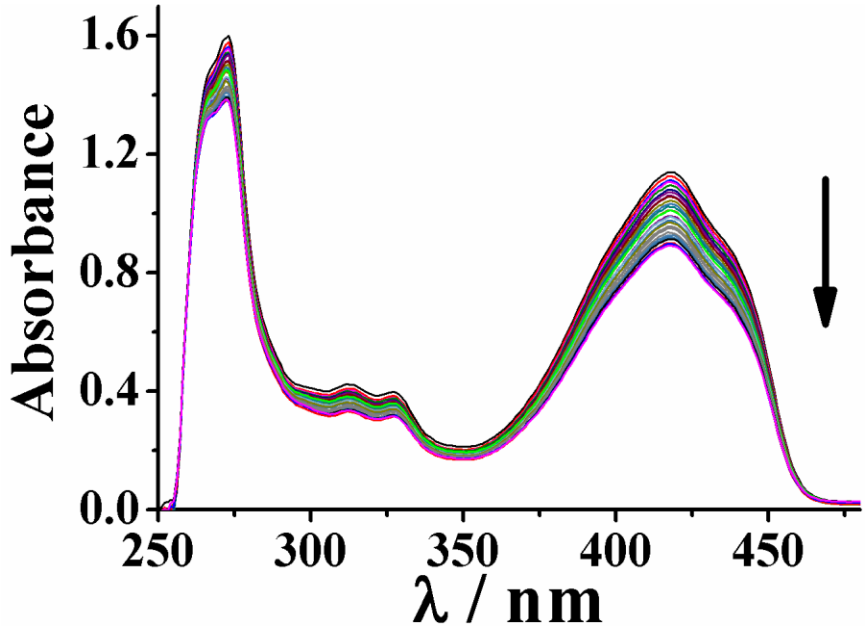

Figure S66 UV-visible absorption spectral decay of DPBF (1,3-diphenylisobenzofuran) in the presence of complex **2** (concentration = 3.0 μM) on light irradiation proving the formation of singlet oxygen qualitatively. The duration of each exposure was 5 sec. Light source used: λ = 400-700 nm, 10 *J* cm^{-2}.

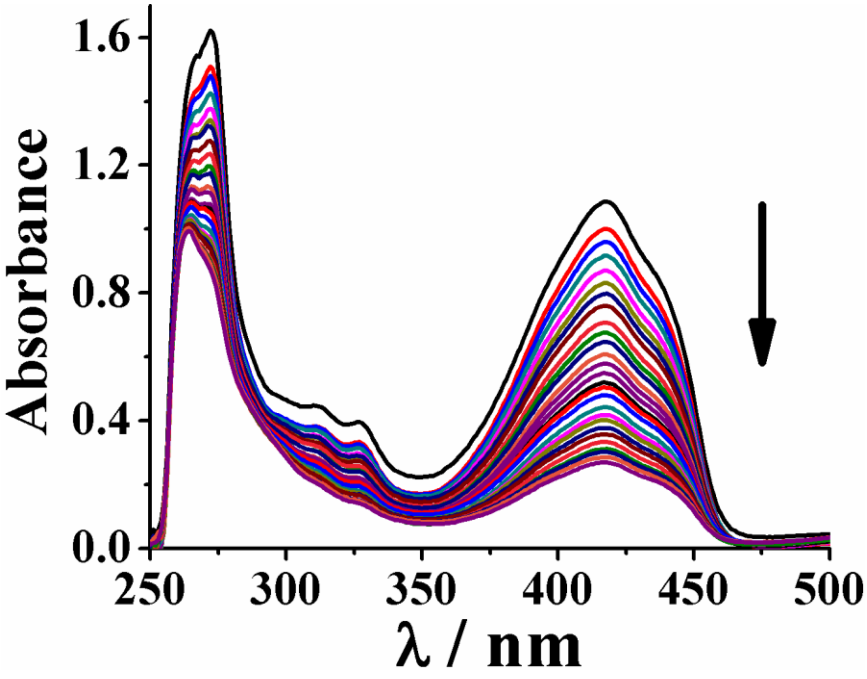

Figure S67 UV-visible absorption spectral decay of DPBF (1,3-diphenylisobenzofuran) in the presence of complex **3** (concentration = 0.3 μM) on light irradiation proving the formation of singlet oxygen qualitatively. The duration of each exposure was 5 sec. Light source used: λ = 400-700 nm, 10 *J* cm^{-2}.

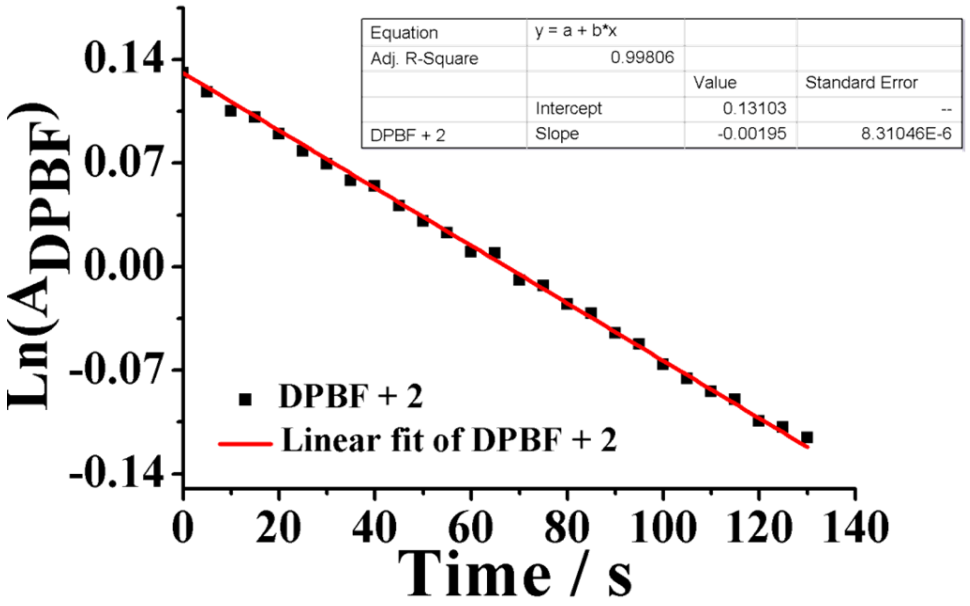

Figure S68 Plot for determination of the rate constant for the 1st order decay of DPBF (1,3-diphenylisobenzofuran) in presence of complex **2** (concentration = 3.0 µM) on light irradiation. The duration of each exposure was 5 sec. Light source used: λ = 400-700 nm, 10 *J* cm^{-2}.

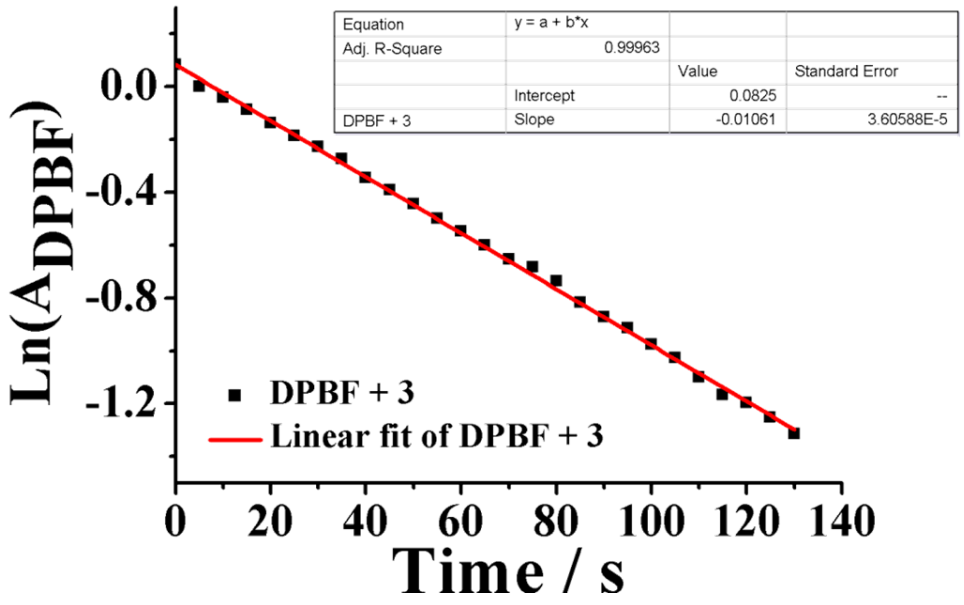

Figure S69 Plot for determination of the rate constant for the 1st order decay of DPBF (1,3-diphenylisobenzofuran) in presence of complex **3** (concentration = 0.03 µM) on light irradiation. The duration of each exposure was 5 sec. Light source used: λ = 400-700 nm, 10 *J* cm^{-2}.

(a)

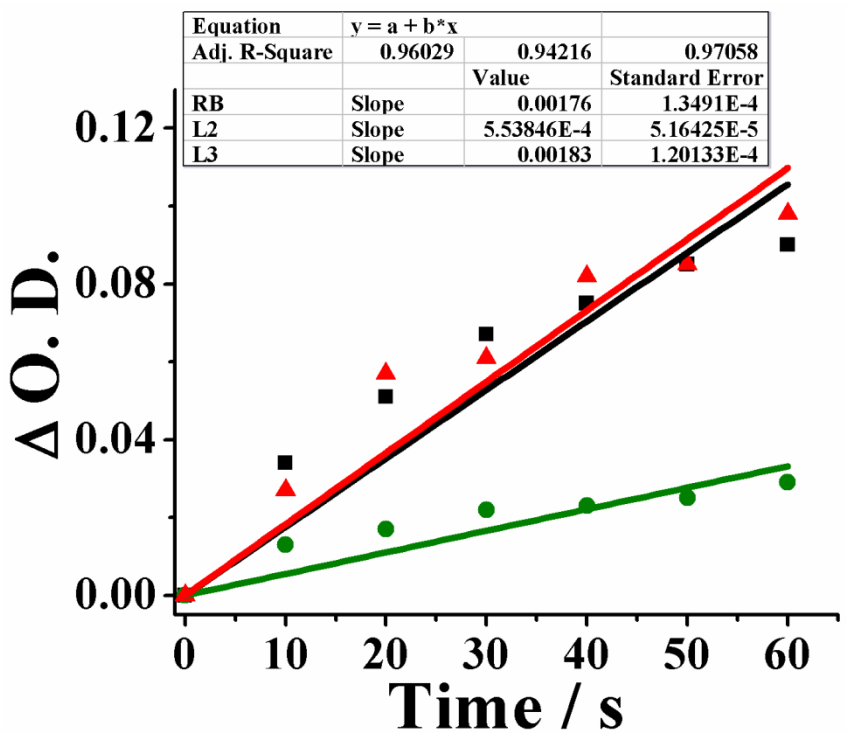

(b)

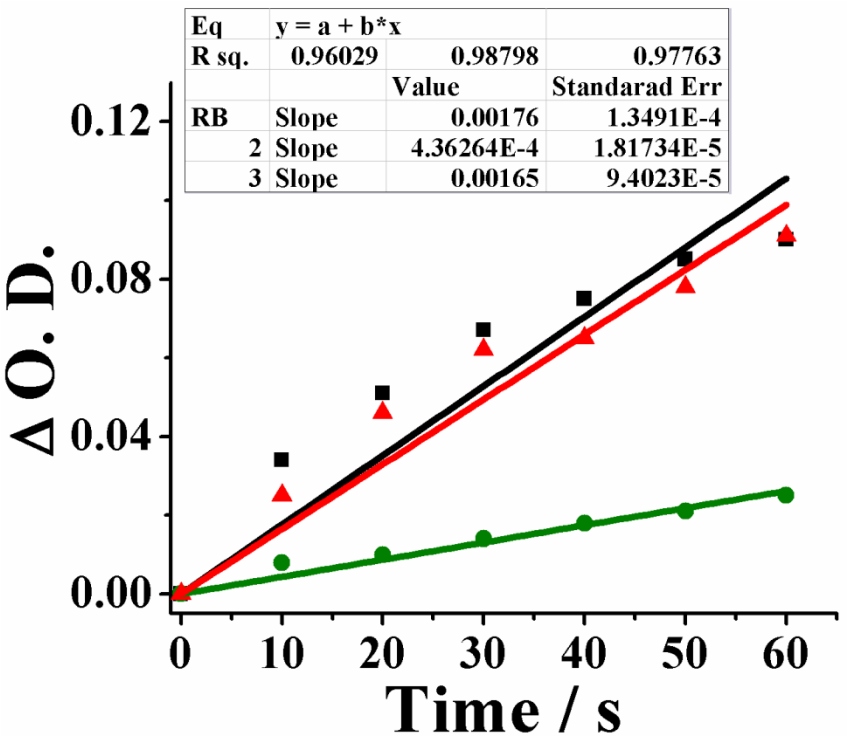

Figure S70 Plot for quantitative singlet oxygen detection and determination of single oxygen quantum yields by measuring the spectral decay of DPBF in the presence of Rose Bengal (R.B., black) as standard, and ligand L^2 (green), ligand L^3 (red) in figure (a) and complex **2** (green), complex **3** (red) in figure (b). The duration of each exposure was 10 sec. Light source used: λ = 400-700 nm (10 *J* cm^{-2}).

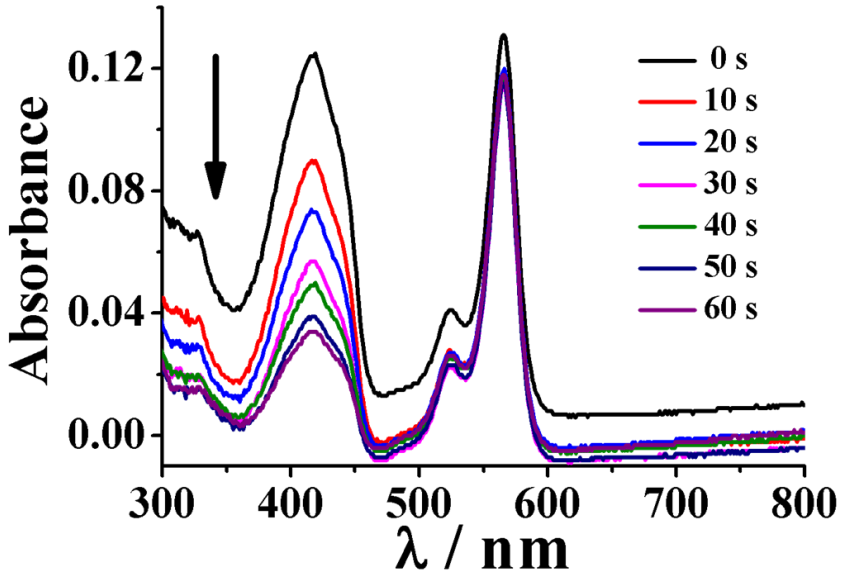

Figure S71 UV-visible absorption spectral decay of DPBF (1,3-diphenylisobenzofuran) in the presence of standard R.B. (Rose Bengal) on light irradiation for the singlet oxygen quantum yield calculations. Optical densities of DPBF and RB are taken in the 0.1-0.2 range to exclude their singlet oxygen quenching possibilities. The duration of each exposure was 10 sec. Light source used: λ = 400-700 nm, 10 *J* cm^{-2}.

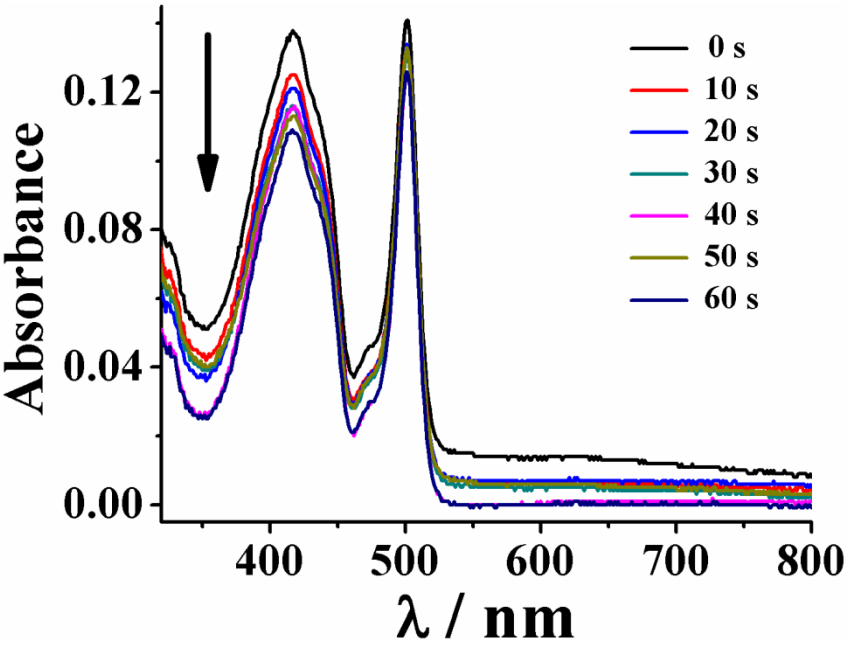

Figure S72 UV-visible absorption spectral decay of DPBF (1,3-diphenylisobenzofuran) in the presence of ligand L^2 on light irradiation for the singlet oxygen quantum yield calculations. Optical densities of DPBF and ligand L^2 are taken in the 0.1-0.2 range to exclude their singlet oxygen quenching possibilities. The duration of each exposure was 10 sec. Light source used: λ = 400-700 nm, 10 *J* cm^{-2}.

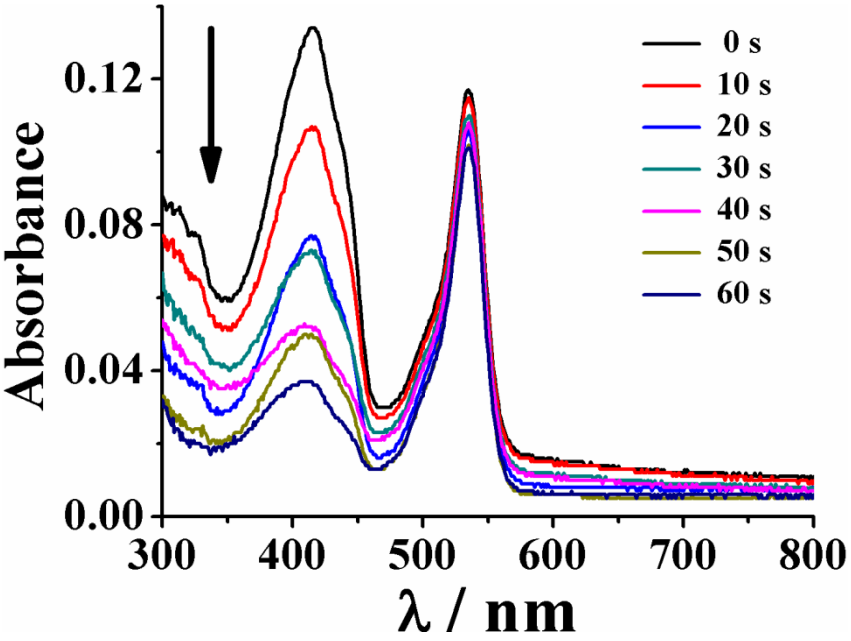

Figure S73 UV-visible absorption spectral decay of DPBF (1,3-diphenylisobenzofuran) in the presence of ligand L^3 on light irradiation for the singlet oxygen quantum yield calculations. Optical densities of DPBF and ligand L^3 are taken in the 0.1-0.2 range to exclude their singlet oxygen quenching possibilities. The duration of each exposure was 10 sec. Light source used: λ = 400-700 nm, 10 *J* cm^{-2}.

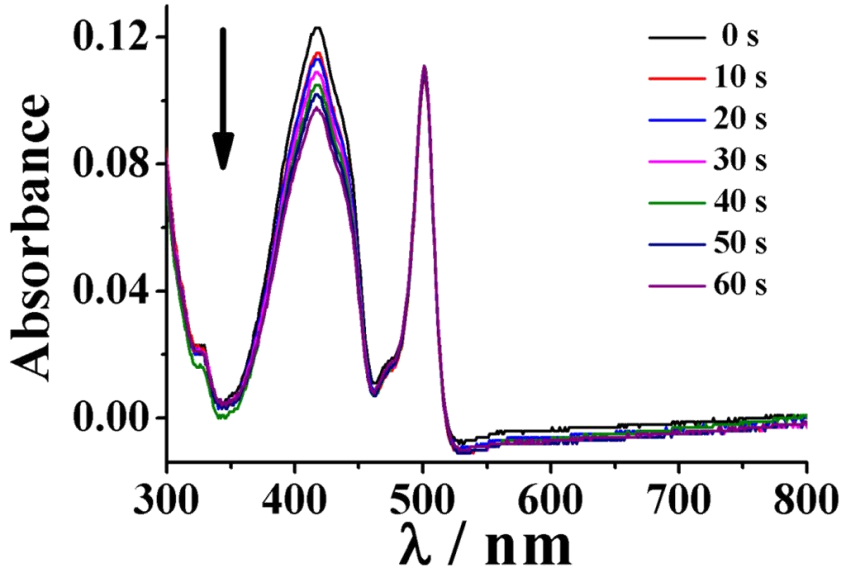

Figure S74 UV-visible absorption spectral decay of DPBF (1,3-diphenylisobenzofuran) in the presence of complex **2** on light irradiation for the singlet oxygen quantum yield calculations. Optical densities of DPBF and complex **2** are taken in the 0.1-0.2 range to exclude their singlet oxygen quenching possibilities. The duration of each exposure was 10 sec. Light source used: λ = 400-700 nm, 10 *J* cm^{-2}.

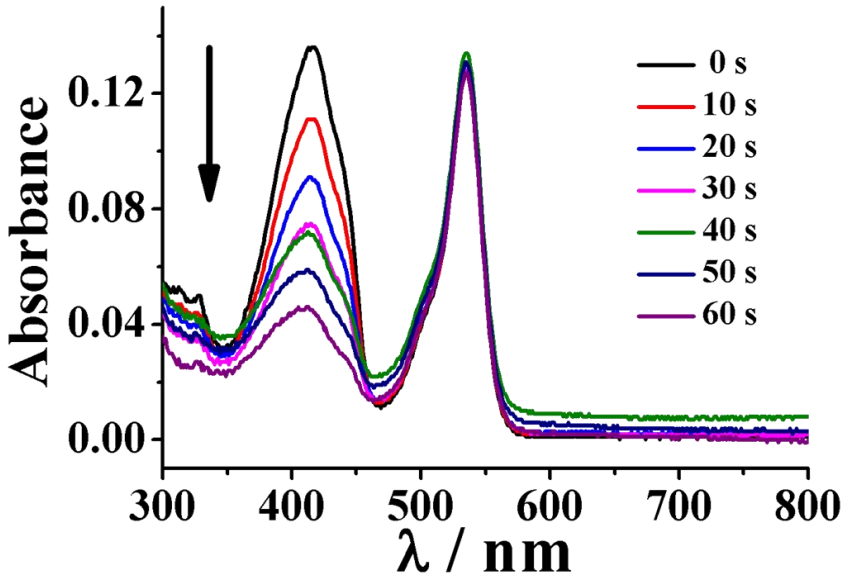

Figure S75 UV-visible absorption spectral decay of DPBF (1,3-diphenylisobenzofuran) in the presence of complex **3** on light irradiation for the singlet oxygen quantum yield calculations. Optical densities of DPBF and complex **3** are taken in the 0.1-0.2 range to exclude their singlet oxygen quenching possibilities. The duration of each exposure was 10 sec. Light source used: λ = 400-700 nm, 10 *J* cm^{-2}.

Tables

Table S1 Selected bond lengths (Å) and bond angles (°) from the crystal structures of complexes **2** and **3** with e.s.d.s in the parenthesis

Entry	Complex **2**	Complex **3**	Entry	Complex **2**	Complex **3**
Zn(1)-N(1)	2.098(2)	2.115(5)	N(1)-Zn(1)-Cl(1)	115.80(7)	129.10(16)
Zn(1)-N(2)	2.124(2)	2.115(6)	N(2)-Zn(1)-Cl(1)	117.21(7)	111.68(15)
Zn(1)-N(3)	2.404(2)	2.376(4)	N(3)-Zn(1)- Cl(1)	91.78(6)	91.57(12)
Zn(1)-Cl(1)	2.2554(8)	2.2861(19)	N(1)-Zn(1)-Cl(2)	97.25(7)	96.21(15)
Zn(1)-Cl(2)	2.2940(9)	2.375(2)	N(2)-Zn(1)-Cl(2)	98.21(7)	99.38(16)
B(1)-N(4)	1.534(5)	1.569(10)	N(3)-Zn(1)-Cl(2)	163.44(6)	166.63(13)
B(1)-N(5)	1.541(5)	1.581(10)	Cl(1)-Zn(1)-Cl(2)	104.76(4)	101.80(8)
B(1)-F(1)	1.384(4)	1.397(9)	N(4)-B(1)-N(5)	107.2(3)	106.7(5)
B(1)-F(2)	1.389(4)	1.408(9)	F(1)-B(1)-F(2)	109.2(3)	110.3(6)
I(1)-C(23)		2.098(7)	F(1)-B(1)-N(4)	110.6(3)	110.6(6)
I(2)-C(27)		2.101(7)	F(2)-B(1)-N(4)	110.2(3)	109.8(6)
N(1)-Zn(1)-N(2)	118.02(9)	111.7(2)	F(1)-B(1)-N(5)	110.1(3)	110.2(6)
N(1)-Zn(1)-N(3)	74.29(8)	74.98(18)	F(2)-B(1)-N(5)	109.6(3)	109.3(6)
N(2)-Zn(1)-N(3)	74.32(9)	75.28(19)			

Table S2 The optimized coordinates of the atoms in complex **1** obtained from DFT calculations

---

Center Number	Atomic Number	Atomic Type	Coordinates (Angstroms) X	Y	Z
1	6	C	3.706770	-1.644345	-0.391994

2	1	H	3.924120	-2.707002	-0.402798
3	6	C	3.054278	1.012256	-0.383233
4	1	H	2.733280	2.048668	-0.389153
5	6	C	4.387572	0.655526	-0.549777
6	1	H	5.142832	1.422144	-0.678968
7	6	C	4.717955	-0.700096	-0.554701
8	1	H	5.746565	-1.017716	-0.691203
9	1	H	0.000004	-1.517884	-1.461648
10	30	Zn	-0.000067	0.547999	0.182289
11	17	Cl	0.000657	0.492971	2.529963
12	17	Cl	-0.000351	2.712471	-0.756045
13	7	N	-0.000007	-1.544573	-0.442278
14	7	N	2.079016	0.103056	-0.217195
15	6	C	-4.387698	0.655418	-0.549406
16	1	H	-5.142996	1.422023	-0.678462
17	7	N	-2.079087	0.103024	-0.217050
18	6	C	-2.395336	-1.204404	-0.216125
19	6	C	-3.706791	-1.644433	-0.391875
20	1	H	-3.924085	-2.707100	-0.402765
21	6	C	-1.246656	-2.166339	0.016181
22	1	H	-1.150922	-2.355604	1.091884
23	1	H	-1.449571	-3.127643	-0.469557
24	6	C	-3.054412	1.012194	-0.382938
25	1	H	-2.733453	2.048614	-0.388840
26	6	C	-4.718030	-0.700217	-0.554424

27	1	H	-5.746635	-1.017864	-0.690893
28	6	C	1.246655	-2.166297	0.016213
29	1	H	1.449577	-3.127631	-0.469463
30	1	H	1.150943	-2.355474	1.091932
31	6	C	2.395308	-1.204356	-0.216202

Table S3 The optimized coordinates of the atoms in complex **2** obtained from DFT calculations

Center Number	Atomic Number	Atomic Type	Coordinates (Angstroms) X	Y	Z
1	30	Zn	4.889123	-0.448267	-0.437824
2	7	N	4.332702	-1.325464	1.380323
3	7	N	4.866839	1.641446	-0.602119
4	7	N	2.633951	0.072886	-0.246773
5	7	N	-5.817196	1.322087	0.562532
6	7	N	-6.282968	-0.910942	-0.429961
7	17	Cl	4.710736	-1.436651	-2.561076
8	17	Cl	7.291651	-0.704049	0.005494
9	5	B	-6.958468	0.357297	0.151308
10	9	F	-7.773299	0.957850	-0.819105
11	9	F	-7.735038	0.023417	1.268851
12	6	C	5.017891	-2.305640	1.994190

13	1	H	5.922796	-2.630399	1.493828
14	6	C	4.606595	-2.855128	3.203452
15	1	H	5.184955	-3.648974	3.661289
16	6	C	3.447134	-2.361781	3.800207
17	1	H	3.096272	-2.765493	4.744242
18	6	C	2.737691	-1.343967	3.164466
19	1	H	1.831369	-0.936615	3.598851
20	6	C	3.208873	-0.848704	1.950666
21	6	C	2.524797	0.278563	1.209080
22	1	H	1.486127	0.385729	1.541534
23	1	H	3.034404	1.215540	1.459687
24	6	C	2.479235	1.323625	-1.002961
25	1	H	1.562228	1.867977	-0.744371
26	1	H	2.405788	1.056211	-2.063244
27	6	C	3.678055	2.232809	-0.831355
28	6	C	3.562339	3.616883	-0.952929
29	1	H	2.588582	4.062433	-1.124024
30	6	C	4.706236	4.405084	-0.852091
31	1	H	4.637577	5.483866	-0.945979
32	6	C	5.934999	3.787593	-0.620741
33	1	H	6.849235	4.362440	-0.530367
34	6	C	5.971194	2.404220	-0.496995
35	1	H	6.892245	1.863912	-0.307202

36	6	C	1.745547	-1.020434	-0.745011
37	1	H	2.032710	-1.927885	-0.207074
38	1	H	2.011863	-1.175623	-1.792317
39	6	C	0.252630	-0.791538	-0.597832
40	6	C	-0.434984	-1.243876	0.537904
41	1	H	0.100859	-1.785362	1.312608
42	6	C	-1.805183	-1.028158	0.684218
43	1	H	-2.317873	-1.386370	1.571577
44	6	C	-2.525937	-0.358752	-0.312421
45	6	C	-1.851593	0.079692	-1.459334
46	1	H	-2.401477	0.585673	-2.246858
47	6	C	-0.481264	-0.138157	-1.598494
48	1	H	0.016888	0.193474	-2.504896
49	6	C	-3.994266	-0.123907	-0.157526
50	6	C	-4.444187	1.080253	0.409759
51	6	C	-3.739471	2.220200	0.921203
52	6	C	-4.715493	3.109230	1.361487
53	1	H	-4.543813	4.079129	1.808724
54	6	C	-5.980722	2.536376	1.131306
55	6	C	-4.902345	-1.110499	-0.576358
56	6	C	-4.707417	-2.398416	-1.177874
57	6	C	-5.979565	-2.929255	-1.368677
58	1	H	-6.213312	-3.892405	-1.802173

59	6	C	-6.928350	-1.999092	-0.902925
60	6	C	-8.416407	-2.125824	-0.899793
61	1	H	-8.718283	-3.073726	-1.348015
62	1	H	-8.807397	-2.073487	0.121106
63	1	H	-8.874955	-1.303728	-1.457745
64	6	C	-3.433249	-3.093263	-1.555552
65	1	H	-2.837193	-2.503196	-2.257987
66	1	H	-2.797562	-3.285219	-0.686054
67	1	H	-3.663125	-4.052499	-2.026037
68	6	C	-2.263510	2.473726	1.001608
69	1	H	-1.742215	1.690497	1.559645
70	1	H	-1.800492	2.517153	0.010871
71	1	H	-2.081127	3.428054	1.501961
72	6	C	-7.322485	3.113054	1.443117
73	1	H	-7.218083	4.116365	1.859167
74	1	H	-7.941353	3.161443	0.542032
75	1	H	-7.856570	2.483486	2.161789

Table S4 The optimized coordinates of the atoms in complex **3** obtained from DFT calculations

---

Center Number	Atomic Number	Atomic Type	Coordinates (Angstroms) X	Y	Z

1	53	I	-5.365933	-5.014193	-0.292133
2	53	I	-3.001008	5.664859	0.315692
3	30	Zn	6.094574	-1.032801	-0.216739
4	17	Cl	5.697433	-2.822126	-1.691196
5	17	Cl	8.461353	-1.364418	0.254765
6	9	F	-6.476552	0.909551	-1.168273
7	9	F	-6.506526	0.771192	1.116076
8	7	N	5.577002	-0.904891	1.816238
9	7	N	3.903123	-0.256914	-0.252416
10	7	N	-5.070118	-0.748722	-0.101244
11	7	N	6.239141	0.746963	-1.302472
12	7	N	-4.530370	1.677004	0.050204
13	6	C	-1.298648	-0.313407	-0.100750
14	6	C	1.446072	-0.979985	-0.165264
15	6	C	-2.756567	0.013423	-0.069379
16	6	C	2.912154	-1.372356	-0.197080
17	1	H	3.151077	-1.960245	0.693597

18	1	H	3.120443	-2.007669	-1.060107
19	6	C	4.521195	-0.124756	2.119387
20	6	C	5.093118	2.482738	-2.486516
21	1	H	4.153712	2.902995	-2.829002
22	6	C	-0.590466	-0.516990	1.090054
23	1	H	-1.100947	-0.429119	2.044228
24	6	C	3.875092	0.591276	0.953081
25	1	H	2.860619	0.915342	1.213117
26	1	H	4.451749	1.499169	0.743748
27	6	C	5.094832	1.292857	-1.759273
28	6	C	-2.416700	2.575476	0.089466
29	6	C	6.224734	-1.548221	2.803575
30	1	H	7.074763	-2.145962	2.494908
31	6	C	-3.533429	-2.454051	-0.189060
32	6	C	-3.698991	-1.030079	-0.121349
33	6	C	-4.669012	3.014872	0.141955
34	6	C	3.814222	0.529354	-1.491216
35	1	H	2.963063	1.221914	-1.496530

36	1	H	3.661045	-0.176374	-2.315596
37	6	C	-5.761974	-1.904887	-0.152986
38	6	C	0.763735	-0.850390	1.053353
39	1	H	1.288532	-1.031896	1.987303
40	6	C	-4.830162	-2.966020	-0.206588
41	6	C	-3.168414	1.355685	0.016758
42	6	C	0.726419	-0.775806	-1.352158
43	1	H	1.219988	-0.897547	-2.312133
44	6	C	-3.375959	3.584623	0.168276
45	6	C	4.083502	0.037219	3.432608
46	1	H	3.231620	0.674527	3.643494
47	6	C	-0.627992	-0.444578	-1.324046
48	1	H	-1.169795	-0.301560	-2.254009
49	6	C	-7.252868	-1.950450	-0.133668
50	1	H	-7.662811	-1.209713	-0.823798
51	1	H	-7.630115	-1.708389	0.865862
52	1	H	-7.613703	-2.941628	-0.409379
53	6	C	5.843960	-1.440695	4.136770

54	1	H	6.390660	-1.981381	4.900670
55	6	C	7.410081	1.358828	-1.562349
56	1	H	8.290595	0.866683	-1.163185
57	6	C	4.755189	-0.629868	4.456338
58	1	H	4.429376	-0.521575	5.485795
59	6	C	-0.930941	2.760391	0.085612
60	1	H	-0.468710	2.303976	-0.793481
61	1	H	-0.466242	2.304121	0.964696
62	1	H	-0.685566	3.823804	0.087228
63	6	C	6.305324	3.112350	-2.760837
64	1	H	6.325430	4.038167	-3.326651
65	6	C	-2.266747	-3.250751	-0.230587
66	1	H	-2.497349	-4.317113	-0.245897
67	1	H	-1.634531	-3.050115	0.638350
68	1	H	-1.672349	-3.018334	-1.118690
69	6	C	7.487345	2.539545	-2.291122
70	1	H	8.451610	2.997928	-2.477880
71	6	C	-6.002429	3.679715	0.208367

72	1	H	-6.642149	3.326244	-0.604276
73	1	H	-5.898469	4.762385	0.141582
74	1	H	-6.506378	3.430627	1.147906
75	5	B	-5.708327	0.665917	-0.023927

Table S5 Molar conductivity data (Λ_M / S m^2 mol^{-1}) of complexes **1-3** in different solvents[S5]

Complex	MeCN	Acetone	DMF	DMSO	H_2O:DMSO (H_2O:DMF) [v/v]				
					1:9	1:3	1:1	3:1	9:1
1	17	3	12	18	29(20)	44(43)	78(75)	171(167)	217(211)
2	12	2	10	10	17(15)	29(35)	61(65)	151(149)	188(178)
3	14	2	12	15	29(19)	38(41)	73(71)	162(154)	202(195)

Table S6 IC_{50} values of complexes **1-3** (μM) with relevant zinc-porphyrin (ZnPP), zinc-phthalocyanine (ZnPc) derivatives and metal-BODIPY conjugates[S16-S25]

Entry	HeLa		MCF-7	
	Dark	Light	Dark	Light
Complex **1**[a]	94.4±0.3	74.5±0.2	110.5±1.0	97.5±0.3
Complex **2**[a]	56.2±0.3	2.4±0.1	51.4±0.2	3.8±0.1
Complex **3**[a]	55.2±0.4	0.015±0.005	57.3±0.3	0.035±0.007
(Methoxyphenylethynyl)-ZnPP conjugate (NP)[b]	>15	3.6	n.d.	n.d.

(TEG-phenylethynyl)-ZnPP conjugate (NP)[c]	>20	11.7	n.d.	n.d.
[{(Quaternized triazolyl)methyl}phenoxy]-ZnPc conjugate[d]	369±53	0.012±0.004	n.d.	0.0053±0.0008
[{(Triethylammonio)ethyl}sulfanyl]-ZnPc conjugate[e]	192±14	0.31±0.121	n.d.	n.d.
Tamoxifen-ZnPc conjugate[f]	n.d.	n.d.	12.5	0.0138±0.0019
Ru^{II}-(Pyrazoylquinoline-BODIPY) conjugate[g]	>100	12.87	n.d.	n.d.
Ir^{III}-(phenylcyanamide-BODIPY) conjugate[h]	60.11±0.2	0.53±0.1	n.d.	n.d.
Pt^{II}-(pyridyl-diiodoBODIPY) conjugate[i]	n.d.	n.d.	>100	0.07±0.02
Au^{I}-(alkynyl-BODIPY) conjugate[j]	0.16	0.0025	n.d.	n.d.
Photofrin®[k]	>41	4.3±0.2	n.d.	2.0±0.2

[a] Used in current study; light source used for photoirradiation: λ = 400-700 nm, fluence rate = 2.4 mW cm^{-2}, light dose = 10 *J* cm^{-2}, exposure time = 1 h. [b] Data from reference S16; Light source: Xe Lamp, λ = 660 nm, power density = 0.75 W cm^{-2}, 8 min; IC_{50} values are reported in μg/mL. [c] Data from reference S17; light source: λ = 650 nm laser, 4.2 mW cm^{-2}, 10 min; IC_{50} values are reported in μg/mL. [d] Data from reference S18; light source: Xe lamp, λ > 570 nm, 12.4 mW cm^{-2}, 11.2 *J* cm^{-2}, 15 min. [e] Data from reference S19; light source: Xe lamp, λ > 570 nm, 12.4 mW cm^{-2}, 11.2 *J* cm^{-2}, 15 min. [f] Data from reference S20; light source: red light, λ = 670 nm, 80 mW cm^{-2}, 1.5 J cm^{-2}. [g] Data from reference S21; light source: λ = 400-700 nm, 2.4 mW cm^{-2}, 10 *J* cm^{-2}, 1 h. [h] Data from reference S22; light source: visible light, λ = 500 nm, 10 *J* cm^{-2}, 20 min. [i] Data from reference S23; light source: λ = 400-700 nm, 2.4 mW cm^{-2}, 10 *J* cm^{-2}, 1 h. [j] Data from reference S24; light source: green LED, λ = 525 nm, 3.3 mW cm^{-2}, 30 min; IC_{50} values in A549 lung cancer cells. [k] Data from reference S25; light source: λ = 633 nm, 5 J cm^{-2}, 2 h. n.d. = not determined.

References:

S1. D. D. Perrin, W. L. F. Armarego and D. R. Perrin, *Purification of Laboratory Chemicals*, Pergamon Press, Oxford, U.K., 1980.

S2. N. M. F. Carvalho, A. Horn Jr., A. J. Bortoluzzi, V. Drago and O. A. C. Antunes, *Inorg. Chim. Acta*, 2006, **359**, 90–98.

S3. B. W. Michel, A. R. Lippert and C. J. Chang, *J. Am. Chem. Soc.*, 2012, **134**, 15668-15671.

S4. C. Fernandes, A. Horn Jr, O. Vieira-da-Motta, M. M. Kanashiro, M. R. Rocha, R. O. Moreira, S. R. Morcelli, B. F. Lopes, L. D. S. Mathias, F. V. Borges, L. J. H. Borges, W. R. Freitas, L. C. Visentin, J. C. d. A. Almeida and G. Schenk, *Inorg. Chim. Acta*, 2014, **416**, 35–48.

S5. W. J. Geary, *Coord. Chem. Rev*., 1971, **7**, 81-122.

S6. (*a*) A. D. Becke, *Phys. Rev. A: At. Mol., Opt. Phys.*, 1988, **38**, 3098−3100; (*b*) A. D. Becke, *J. Chem. Phys.*, 1993, **98**, 5648−5662; (*c*) W. R. Wadt, and P. J. Hay, *J. Chem. Phys.*, 1985, **82**, 284−298.

S7. T. Mosmann, *J. Immunol. Methods*, 1983, **65**, 55–63.

S8. *Prism 6 Statistics Guide*, GraphPad Software, Inc., San Diego, CA, 2014, http://www.graphpad.com.

S9. I. Vermes, C. Haanen, H. Steffens-Nakken and C. A. Reutelingsperger, *J. Immunol. Methods*, 1995, **184**, 39–51.

S10. R. Brandt, and A. S. Keston, *Anal. Biochem.*, 1965, **11**, 6–9.

S11. A. Bhattacharyya, A. Jameei, A. Garai, R. Saha, A. A. Karande and A. R. Chakravarty, *Dalton Trans.*, 2018, **47**, 5019–5030.

S12. (*a*) J. D. McGhee, and P. H. von Hippel, *J. Mol. Biol.*, 1974, **86**, 469–489; (*b*) M. T. Carter, M. Rodriguez and A. J. Bard, *J. Am. Chem. Soc.*, 1989, **111**, 8901–8911.

S13. (*a*) D. Mustard and D. W. Ritchie, *Proteins: Struct. Funct. Genet.*, 2005, **60**, 269−274; (*b*) M. A. Husain, T. Sarwar, S. U. Rehman, H. M. Ishqi and M. Tabish, *Phys. Chem. Chem. Phys.*, 2015, **17**, 13837−13850.

S14. (*a*) F. M. Ausubel, R. Brent, R. E. Kingston, D. D. Moore, J. G. Seidman, J. Smith and K. Struhl, *Cur. Protocols in Mol Biol.* John Wiley & Sons, New York, 2003; (*b*) J. Bernadou, G. Pratviel, F. Bennis, M. Girardet and B. Meunier, *Biochemistry*, 1989, **28**, 7268–7275.

S15. (*a*) G. Bartosz, *Clin. Chim. Acta*, 2006, **368**, 53−76. (*b*) N. Adarsh, M. Shanmugasundaram, R. R. Avirah, and D. Ramaiah, *Chem. Eur. J.*, 2012, **18**, 12655–12662.

S16. K. Ding, Y.-W. Zhang, W. Si, X. Zhong, Y. Cai, J. Zou, J. Shao, Z. Yang and X. Dong, *ACS Appl. Mater. Interfaces*, 2018, **10**, 238–247.

S17. D. Pan, P. Liang, X. Zhong, D. Wang, H. Cao, W. Wang, W. He, Z. Yang and X. Dong, *ACS Appl. Bio Mater.*, 2019, **2**, 999−1005.

S18. B. Ghazal, M. Machacek, M. A. Shalaby, V. Novakova, P. Zimcik and S. Makhseed, *J. Med. Chem.*, 2017, **60**, 6060−6076.

S19. M. Machacek, A. Cidlina, V. Novakova, J. Svec, M. Rudolf, M. Miletin, R. Kuccera, T. Simunek and P. Zimcik, *J. Med. Chem.*, 2015, **58**, 1736−1749.

S20. F.-L. Zhang, M.-R. Song, G.-K. Yuan, H.-N. Ye, Y. Tian, M.-D. Huang, J.-P. Xue, Z.-H. Zhang and J.-Y. Liu, *J. Med. Chem.*, 2017, **60,** 6693−6703.

S21. R. P. Paitandi, V. Sharma, V. D. Singh, B. K. Dwivedi, S. M. Mobin and D. S. Pandey, *Dalton Trans.*, 2018, **47**, 17500–17514.

S22. L. Tabrizi, and H. Chiniforoshan, *RSC Adv.*, 2017, **7**, 34160–34169.

S23. M. K. Raza, S. Gautam, P. Howlader, A. Bhattacharyya, P. Kondaiah and A. R. Chakravarty, *Inorg. Chem.*, 2018, **57**, 14374–14385.

S24. M. Ucuncu, E. Karakus, E. K. Demirci, M. Sayar, S. Dartar, M. Emrullahoglu, *Org. Lett.*, 2017, **19**, 2522–2525.

S25. (*a*) E. Delaey, F. Van Laar, D. De Vos, A. Kamuhabwa, P. Jacobs and P. A. De Witte, *J. Photochem. Photobiol. B*, 2000, **55**, 27−36. (*b*) F. Menard, V. Sol, C. Ringot, R. Granet, S. Alves, C. Morvan, Y. Le Queneau, N. Ono and P. Krausz, *Bioorg. Med. Chem.*, 2009, **17**, 7647−7657.